Excitatory effects of dentate gyrus mossy cells on granule cells and area CA3: an vitro and in vivo study in adult mice.

Running title: Dentate gyrus mossy cell excitation of granule cells.

Hannah L. Bernstein[1,2,3], Yi-Ling Lu[1], Paige Leary[1,2], Swati Jain[1], Clay O. Lacefield[4]*, Justin J. Botterill[1,5*], Helen E. Scharfman[1,2,6]

[1]Center for Dementia Research
The Nathan Kline Institute for Psychiatric Research
140 Old Orangeburg Road, Building 35
Orangeburg, NY 10962

[2]Department of Neuroscience & Physiology and
The Neuroscience Institute
New York University Langone Health
500 First Avenue
New York, NY 10016

[3]Current address:
Department of Psychiatry
University of Austin
Austin, TX 78705

[4]Department of Psychiatry
Columbia University, College of Physicians & Surgeons
1051 Riverside Drive
New York, NY 10032

[5]Current address:
Department of Anatomy, Physiology & Pharmacology
University of Saskatchewan
Saskatoon S7N 5A2, Canada

[6]Departments of Child & Adolescent Psychiatry and Psychiatry
New York University Langone Health
1 Park Avenue
New Yor, NY 10016

Abstract: 278 words
Significance: 133
Introduction: 864
Discussion: 3243
Figures: 11
Appendix Figures: 14

Keywords: hilus, potentiation, NMDA, CA3, perforant path, acetylcholine, sharp wave-ripples

Conflict of interest: The authors have no competing financial interests.

Acknowledgements: We thank Karl Deisseroth and Charu Ramakrishnan for advice regarding optogenetics, Charlie Schroeder and Thomas Radman for assistance with CSD analysis, and Lawrence Bernstein for comments on the manuscript. This project was supported by National Institutes of Health (NIH) F30 MH-110165 (HLB), NIH R01 MH-109305 and NIH R37 NS-126529 HES), NIH R37 NS-128177 (COL), the Savoy Foundation and Natural Sciences and Engineering Research Council of Canada (NSERC; JJB), and the New York State Office of Mental Health (HES).

Additional Information: All data are available by contacting the corresponding author.

KEY POINTS

- In hippocampal slices, MC excitation of GCs is widespread but is usually subthreshold.
- MC input to GCs can increase entorhinal cortical excitation of GCs, but only within a restricted temporal window.
- MC activation of GCs can be strengthen by increasing MC activity, GC depolarization, NMDA receptors, or a muscarinic agonist.
- After MC stimulus trains or reduced $[Mg^{2+}]_o$ in vitro, MC excitation of GCs can trigger CA3 sharp wave-ripples.
- During exploration of novel objects, chemogenetic excitation of MCs leads to increased CA3 c-Fos immunoreactivity.
- During in vivo recording, calcium imaging of GCs shows that a subset of GCs are activated strongly by MCs.

SIGNIFICANCE

Here we show that the direct activation of dentate gyrus (DG) granule cells (GCs) by mossy cells (MCs) is widespread and, even when weak, has important effects, such as gating entorhinal input to GCs with high temporal precision. We also show that a subset of GCs is strongly activated by MCs. In addition, MC excitation of GCs can strengthen greatly under specific conditions. After strengthening, MC activation can increase neural activity in area CA3, and induce sharp wave-ripples (SPW-Rs) in CA3 pyramidal cells, which is significant because SPW-Rs are implicated in memory consolidation. Taken together with the understanding that MCs also inhibit GCs by exciting intermediary GABAergic neurons, the results suggest that MCs usually inhibit GCs, but activate GCs under select conditions. These roles are ideal for a structure that requires selective activation.

ABSTRACT

Understanding dentate gyrus (DG) circuitry is important to clarify DG function. The effects of glutamatergic mossy cells (MCs) on the primary cell DG type, granule cells (GCs) are puzzling because MCs project directly to GCs while also innervating GABAergic neurons that inhibit GCs. Because MCs appear to primarily inhibit GCs in vivo, we hypothesized that MC→GC excitation is weak, but important nevertheless because it can facilitate other inputs and strengthen under specific conditions. Furthermore, we hypothesized that a GC subpopulation might be activated strongly by MCs, even under normal conditions. To test these hypotheses, mice with Cre-recombinase located preferentially in MCs were injected with adeno-associated virus (AAV) to express an excitatory opsin (channelrhodopsin) in MCs, or with an AAV for chemogenetics. A combination of in vitro and in vivo methods was used to assess responses of GCs to optogenetic stimulation of MCs. The results supported the idea that MC excitation is weak but in almost all GCs, and that it can increase the perforant path input to GCs, although precise timing is required. We show that MC→GC synapses strengthen after GC depolarization, trains of MC optogenetic stimuli, reduced $[Mg^{2+}]_o$, and exposure to the cholinergic muscarinic agonist carbachol. Optogenetic stimulation of MCs in slices can lead to CA3 sharp wave-ripples (SPW-Rs) by a MC→GC→PC pathway, and chemogenetic activation of MCs during exploration in vivo can strongly activate area CA3, reflected by c-Fos protein expression. Two-photon calcium imaging in awake head-fixed mice showed that a subset of GCs are strongly activated by MCs. Together the data suggest that the MC→GC synapse is well suited for selective, conditional GC excitation, consistent with a structure that performs pattern separation.

INTRODUCTION

Mossy cells (MCs) of the dentate gyrus (DG) play an important role in many cognitive and behavioral functions of the DG, such as spatial memory, recognition of novelty in the environment, and regulating anxiety(Scharfman, 2016; Danielson et al., 2017; Nakazawa, 2017; Senzai and Buzsaki, 2017; Botterill et al., 2021b; Fredes and Shigemoto, 2021; Wang et al., 2021; GoodSmith et al., 2022; Miller et al., 2022; Kim et al., 2023). MCs also contribute to diseases where the DG is implicated, such as temporal lobe epilepsy (Sloviter, 1994; Blumcke et al., 2000; Ratzliff et al., 2002; Jinde et al., 2012; Scharfman, 2016; Bui et al., 2018; Botterill et al., 2019). MCs are also potentially important in the response to traumatic brain injury, where they are highly vulnerable (Santhakumar et al., 2000; Ratzliff et al., 2002; Grovola et al., 2020). MCs have also been implicated in schizophrenia (Wang et al., 2014; Yuan et al., 2015; Bauer et al., 2021) and depression (Oh et al., 2013; Oh et al., 2020). Despite their diverse roles, there are many questions about MCs and how they influence the primary cell type, glutamatergic granule cells (GCs). Although MCs are glutamatergic, and project primarily to GC dendrites (Amaral et al., 2007; Scharfman and Myers, 2012), they contact DG GABAergic neurons also, making it possible for MCs to excite or inhibit GCs.

Although MCs mostly contact GCs (Ribak et al., 1985; Buckmaster et al., 1996; Scharfman and Myers, 2012), DG GABAergic neurons innervate so many GCs (Amaral et al., 2007), that MC excitation of a small number of GABAergic neurons may lead to strong inhibition of GCs. Indeed, GC inhibition does appear to be a major role of MCs in vivo (Sloviter, 1994; Jinde et al., 2013; Senzai and Buzsaki, 2017; Bui et al., 2018).

The present study was undertaken to test several hypotheses why MC→GC excitation may be underestimated. First, we hypothesized that MC→GC excitation was robust, but it has often been missed in vivo, where the measurements are typically suprathreshold events, because MC→GC excitation does not usually reach threshold. That would make studies which only look at GC firing easy to underestimate MC→GC excitation. Second, the excitation of GCs may be able to modulate other inputs even when weak, but this might be easily missed because the timing that is required could be restricted. Third, MC→GC synapses might strengthen under several conditions, leading to greater excitation of GCs if conditions are used that are not standard. Fourth, a subset of GCs might be particularly affected by MC input, and their activation might be enough to have significant effects in their CA3 pyramidal cell targets even under normal conditions. But the subset may not usually be sampled because they are a minority of GCs.

To address these hypotheses, two mouse lines with Cre recombinase (Cre) in MCs were used with Cre-dependent adeno-associated viruses (AAVs). For experiments in vitro, a virus encoding the excitatory opsin channelrhodopsin (ChR2) was first injected in the hilus for recordings in hippocampal slices several weeks later, when ChR2-eYFP was expressed in the MC axons. Recordings were made of GC responses to optogenetic stimulation of the MC axons in the inner molecular layer (IML), where MC innervation of GCs is strong. For behavioral experiments, a different AAV was injected to allow chemogenetic activation of MCs during behavior. For in vivo calcium imaging of GCs in head-fixed mice, two viruses were injected, one that would express a red-shifted opsin in MCs and the other encoding GCaMP6s to image calcium fluctuations in GCs.

Calcium events were recorded as mice ran on a treadmill with and without MC optogenetic stimulation.

The in vitro results suggest that optogenetic activation of MCs leads to subthreshold excitation of GCs throughout the septotemporal extent of the DG, but the weak nature of excitation makes it easily missed. Similar results were found with extracellular, intracellular and patched GCs, both sexes, different survival times, ages, transgenic mice, and in different DG locations. Notably, excitation could facilitate the response of GCs to the entorhinal cortical input, the perforant path (PP), but it required precise timing, making it easy to overlook. We also show that several conditions can greatly strengthen MC→GC excitation: increasing the frequency of presynaptic (MC) stimuli, depolarizing postsynaptic GCs, activating GC NMDA receptors, and exposure to the muscarinic cholinergic agonist carbachol.

Moreover, we demonstrate that after trains of optogenetic stimuli or transiently lowering $[Mg^{2+}]_o$, MCs could trigger sharp wave-ripples in CA3 and this was GC-dependent. This result was complemented by chemogenetic activation of MCs during exploration of novel objects in the home cage; a task that has been shown to recruit MCs and a small number of GCs. When MCs were activated by chemogenetics during the task, CA3 c-Fos immunoreactivity (ir) was increased, compared to CA3 c-Fos-ir after the same behavior, but without MC activation. Interestingly, GC c-Fos was not elevated, suggesting few GCs were required for CA3 activity to increase. These data led to the idea that only a small subset of GCs may need to be activated by MCs for a significant effect to occur in CA3. The idea that MCs could activate a subset of GCs strongly was supported by optogenetic stimulation of MCs in vivo while recording calcium fluctuations of GCs. Upon optogenetic stimulation of MCs, a subset of GCs showed increased calcium event rates, especially in dorsal DG.

The characteristics of MC→GC excitation that were identified support DG functions such as pattern separation (Leutgeb et al., 2007; Myers and Scharfman, 2009; Yassa and Stark, 2011; Newman and Hasselmo, 2014; Knierim and Neunuebel, 2016). Thus, MCs would keep the GCs inhibited most of the time but there would also be opportunities for selective GC activation by MCs.

METHODS

All in vitro and chemogenetic experiments were conducted at the Nathan Kline Institute and approved (Protocol #AP-2001-678) by the Institutional Animal Care and Use Committee (IACUC) of The Nathan Kline Institute (NKI). All calcium imaging experiments were conducted at Columbia University and approved by the Columbia University and New York State Psychiatric Institute IACUC (#1651).

I. Animals and genotyping

A. In vitro optogenetics and chemogenetics

Adult mice (male and female) were used. Two mouse lines were used that had Cre recombinase (Cre) expression in MCs. One mouse line expressed Cre in cells that have the dopamine receptor type 2 (Drd2), which, in the DG, are primarily localized to MCs (Gangarossa et al., 2012; Puighermanal et al., 2015). It has been reported that some GABAergic neurons express Cre in the mice (Puighermanal et al., 2015; Azevedo et al., 2019), so another mouse line with Cre in cells that have the calcitonin receptor-like

receptor (Crlr; Jinde et al., 2012) was also used. The *Drd2*-Cre mice and *Crlr*-Cre mice were graciously provided by Drs. E. Valjent and Dr. K. Nakamura respectively. Hemizygous *Drd2*-Cre males were bred to C57BL/6NCrl females (#027, Charles River Laboratories). Hemizygous *Crlr*-Cre males were bred in-house to C57BL/6J female mice (#000664, Jackson Laboratories). Hemizygous *Drd2*-Cre or *Crlr*-Cre offspring were used for experiments except for in vivo calcium imaging which only used *Drd2*-Cre mice. In a subset of experiments, mice with Cre in proopiomelanocortin (POMC)-expressing cells (*POMC*-Cre mice) mice (kindly provided by Dr. Rene Hen) were bred with a ChR2 reporter line (Ai32(RCL-ChR2(H134R)/eYFP; #012569, Jackson Laboratories). Hemizygous mice were used.

Mice were bred in-house. At NKI, breeders were provided a nestlet (2"x2"; W.F. Fisher) and fed Purina 5008 chow (W.F. Fisher). After weaning at 25-30 days of age, mice were housed with others of the same sex (2-4/cage) and fed Purina 5001 chow (W.F. Fisher) and water *ad libitum*. They were housed in standard mouse cages with a 12 hr light:dark cycle and relative humidity between 64-78%. Breeding and housing were similar at Columbia University. For slice electrophysiology, mice were housed overnight in the laboratory (2-4/cage) prior to experiments because non-acclimatized animals exhibit poor DG and CA3 synaptic responses in hippocampal slices (Fig. 6 of 25058745). Tail samples were frozen and genotyped later (either in-house or by the Mouse Genotyping Core, New York University Medical Center).

II. Viruses

A. Viral expression for optogenetics in vitro

The viruses used for optogenetics in slices were adeno-associated virus (AAV) serotype 2(AAV2)-Ef1a-DIO-hChR2(H134R)-eYFP or AAV5-Ef1a-DIO-hChR2(H134R)-eYFP to express humanized ChR2 tagged with eYFP in Cre-expressing cells. Viruses were obtained from the Karl Deisseroth laboratory or the University of North Carolina (UNC) Vector Core. Titers were ~10^{12} vector genomes (vg) per ml. Aliquots of 5 µl of each virus were stored at -80°C until the day of use.

B. Viruses for chemogenetics

The virus that was used to express hM3D(Gq), an excitatory designer drug acting exclusively on designer receptors (eDREADDs) in MCs was AAV2-hSyn-DIO-hM3D(Gq)-mCherry (#44361, Addgene). Controls were injected with AAV5-EF1a-DIO-mCherry (UNC Vector Core). Titers and storage were the same as above.

C. Viruses for calcium imaging

A Cre-inducible AAV encoding a red-shifted excitatory opsin (bReaches, AAV2-hSyn-FLEX-bReaches-tdTomato, custom-synthesized) was used for experiments in dorsal DG. For ventral DG, bReaches was no longer available so AAV2-hSyn-FLEX-ChRimson-tdTomato (UNC Vector Core) was used. In addition, an AAV encoding the calcium indicator GCaMP6s (AAV2-hSyn-GCaMP6s; Addgene) was injected.

D. Surgical injection of viruses

1) ChR2

Animals (6-8 weeks old) were anesthetized with 4% inhaled isoflurane (Aerrane; Piramal Enterprises) in an induction chamber (#V711801; SurgiVet), then transferred to a rodent stereotaxic apparatus (#502063; World Precision Instruments; WPI). Body temperature was maintained at 37°C with a homeothermic heating pad (#507220F; Harvard Apparatus) for the duration of surgery. Isoflurane (1-2%) mixed with oxygen was delivered through a nose cone (WPI). Buprenex® (buprenorphine; 0.1 mg/kg, subcutaneous; Reckitt-Benkiser Pharmaceuticals) was administered shortly after the onset of anesthesia to reduce discomfort. The skin of the head was shaved, sterilized with Betadine (Purdue Products) and 70% ethanol (100% ethanol from Pharmaco-Aaper, diluted in double-distilled H_2O or ddH_2O), and then an incision was made. A hand drill (#177001; Dremel Instruments) was used to create a craniotomy above the injection site. Using a nanoliter-precision automated syringe pump (#UMP3; WPI) with a syringe (#Nanofil; WPI) and 33-gauge needle (#INanofil-10F; WPI), 150 nL of virus was injected into hippocampus at 100 nL/min. For extracellular and sharp intracellular recordings there was one injection site, either the left dorsal or left ventral hippocampus (Table 1). For whole-cell recording, the same injection sites were used or there were 2-3 sites in one hemisphere and slices were used from the contralateral DG (Table 1). The needle was left at the injection depth for 5 min to allow diffusion of the virus before being slowly retracted. The incision was closed with Vetbond (3M Inc.). Animals were transferred to a clean cage at the end of the surgery and placed on a heating blanket (37 °C) until they recovered from anesthesia. They were housed alone until use.

2) Chemogenetics

Methods were the same as for ChR2 except for the following: a different drill (Model C300, Grobert) was used to make craniotomies and they were made bilaterally over the rostral (-2 mm anterior-posterior, ±1.2 mm medial-lateral) and caudal hippocampus (-3.2 mm anterior-posterior, ± 2.3 mm medial-lateral), relative to Bregma. A 500 nL Neuros Syringe (#65457-02, Hamilton) attached to the stereotaxic apparatus was positioned over each craniotomy and lowered 2.0 mm (for rostral injections) or 2.6 mm (for caudal injections) below the skull surface. Each of the four injection sites was injected with 160 nL of virus at 80 nl/minute.

3) Calcium imaging

For dorsal injection, a total volume of 400nL of AAV (200 nL/virus, mixed 1:1) was injected slowly over the course of 5 minutes into the target location (AP:-2.0, ML:-1.2, DV:-2.0 from Bregma), using a microinjector (Drummond Inc.). For ventral injection, 200 nL of virus to express GCaMP6s was injected dorsally and 400 nL of the virus to express the red-shifted opsin was injected ventrally. The 400 nL was composed of 200 nL virus and 200 nL artificial cerebrospinal fluid (ACSF, composition described below in Section VA1).

III. Evaluation of expression

A. Perfusion-fixation

Animals were deeply anesthetized with isoflurane (by inhalation in a closed glass jar) followed by urethane (2.5 g/kg, intraperitoneal or i.p.). The abdominal cavity was opened and the animal was transcardially perfused with ~10 ml 0.9% NaCl in ddH_2O

followed by 20 mL 4% paraformaldehyde (#158127; Millipore Sigma) in 0.1M phosphate buffer (PB; pH 7.4), using a 25-gauge butterfly needle attached to a peristaltic pump (#Minipuls 2; Rainin). Brains were removed and postfixed overnight at 4°C and then cut into 50 µm coronal sections using a vibratome (#TPI1000; Ted Pella, or VT1000P; Leica). Sections were collected in cryoprotectant (25% glycerol, 30% ethylene glycol, 45% 0.1M PB) and stored at 4°C. For eDREADDs, the same procedures were used but the brains were hemisected before post-fixation. One hemisphere was cut coronally and the other horizontally.

B. Immunofluorescence

Free-floating sections were washed in 0.1M PB (3 x 5 min each) and transferred to blocking serum. Blocking sera were 10% normal donkey serum (#017-000-121; Jackson ImmunoResearch) for parvalbumin (PV) or 10% normal goat serum (#S-1000; Vector) for GluR2/3 and neuropeptide Y (NPY). Blocking sera included 0.25% Triton-X 100 (#11332481001; Millipore Sigma) diluted in 0.1M PB, and sections were incubated for 1 hour. Sections were then transferred to primary antibody solution (in 0.25% Triton X-100 diluted in 0.1M PB). For primary antibody, a mouse monoclonal antibody to PV (1:500; #MAB1572; Millipore), rabbit polyclonal antibody to GluR2/3 (1:100; #AB1506; Millipore) or a rabbit polyclonal antibody to NPY (1:1000; #T-4070; Peninsula) was used. Sections were gently agitated on a rotator overnight at 4°C. The next day, sections were washed in 0.1M PB (3 x 5 min each) and then incubated with secondary antibody (AlexaFluor 546 donkey anti-mouse for PV, goat anti-rabbit for GluR2/3 or NPY, both 1:400, Thermo Fisher). Secondary antibody was dissolved in 1% normal donkey serum for PV or 1% normal goat serum for GluR2/3 or NPY, and 0.25% Triton-X 100, diluted in 0.1M PB. After washing in 0.1M PB (3 x 5 min each), sections were mounted and allowed to dry at room temperature overnight. Slides were coverslipped using ProLong Gold antifade solution (Thermo Fisher) and stored at 4°C.

Stained sections were imaged on a laser scanning confocal microscope (#LSM 510; Zeiss). Double fluorescent labeling was quantified using LSM ImageBrowser software (Zeiss). Double labeling was determined by acquiring z-stack images at 1.5-2.0 µm intervals of a cell and locating the brightest optical section of the cell for each color channel.

C. Immunohistochemistry for analysis of c-Fos

C-Fos was analyzed after injection of the DREADD activator clozapine-N-oxide (10 mg/kg, s.c.) as described previously (Botterill et al., 2021b). Sixty min after CNO injection, novel objects were explored in the home cage. This task, called Home Cage Novel Object Exploration (HCNOE), was chosen because we had found that it increases c-Fos protein in MCs (Bernstein et al., 2019).

The task was performed as follows. For acclimation, the home cage was placed in the behavioral testing room for 5 min. Then mice were returned to their home cage. The next day, the home cage was brought to the behavioral testing room. Two identical novel objects [(Legos: 3 cm x 4.5 cm x 5 cm, shown in (Chartampila et al., 2023)] were placed in the home cage, spaced approximately 15 cm apart and 5 cm from the cage walls. Mice were allowed to explore the objects. The percent of time spent exploring objects was calculated for the first 4 min. The amount of time (sec) mice spent exploring

was divided by the total time (240 sec or 4 min). Exploration of an object was defined as having the nose pointed towards the object for >1 sec. Mice were perfusion-fixed 90 min after the task to allow sufficient time for c-Fos to be expressed.

Brains were hemisected and 50 μm-thick sections were cut in the coronal or horizontal plane (Vibratome 3000; Ted Pella). Coronal sections were used to evaluate dorsal DG because the coronal plane maintains the dorsal DG lamination well. For the ventral DG, where the DG lamination is hard to interpret in the coronal plane, horizontal sections were used. Sections were 600 μm apart. At least 3 sections 300 μm apart were used for dorsal and at least 3 for ventral measurements. Mean values for the 3 sections were used to give a dorsal value and a ventral value for every mouse.

Sections were rinsed in 0.1M Tris buffer (TB; 3 x 5 min) followed by 1% H_2O_2 in 0.1M TB for 5 min. Sections were washed in Tris A (0.1M TB in 0.25% Triton-X 100) and Tris B (Tris A and 1% bovine serum albumin; Millipore Sigma) for 10 min each and then incubated for 30 min in 5% normal goat serum diluted in Tris B (blocking solution). The sections were then incubated overnight at 4°C in an antibody to c-Fos (rabbit polyclonal, 1:2000; #226003, Synaptic Systems) diluted in blocking solution. This antibody has been shown to be highly specific for c-Fos protein (Zhou et al., 2019; Kim and Cho, 2020). On the following day, sections were rinsed in 0.1M TB (3 x 5 min) and incubated in biotinylated goat anti-rabbit secondary antibody (1:500, Vector) diluted in Tris B for 2 hours. The sections were then rinsed in 0.1M TB (2 x 5 min) and incubated in avidin-biotin complex (1:500, #PK-6100 Elite kit, Vector) for 1 hour. Sections were transferred to a solution containing 0.5 mg/ml 3,3'-diaminobenzidine tetrahydrochloride (#D12384; Millipore Sigma), 40 μg/ml ammonium chloride (#213330; Millipore Sigma), 25 mg/ml (D+)-glucose (#G5767; Millipore Sigma), and 3 μg/ml glucose oxidase (#G7141; Millipore Sigma) in 0.1M TB. The reaction was terminated by washing sections in 0.1M TB (3 x 5 min). Sections were mounted on gelatin-coated slides and when c-Fos immunoreactivity was black in some cells but background was still pale. To make the sections from different animals comparable, mice from each group were processed together, which is an approach we previously validated (Bernstein et al., 2019).

Sections were dried overnight at room temperature. On the following day, the sections were dehydrated using a graded series of ethanol solutions (70%, 95%, 100%, 10 min each), cleared in Xylene (~10 min; Fisher Scientific), and coverslipped with Permount (Electron Microscopy Sciences). Photomicrographs used a brightfield microscope (Model BX51, Olympus) with a CCD camera (Retiga 2000R, QImaging).

C-Fos-ir cells were counted manually at 16x using criteria previously reported by our laboratory (Duffy et al., 2013; Moretto et al., 2017; Bernstein et al., 2019). Immunoreactive cells were counted at similar locations across the septotemporal axis using landmarks in the extrahippocampal part of each section (Moretto et al., 2017; Botterill et al., 2021a; Botterill et al., 2021b).

V. In vitro electrophysiology

A. Field recordings and sharp intracellular recordings

1) Slice preparation

Mice were rapidly anesthetized with isoflurane by inhalation in a covered glass jar. While deeply anesthetized, mice were decapitated, the brain was rapidly dissected and

placed in a 4-8°C ACSF with sucrose instead of NaCl (in mM: 252 sucrose, 3.5 KCl, 2.0 $MgSO_4$-$7H_2O$, 2.4 $CaCl_2$, 1.25 NaH_2PO_4, 26 $NaHCO_3$, 10 D-glucose, pH 7.4). After 1-3 min, the brain was blocked to cut it transversely or horizontally. For transverse sections, slices were cut at an approximately 15° angle to the coronal plane so the dorsal hippocampus would be cut along the transverse axis. For horizontal sections, the dorsal surface of the brain was trimmed so it would lie flat when glued to the vibratome stage. Horizontal sections were cut and ventral sections that were approximately transverse to the long axis of the hippocampus were selected.

For all sections, the blocked brain was glued to a metal plate using cyanoacrylate. The metal plate was placed in a holding container filled with semi-frozen sucrose-based ACSF and cut (400 µm thick) using a vibratome (#Microm HM 650V, Richard-Alan Instruments). Sections containing hippocampus and adjacent regions were trimmed with a fine scissors (Fine Science Tools) and then placed in room temperature sucrose-based ACSF in a beaker with carbogen (5% CO_2/95% O_2) for 1-5 min. Slices were transferred to an interface-style recording chamber (made in-house; Scharfman 2001). Using this chamber, 2-3 septal and 2-3 temporal slices could fit in the inner compartment so recordings could be made of slices exposed to similar conditions. Slices were placed on a nylon mesh, ACSF entered from below, and ACSF was wicked over the mesh and to a distant exit port with Kimwipes®. This arrangement kept slices submerged up to their upper surfaces. Warmed (32°C) humidified air was vented over the surfaces. Slices were in the chamber for 30 min with sucrose-based ACSF at 1-2 mL/min (#Minpuls 2, Gilson) and then NaCl-based ACSF (125 mM NaCl instead of sucrose) was used. Recordings began at least 30 min after the switch from sucrose-based ACSF to NaCl-based ACSF and terminated approximately 6 hours later. Slices were removed and fixed by immersion in 4% paraformaldehyde in 0.1M Tris buffer.

Slices were screened for viability using field potential recordings of the response to an electrical stimulus to the PP while recording in the GC layer (GCL). For PP stimulation, a stimulating electrode was placed on the slice surface at the point along the hippocampal fissure just below the subiculum where the PP is a white fiber bundle as it enters the DG. Field recordings were made in the GCL at the border with the hilus, either near the crest, or near the center of the superior blade, approximately 250 µm from the stimulating electrode. To assess viability, the population spike was not used because the GCs do not generate many APs normally, so the population spike is normally small. The amplitude of the positivity, upon which the population spike is superimposed, was used instead, since past studies found that when the positivity is >3 mV and the population spike is small (<2 mV) GCs are recorded with characteristics of healthy GCs (Scharfman, 1991, 1994a; Scharfman et al., 2000; Scharfman et al., 2002).

2) Stimulating and recording electrodes

Monopolar electrodes used for stimulation were made from 35 µm-diameter Teflon-coated stainless-steel wire (A-M Systems Inc.) and triggered in pClamp (Molecular Devices) using 50 µA amplitude, 10-100 µsec duration square pulses, generated from a stimulus isolation unit (#Isoflex, AMPI Instruments).

Electrodes used for extracellular recording were 1-5 MΩ and filled with NaCl-based ACSF. Intracellular “sharp" electrodes were 60-90 MΩ and filled with filtered (0.2 µm polypropylene filters, Nalgene) 1 M potassium acetate in ddH_2O. Electrodes were pulled

from capillary-filled 1.2 mm outer diameter, 0.85 mm inner diameter borosilicate glass (WPI) using a horizontal puller (#P-87, Sutter Instruments). Signals were digitized at 10 kHz for field and 30 kHz for intracellular recordings (#Axoclamp2B and Digidata 1440A, Molecular Devices). For sharp intracellular recordings, the bridge was balanced whenever current was passed. Cells were not accepted unless their resting potentials were hyperpolarized to -60 mV, action potentials were >90 mV, and their input resistance at -60 mV was >70 MΩ.

3) Analysis

The latency to onset was measured from the end of the light pulse to the fEPSP onset. The fEPSP slope was the maximum slope of the rising phase. The amplitude was measured from the pre-stimulus baseline to the peak.

B. Whole-cell recording

1) Slice preparation

Mice were prepared as described above, but the sucrose ACSF contained (in mM): 90 sucrose, 80 NaCl, 2.5 KCl, 1.25 NaH_2PO_4, 25 $NaHCO_3$, 10 D-glucose, 4.5 $MgSO_4$-$7H_20$, and 0.5 $CaCl_2$. Only horizontal slices were cut and they were 350 µm thick instead of 400 µm. After slice preparation, slices were placed in a holding chamber (made in-house) in oxygenated (95% O_2, 5% CO_2) sucrose-based ACSF. The holding chamber was placed in a water bath (Poly Pro Water Bath; Revolutionary Science), and the temperature was increased incrementally to 35°C over 15-20 min and maintained at 35°C thereafter. After slices had been in the holding chamber for 45 min, slices were kept in sucrose-based ACSF at room temperature until use.

Slices were placed in a recording chamber (Model #RC-27LD; Warner Instruments), held down with a nylon mesh (Item #SS-4-500H; Warner), warmed to 32°C with an in-line heater (Item #SH-27B; Warner), and perfused at 6-7 mL/min by a peristaltic pump (#Masterflex C/L; Cole-Parmer) on an infrared differential interference microscope (#BX51WI; Olympus). Slices were perfused with NaCl-ACSF containing the same constituents as described above except 1) 130 mM NaCl was used instead of 126 mM for extracellular and sharp recordings, and 2) 2.5 mM KCl was used instead of 3.5 mM.

2) Recording electrodes

Recording electrodes were pulled from borosilicate glass (1.5 mm outer diameter and 0.86 mm inner diameter, Sutter Instruments) using a micropipette puller (#P-97; Sutter) with tip resistance between 5-10 MΩ. Internal solution was filtered (#0.02 µm, Whatman Anotop 10 syringe filter; Fisher) and contained (in mM): 130 potassium gluconate, 4 KCl, 2 NaCl, 10 4-(2-hydroxyethyl)-1-piperazine ethanesulfonic acid (HEPES), 0.2 ethylene glycol-bis(β-aminoethyl ether)-N,N,N′,N′-tetraacetic acid (EGTA), 4 adenosine triphosphate magnesium salt, 0.3 guanosine triphosphate tris salt, 14 di-tris phosphocreatine, 0.2-0.5% biocytin, and was adjusted to pH 7.25 using 1M potassium hydroxide. Final osmolarity was 280-290 mOsm without biocytin. Aliquots were frozen (-20°C) and used within 6 months.

3) Analysis

Recordings were analyzed offline using Clampfit (v. 10.7 or 11.1; Molecular Devices). Resting membrane potential (RMP) was defined as the difference between the MP during recording (without current injection) and the extracellular potential after the recording. R_{in} (input resistance) was calculated from the slope of the voltage-current (V-I) relation based on steady state measurements of responses to current commands (5 pA steps, -45 pA to +45 pA) from RMP. Time constant (τ) was defined as the point when the MP reached 0.63% of the response at steady state. It was determined from the exponential fit to the onset of the response to a hyperpolarizing 5-10 pA step at RMP using Clampfit. Action potential (AP) amplitude was defined at RMP, using the AP elicited by a 500-1500 msec depolarizing current step that was approximately at threshold for AP generation. AP amplitude was measured from 1) RMP to the AP peak and 2) from the point during the depolarizing step that the rapid rising phase began. Threshold was defined in two ways because the use of this term varies in the literature. One definition was the MP where a spontaneous AP was triggered if cells were depolarized. Second, threshold MP was the MP where an AP was evoked in approximately 50% of trials using a depolarizing step. A three-point tangent slope vector was used in Clampfit to find the MP where the rapid rise of the AP stared (slope $\geq$ 10 V/sec). Half-width was defined as the time between AP onset (the time an AP initiated its rapid rising phase) to the time the AP reached half its amplitude. AP rising slope and decay slope were defined as the maximum slope of the rising and decay phases, respectively.

C. Optogenetics in vitro

A 200 µm-diameter fiber optic cable (#M86L01I; Thorlabs) was modified by removing the ferrule and rubber coating from the tip, stripping approximately 2 cm of covering (cladding), and polishing the bare fiber tip with fine emery cloth. The fiber tip was approximately 150 µm thick and threaded through a glass Pasteur pipette with the tip extruding approximately 2 cm. For field potentials and sharp intracellular recordings, the Pasteur pipette was held by a micromanipulator (#NMN-21; Narashige) so that it was approximately 3 cm from the slice surface. The glass holder was slanted 15-20° from vertical. For whole-cell recording, the light fiber was positioned 55° from vertical (35° from horizontal) using the micromanipulator. Blue light was generated by attaching the fiber to a 473 nm DPSS laser (#LRS-0473; Laserglow), after power was adjusted to 10 mW with a power meter (#PM100D; Thorlabs). Light pulses (typically <2 msec duration) were triggered 1/min or in pairs 10-200 msec apart (1 pair, every 1-2 min), or trains of 3-5 pulses at 5, 25 or 100 Hz (1 train/1-2 min).

VI. Chemogenetics

Three weeks after viral injection, mice were used for behavioral experiments. Results were published (Botterill et al., 2021b). After the last task, mice were perfused and c-Fos-ir was examined. Unpublished data are used in the present paper.

Behaviors were tested 1/week for 6 weeks. Each week CNO (10 mg/kg, s.c.). was injected and then behavior was tested for 1-3 hrs. Different behaviors were tested each week (Botterill et al., 2021b). On the 6th week, mice were injected again with CNO and 60 min later they were allowed to explore two objects in their home cage for 5 minutes.

This task, called Home Cage Novel Object Exploration (HCNOE), was chosen because we found it increases c-Fos in MCs (Bernstein et al., 2019). The task was performed as follows. Two identical novel objects (decribed above) were placed in the home cage, spaced approximately 15 cm apart and 5 cm from the cage walls. Mice were allowed to explore the objects for 5 min. Mice were perfusion-fixed 90 min after the task to allow sufficient time for c-Fos to be expressed. The brain was removed and post-fixed in 4% paraformaldehyde at 4°C for at least 1 day. Then coronal sections were made from one hemisphere and horizontal sections from the second hemisphere (50 µm thick). The dorsal coronal sections and ventral horizontal sections were used to assess dorsal and ventral DG, respectively (Moretto et al., 2017; Botterill et al., 2021a; Botterill et al., 2021b). Immunocytochemistry was conducted as described above using an antibody to c-Fos.

VII. Imaging GCs in head-fixed mice during MC optogenetic stimulation

A. Surgery

To image calcium fluctuations in large populations of GCs while optogenetically stimulating MCs, we injected two adeno-associated viruses (AAVs) into the hilus of 8-12 week-old *Drd2*-Cre mice. Mice were anesthetized with isoflurane, placed in a stereotaxic apparatus, and a hole was drilled in the skull above the dorsal DG. After viral injection, mice were allowed to recover for one week before implantation of a chronic imaging cannula over the injected region of the left DG. Isoflurane-anesthetized mice were injected with dexamethasone to prevent brain edema during surgery, placed in a stereotaxic apparatus, and a 2mm hole drilled above the DG. The brain tissue overlying the DG was aspirated and a 2mm imaging cannula was gently pressed into the hole to contact the dorsal surface of the DG molecular layer and cemented into the hole with dental arcylic. A stainless steel headpost was then cemented to the skull surrounding the implant and the animal was allowed to recover for at least one week before 2P imaging.

B. 2P imaging and optogenetic stimulation

After recovery from surgery, animals were habituated to head fixation on a 2m-long circular treadmill for increasing periods of time over two weeks, during which time 2P imaging was performed to assess expression of GCaMP6s in the dorsal GCL and red bReaches/ChRimson-tdTomato axons from MCs in the IML. Animals were used for experiments when both GCaMP6s fluorescence could be observed in the GCL, and red tdTomato-expressing MC axons were observed in the IML.

Imaging was performed on a Bruker Ultima II microscope with resonant-galvanometer scanners and GAsP photomultiplier tubes (Hammamatsu), with a tunable pulse laser tuned for 940nm excitation (Insight Deep-See, Spectra-Physics). Two-photon imaging was performed at 10 frames/sec (fps) with optogenetic stimulation via a red LED coupled to the beam path (620nm, 10mW). Optogenetic stimulation was triggered during the inter-frame intervals using a custom-made control circuit. Both optogenetic stimulation and 2P excitation light were focused on the DG through the objective lens (40x, 1.0NA, Nikon).

To image GC calcium fluctuations while optogenetically stimulating dorsal MCs, mice ran on the motorized treadmill for a minimum of 20 laps, during which optogenetic stimulation was triggered in a location at the center of the treadmill belt (at 700-1300cm

of the 2m-long track). These laps were interspersed with laps with no optogenetic stimulation using Arduino/Java-based behavioral software (Behavior Mate, kindly provided by Attila Losonczy, Columbia University). The position of the mouse was recorded and optogenetic stimulation triggered using Behavior Mate.

C. Data analysis

Movies of GCaMP fluorescence signals from the GCL were preprocessed and then motion corrected and segmented using the CaImAn Python package, which implements a sparse non-negative matrix factorization (CNMFe) to decompose patterns of pixel intensity values into single cell calcium signals (Pnevmatikakis et al., 2016; Giovannucci et al., 2019). Imaging sessions yielded 150-250 individual cells, whose activity was registered to the animal's position on the treadmill belt during laps with and without optogenetic stimulation. Calcium events in putative single cells were detected based on the slope of the rising phase of an event, and were included if the slope was >3x the SD of baseline noise. Spatial tuning of single-cell event rates was assessed by bootstrapping. Significantly tuned cells were defined as cells whose calcium event rates on laps with optogenetic stimulation exceeded 95% of shuffled rates (1000 shuffle iterations) either at the start of the lap ("Start" cells) or during optogenetic stimulation. Calcium event rates were compared between laps with and without optogenetic stimulation of MCs.

VIII. Pharmacology

The AMPA receptor antagonist cyanquixaline (6-cyano-7-nitroquinoxaline-2,3-dione; CNQX disodium salt; #1045; Tocris Biosciences) or 6,7-Dinitroquinoxaline-2,3(1H,4H)-dione (DNQX disodium salt; #2312/10; Tocris) was dissolved in 0.9% NaCl to make a 10 mM stock solution, stored at -20°C and defrosted on the day of the experiment. Stock solutions of the NMDA receptor antagonist DL-2-amino-5-phosphonovaleric acid (DL-APV; #5282; Millipore Sigma), $GABA_A$ receptor antagonist bicuculline methiodide (#14343; Millipore Sigma) and gabazine (#1262; Tocris) were prepared in a similar manner.

IX. Statistics

Results are expressed as means ± standard error of the mean (SEM). Power analysis was used to determine if sample size was adequate, for α=0.05 and 80% power (Statmate2; Graphpad). Sample size was assessed using each mouse as one data point. When there was more than one slice/mouse, the data from each slice was averaged to produce a single value for that animal.

Statistics were conducted using Prism (v. 9; GraphPad). Comparisons of two groups were made using Student's t-test (unpaired, two-tailed) and one- or two-way Analysis of Variance (ANOVA) or repeated measures ANOVA (RMANOVA) for more than two groups. For ANOVAs, post-hoc tests were conducted with corrections for multiple comparisons (Tukey-Kramer or Dunnett's) tests to assess statistical differences between groups.

Nonparametric tests were conducted when data were not normally distributed as defined by the Shapiro-Wilk test. For two groups, a Mann-Whitney *U* test was used for two groups and the Kruskal-Wallis test for more than two groups. If there was

heteroscedasticity of variance, determined by the Brown-Forsythe test, and it could not be resolved by log or reciprocal transformation of the data, non-parametric statistics were also employed. If heteroscedasticity could be resolved, statistics were conducted on the transformed data. However, graphs in the Figures show raw data.

RESULTS

I. MC→GC excitation is common but weak

A. MC→GC excitation can be detected by extracellular recording as fEPSPs

Extracellular recordings were made to test the hypothesis that MC excitation of GCs was so common that a fEPSP could be recorded in the IML. There were 26 animals injected with virus encoding ChR2 that were used for extracellular recordings (*Drd2*-Cre, n=18; *Crlr*-Cre, n=8; Fig. 1). They were 80.3 ± 7.6 days-old. Of the 26 mice, 19 received dorsal injections and the 7 others had ventral injections. All *Crlr*-Cre mice had dorsal injections because of decreased specificity for MCs in ventral levels (see below, Section 1D).

For fEPSPs, slices were made distal to the injection site to capture the location where MC projections to the IML dendrites of GCs are most robust (Buckmaster et al., 1996). Thus, slices ipsilateral to the injection site were >2 slice widths (>800 μm) from the injection site. Slices contralateral to the injection site were selected throughout the septotemporal axis.

Initial experiments using *Drd2*-Cre mice tested whether any subfield (DG, CA1, CA3) showed a field potential in response to light (1-6 slices /mouse, 6 mice). The one combination of optic fiber position and recording site that was successful used light directed at the IML with a recording position that was either in the GCL, or ML (Fig. 1A-B). The largest response was always in the IML.

The response was a field excitatory postsynaptic potential (fEPSP; Fig. 1A-B). Responses are called fEPSPs because they were graded like an EPSP, i.e., increasing the duration of the light pulse led to a graded increase in slope and amplitude (Fig. 1A). Interestingly, the fEPSP was not very large (typically < 3 mV), and a maximum was obtained after only a brief light pulse (typically <2 msec). After reaching the maximum, the fEPSP did not increase even with prolongation of the light pulse duration (Fig. 1A). The maximum fEPSP recorded in the IML was 1.78 ± 0.39 mV; n=19 slices, 16 mice. It appeared weak because population spikes were not elicited. However, recordings in the GCL showed units or a very small population spike at the peak of the fEPSP (see below, Fig. 2B2). These data suggested that possibly a small subset of GCs were activated, but most were not.

Consistent with the idea that fEPSPs are excitatory, and glutamate is the neurotransmitter of MCs (Soriano and Frotscher, 1994; Scharfman, 1995a), the AMPA receptor antagonist CNQX (10 μM) decreased the fEPSP (to 11.7±4.1% of control after 30 min, n=3 slices, 1 slice/mouse), but the $GABA_A$ receptor antagonist bicuculline methiodide did not (BMI; 10 μM; 99.5 ± 5.2% of control at 30 min, n=4 slices, 1 slice/mouse; Appendix Fig. 1). Characteristics of latency, slope and amplitude of fEPSPs are shown in Table 2.

These data suggest that MCs excite so many GCs that the response can be recorded extracellularly. However, the response is small and does not evoke a large population spike, suggesting excitation may be common but it is usually weak.

B. FEPSPs are monosynaptic

fEPSPs had a rapid onset, usually beginning at the end of the light pulse or shortly thereafter, consistent with MC→GC monosynaptic excitation (Fig. 1). To determine the mean latency to onset, responses were chosen that were between 50 and 100% of the maximum response. The latency from the end of the light pulse to the fEPSP onset was 0.69 ± 0.11 msec (n=42 slices, 16 mice). Light pulses were typically <2 msec long, so the latency from the start of the optogenetic pulse to the onset of the fEPSP was <3 msec. These data are consistent with monosynaptic excitation.

C. FEPSPs are specific for MC axons in the IML

As mentioned above, the fEPSP evoked by optogenetic stimulation was highly localized to the IML (Fig. 1B). In 18 slices from 12 mice, minor movements of the optic fiber from the IML towards the MML or the GCL decreased the fEPSP greatly (Fig. 1B). In contrast, movements of the optic fiber along the IML, even relatively far (>250 μm), had little effect on the fEPSP amplitude (<5% change in amplitude for a 250 μm change in optogenetic fiber location, n=12 slices in 6 mice; data not shown). The similarity of responses when the light fiber was moved parallel to the IML is consistent with responses that were due to activation of MC axons in the IML (Buckmaster et al., 1996; Wenzel et al., 1997; Amaral et al., 2007; Scharfman and Myers, 2012). Activation of IML axons was also demonstrated by a fiber volley before the fEPSP (10/34 fEPSPs were preceded by fiber volleys; Fig. 1C). None of these fEPSPs were preceded by fiber volleys when they were recorded in the MML or GCL, consistent with the lack of MC axons in those layers.

To confirm the responses to light were due to activation of MC axons, fEPSPs were tested for sensitivity to WIN 55,212 mesylate (WIN), a cannabinoid receptor type 1 (CB1) agonist which is expressed on MC terminals in the IML (Chiu and Castillo, 2008). Exposure to 5 μM (n=2 slices in 2 different mice) or 10 μM (n=1 slice in a 3rd mouse) WIN for 30 min reduced the slope and amplitude of the light-evoked fEPSP to 44.0 ± 4.9% of control (Fig. 1D). The fact that the fEPSP was not completely blocked may be due to the weak affinity of WIN for CB1 receptors on glutamatergic terminals relative to non-glutamatergic terminals (Hajos and Freund, 2002).

Current source density (CSD) analysis supported the idea that fEPSPs were generated by synapses in the IML (n=5 slices, 5 mice; Fig. 1E). The data for the CSDs were acquired by focusing the optic fiber on the IML and making sequential recordings at locations from the hilus to the hippocampal fissure (along a path oriented perpendicular to the GCL; Fig. 1E). Sequential recording sites were made at similar spatial increments. The results showed a current sink in the IML (n=3 slices, 1 slice/mouse; Fig. 1E1). In contrast, the response to electrical PP stimulation produced a current sink in the area of the OML or MML, where PP synapses are located (n=4 slices, 3 mice; Fig. 1E2).

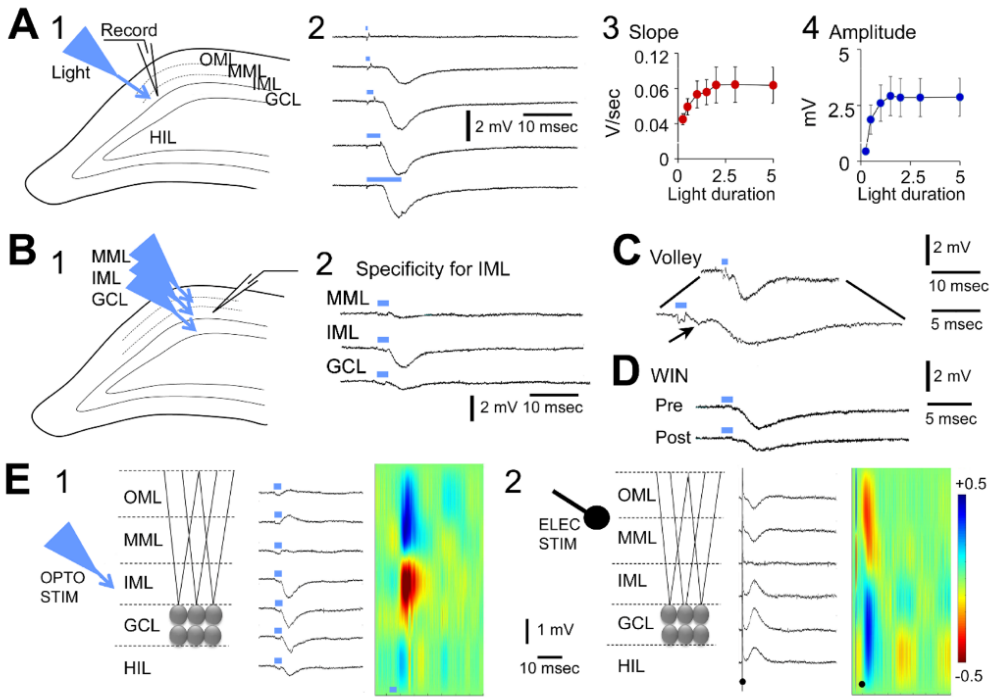

Figure 1. Optogenetic stimulation of MC axons in the IML evoke a fEPSP in GC proximal dendrites.

A. Either *Drd2*-Cre or *Crlr*-Cre mice were used after a single injection in either dorsal (*Drd2*-Cre, *Crlr*-Cre) or ventral (*Drd2*-Cre) DG. Field potentials evoked by light were recorded in the IML.
   1) Light was directed to the IML approximately 200 µm lateral to the recording electrode.
   2) Example of responses to increasing durations of light pulses (blue bars) showed a fEPSP was evoked, and there was a gradual increase in amplitude, consistent with a synaptic potential. Note that after reaching 2-3 mV, a maximum was reached, so that prolonging the pulse further did not increase the fEPSP.
   3-4) FEPSP slope and amplitude are plotted for slices tested with the same light pulse durations (n=11 slices, 1 slice/mouse).

B. FEPSPs were specific to the IML.
   1) The recording electrodes was in the IML while the light fiber was moved from the GCL to the IML and then to the MML, perpendicular to the GCL. The light pulse duration was the same for all recordings.
   2) The fEPSP was maximal when the fiber optic was pointed at the IML, suggesting MC axons were responsible for fEPSPs.

C. Example of a fEPSP recorded in the IML that was preceded by a fiber volley (arrow). The volley was not elicited by light directed at the GCL or MML (not shown). The same trace is shown at two different timescales. The data suggest that the optogenetic stimulus activated MC axons

D. WIN 55,212, an antagonist of MC synapses (Chiu and Castillo, 2008), reduced the fEPSP evoked by IML optogenetic stimulation, consistent with a MC→GC pathway.

E. 1) Left: A diagram shows the layers of the DG where recordings were made in response to optogenetic stimulation of the IML.
   Center: Responses elicited by a fixed light stimulus were recorded in many layers sequentially.
   Right: Current source density (CSD) analysis showed a current sink (red) in the IML, consistent with activation of MC axons.

2) CSD analysis of responses to electrical stimulation of PP axons in the OML and MML. A weak stimulus was used so the CSD only reflected a subthreshold fEPSP. The site of the stimulating electrode is indicated by a black circle with the ball representing the monopolar stimulating electrode tip on the slice, on the border of the OML and MML. The CSD showed a current sink in the OML (red). The recordings in 1 and 2 are from the same slice. They were replicated in 5 slices (5 mice).

Intracellular recordings of GCs showed small depolarizations in response to the same optogenetic stimulus that elicited a fEPSP in the IML (32/34 or 94.1% of GCs recorded at RMP, 5 slices, 1 slice/mouse; Fig. 2A). These data suggest that almost all GCs have a subthreshold depolarizing response to light. The two exceptional GCs had no detectable effects of light, suggesting that some GCs lack input from MCs, which is important if true because thus far it has not been suggested that any GCs lack MC input. However, we cannot rule out that these GCs lacked input from MC axons that expressed ChR2, or expression of ChR2 was insufficient in the MC axons that innervated these GCs.

The onsets of the light-evoked depolarizations in GCs were rapid (<2 msec; Fig. 2A), consistent with the fEPSPs and a monosynaptic MC→GC pathway. None of these GCs had a suprathreshold response to light at the RMP, which is consistent with the small size of most fEPSPs (Fig. 1). However, an AP was elicited at the peak of the EPSP when GCs were depolarized to -50 to -60 mV (n=12/12 cells tested; Fig. 2A1-2) and a small population spike or units were recorded on the fEPSP peak in GCL recordings (Fig 2B), suggesting that a subset of GCs may have been excited over threshold. The idea that a subpopulation of GCs may be excited more than others is supported from in vivo data presented below (Fig. 9, 10C).

These data suggest the fEPSPs and depolarizations were excitatory but weak. These interpretations were supported by moving the recording electrode to CA3 while keeping the optic fiber in the same location. There was no field potential elicited by the optogenetic stimulation either in stratum lucidum or the PCL (Figure 2B).

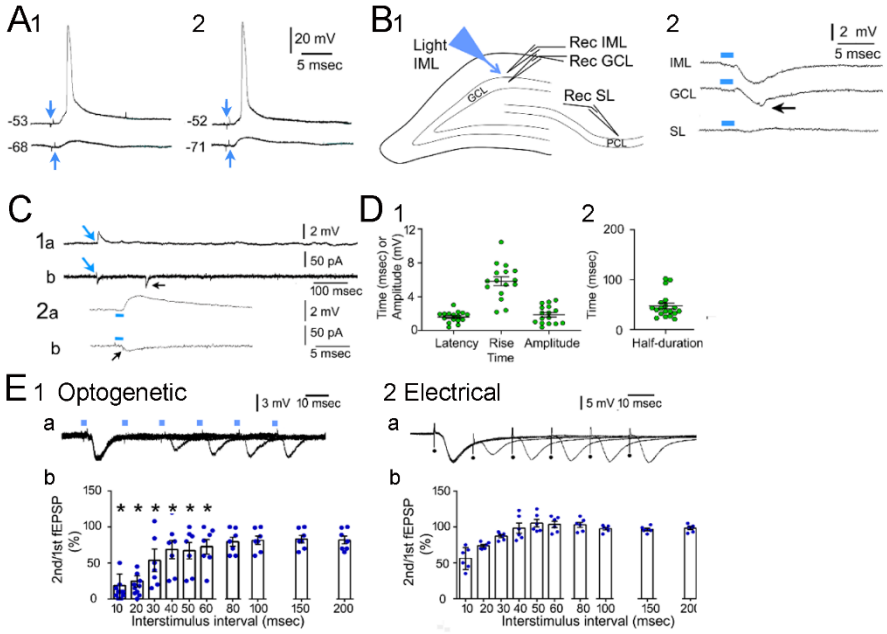

Figure 2. Excitation of GCs by optogenetic activation of MC axons is weak and shows little paired pulse facilitation.

A. 1-2) Intracellular sharp electrode recordings from two different GCs show the - responses to a 1 msec-long light pulse directed to the IML, ~200 µm from the recorded cell. At RMP (-68 or -71 mV in each cell, respectively),

a small depolarization was evoked. After depolarizing the cells (to -53 or -52 mV, respectively), the optogenetic stimulus evoked an AP. These data reflect weak excitation by a more sensitive recording method than extracellular recordings used in Fig. 1.

B. MC→GC excitation is insufficient to activate CA3.

1) The experimental arrangement is illustrated.

2) Top: Recordings were made in the IML in response to an optogenetic stimulus.

Center: Recording in the GCL of the response to the optogenetic stimulus. An arrow points to an extremely small population spike after the peak of the fEPSP reflecting GC firing was weak in response to MC input.

Bottom: The same optogenetic stimulus did not evoke a detectable response in stratum lucidum (SL) of CA3, suggesting that the optogenetic response was too weak to activate GC mossy fiber synapses on PCs.

C. Whole-cell recording of GCs in response to IML optogenetic stimulation.

1) a. A current clamp recording shows a small EPSP. b. The recording in voltage clamp from the same cell shows a small EPSC in response to the same optogenetic stimulus. Later in the recording is an example of a spontaneous EPSC (black arrow).

2) The EPSP/C is shown at higher gain (a, current clamp, b, voltage clamp). In 1a and 2a, the optogenetic stimulus is denoted by a vertical blue arrow. In 1b and 2b, the optogenetic stimulus is denoted by a blue bar. The arrow in 2b points to the artifact of the end of the light pulse, showing that the EPSC often had such a short latency that it began before the light pulse ended, similar to fEPSPs (Fig. 1A). These data corroborate intracellular sharp and extracellular recordings described above.

D. Characteristics of optogenetically-evoked EPSPs. The durations of the light pulses were chosen so that a response was elicited between 50% and 100% of the maximum at RMP. The membrane potential was -65 to -75 mV.

1-2) The latency to onset, rise time and amplitude are shown.

3) The half-durations are plotted.

E. 1) a. Optogenetically-evoked fEPSPs were triggered in pairs with increasing interstimulus intervals. Identical stimuli were used. Traces are superimposed.

b. Comparisons of paired-pulse responses in 6-7 slices from 7 mice. The ratios of the second fEPSP amplitudes to the first are plotted. There was weak facilitation.

2) a. Example of fEPSPs evoked by electrical stimulation (at the dots) of the IML also show weak stimulation.

Note that there was more paired-pulse inhibition at short interstimulus intervals (two-way ANOVA, effect of stimulation type (optogenetic vs. electrical; $F(1,16)=10.64$; $p=0.005$) and interstimulus interval ($F(9,144)=32.13$; $p<0.0001$) with an interaction ($F(9,144)=4.50$; $p<0.0001$). Optogenetic stimulation showed significantly more paired-pulse inhibition at 10-60 msec intervals relative to electrical stimulation (Tukey Kramer post-hoc tests; 10 msec interval, $p=0.037$; 20, $p=0.001$; 30, $p=0.002$; 40, $p=0.003$; 50, $p<0.001$; 60, $p=0.021$). The difference between optogenetic and electrical stimulation may have been technical because of the limit of the frequency ChR2 can be activated (Wang et al., 2007). Support is provided in Appendix Figure 6.

D. Blinding and controls

The experiments described above were conducted by an experimenter who did not know if there was robust expression of virus. Expression was assessed after recordings. In 28 slices (7 mice) there was no detectable fluorescence. In the experiments with those slices, there were no light responses. In contrast, when viral expression was detected, responses had been recorded.

Additional mice were used that lacked Cre recombinase (*Drd2*-Cre$^{-/-}$ mice) and did not have a viral injection. Experiments were blinded. No response to light could be detected (n=5 slices, 3 mice), even long pulse durations (up to 50 msec) with high power (up to 50 mW).

We also compared optogenetic stimulation of the IML to electrical stimulation of the IML (Appendix Fig. 2). To ensure the site of electrical stimulus activated the IML as selectively as possible, recordings were made in the MML and IML to confirm the fEPSP was much smaller in the MML than the IML. If it was larger, we assumed that the electrical stimulus activated the medial PP and did not use the slice.

When this procedure was followed, both electrical and optogenetic stimulation of the IML led to fEPSPs that did not evoke population spikes in the GCL (Appendix Fig. 2; 5 slices, 5 mice). In contrast, when the MML or OML was used as an electrical stimulation site in the same slices, population spikes were readily evoked by the PP stimulus. A comparison of IML and OML electrical stimulation is shown in Appendix Fig. 2. That data supported the idea that the MC input to GCs was weak regardless of the method (optogenetics or electrical stimulation) to stimulate MC axons.

Appendix Fig. 3 confirms for a dorsal injection that there was robust hilar expression dorsally and distal to the injection site there was robust IML expression ipsi- and contralaterally (Appendix Fig. 3A-C). Conversely, ventral MC labeling led to local and distant IML expression in the IML bilaterally (data not shown). This pattern of expression is consistent with the understanding that MCs project to the IML throughout the septotemporal axis bilaterally (Buckmaster et al., 1996; Scharfman and Myers, 2012). In addition, there was some expression of virus from dorsal AAV injection in the MML of caudal sections (Appendix Fig. 3C4-5), consistent with the reports that this occurs (Botterill et al., 2021a; Houser et al., 2021). One might wonder why we took care to examine expression given that several laboratories have used both the *Drd2*-Cre and *Crlr*-Cre mice. One reason is that prior studies have not described the contralateral projection of MCs well. We thought the contralateral expression might be restricted because the contralateral MC axon projection has been considered to be mainly homotopic (Scharfman and Myers, 2012). However, we found robust contralateral expression throughout the septotemporally axis (Appendix Fig. 3C3,C5). Therefore, we used slices from all septotemporal levels ipsi- and contralaterally.

Analyses of MC specificity in *Drd2*-Cre mice are provided in Appendix Fig. 4. Specificity is important because originally there were reports of GABAergic neurons that expressed Drd2 mRNA in *Drd2*-Cre mice (Gangarossa et al., 2012; Puighermanal et al., 2015) and later it was suggested after relatively large (500 nL) viral injections led to non-MC labelling in *Drd2*-Cre mice (Azevedo et al., 2019). Our smaller viral injections (150 nL) showed eYFP-expressing hilar somata expressed GluR2/3, a marker of MCs (Leranth et al., 1996) but not NPY or PV, markers of GABAergic neurons (Freund and Buzsaki, 1996; Houser, 2007; Hosp et al., 2014); Appendix Fig. 4).

Specificity in *Crlr*-Cre mice is addressed in Appendix Fig. 5. As reported before (Jinde et al., 2012; Botterill et al., 2021b) we found dorsal injections of virus led to specificity for MCs, but ventral injections led to MC and CA3 expression. This pattern of expression in CA3 is variable in the literature, sometimes not reported, and has never been shown to be functionally important in those studies where it is mentioned. Therefore, we conducted experiments to show that indeed it was sufficiently robust to

functionally affect CA3 pyramidal cells (PCs; Appendix Fig. 5). Therefore, *Crlr*-Cre mice were only used for dorsal injection of virus.

E. Whole cell recordings confirm MC→GC excitation is common but weak

Although the data suggested MC→GC excitation was common and weak, we wanted to ensure that this was the case with the higher resolution afforded by patching GCs. There were 57 whole-cell recordings of GCs in 31 mice. Most GCs (50/57 or 87.7%) had excitatory optogenetic responses when light was directed to the IML and a GC was recorded approximately 200 µm away. These 50 GCs were from 2-3 months-old mice (98.8 ± 2.9 days) at the time of recording. The majority of the 50 GCs were from *Drd2*-Cre (44 cells) and the others were *Crlr*-Cre mice (6 cells). The majority of the 50 GCs were from males (34 cells) and the rest of the GCs were from females (16 cells). A maximum of 3 cells were sampled per mouse.

1) EPSPs were common

Taken together, 87.7% of tested GCs had robust responses to light. Of the 50 cells with robust responses to light, all had depolarizations at RMP (Fig. 2C). In voltage clamp, EPSPs corresponded to small inward currents (Fig. 2C; n=3). Therefore, whole-cell recordings in current clamp agreed with the recordings in voltage clamp from the same cell.

2) EPSPs were monosynaptic, and had characteristics of small glutamatergic EPSPs

Quantification of EPSPs are shown in Fig. 2D. GCs were included that were stimulated with a light pulse duration that was between 50% and 100% of the maximal response. EPSPs were measured using optogenetic stimuli triggered when GC membrane potential was between -65 and -75 mV. Like the extracellular recordings described above, the average light duration for EPSPs was brief (1.50 ± 0.11 msec; range, 0.50-2.50; n=24 cells). Also like the prior results, the latency from the onset of the light pulse to the onset of the EPSP was consistent with a monosynaptic pathway (3.13 ± 0.12 msec, range, 2.40-4.10; n=16 cells). Measured from the end of the light pulse to the onset of the EPSP, the latency to onset of the EPSP was 1.62 ± 0.17 (range, 0.40-3.04; n=16 cells).

The rise time of the EPSP, measured from the EPSP onset to the EPSP peak, was 5.83 ± 0.54 msec (range, 2.20-10.45; n=16 cells; Fig. 2D). The latency to peak, measured from the end of the light pulse to the peak of the EPSP was 6.59 ± 0.57 msec (range, 3.87-12.40; n=16 cells; see Fig. 2D). The mean peak amplitude of EPSPs was small (1.89 ± 0.27 mV; range, 0.39 - 3.60 mV; n=16 cells; Fig. 2D). Mean half-duration was 45.93 ± 5.70 msec (range, 23.00-99.60; n=16), when measured from the EPSP onset to the point on the EPSP decay when the EPSP had declined to half its peak amplitude. When half-duration was measured from the end of the light pulse, the mean half-duration was 47.55 ± 5.74 msec (range 24.20-100.50, n=16; Fig. 2D).

3) GCs without optogenetic responses

The 7 GCs that lacked robust optogenetic responses deserve comment because they may have represented a special subset of GCs. These GCs had either no response or an inconsistent response that was a small depolarization (<0.3 mV). The

intrinsic properties of the cells with weak responses were not significantly different from other GCs (Table 3) suggesting they were not a unique subpopulation. They did not have characteristics of young adult-born cells, such as a relatively depolarized RMP and relatively high Rin (Overstreet et al., 2004; Schmidt-Hieber et al., 2004; Esposito et al., 2005; Ge et al., 2007); Table 3). There was no evidence that GABAergic neurons were sampled, because the patched cells did not exhibit the large, monophasic afterhyperpolarization (AHP), weak spike frequency adaptation or a brief half-width (Table 3) like DG GABAergic neurons (Scharfman, 1995b; Scharfman et al., 2000; Hosp et al., 2014). However, we cannot exclude the possibility that MCs avoid contact with some GCs.

F. Paired pulse facilitation was weak

Prior studies of the MC→GC synapse with different methods showed paired pulse facilitation (Hashimotodani et al., 2017), although less than the GC→CA3 PC synapse which is striking in facilitation (Salin et al., 1996). We used optogenetic stimuli with a common range of interstimulus intervals to test paired-pulse facilitation (10-200 msec; Fig. 2E1). Stimuli were half-maximal because weak stimuli can lead to an overestimation of facilitation and strong stimuli can underestimate facilitation. The second response of the pair was usually similar or smaller than the first (Fig. 2E1), suggesting weak facilitation at the MC→ GC synapse. Electrical stimulation of the IML led to the same conclusion (Fig. 2E2). Taken together, several studies suggest weak facilitation at the MC→GC synapse.

III. Effect of the MC→GC synapse on the entorhinal cortical input

Next we asked whether the MC→GC synapse could increase the PP input. The question is important because prior studies suggested that the selective activation of MCs only inhibits the PP Input. The investigators timed a prepulse of light to activate ChR2 prior to a PP stimulus (Hsu et al., 2015). However, the prepulse was before the PP stimulus. Figure 3A-D shows that when the optogenetic stimulus occurs at the time or up to 2 msec after the PP stimulus, there was facilitation of the PP-evoked population spike in 5/15 (33%) of the slices. Facilitation was small (mean, 11.34 ± 3.2%; Fig. 3B-D). When the prepulse was >2 msec before PP stimulus, inhibition of the population spike occurred in 15/15 (100%) of slices (mean, 69.3 ± 11.3%, 15 slices, 8 mice; Fig. 3B-D). If the prepulse was between 0 and 2 msec before the PP stimulus there was inhibition or facilitation of the population spike (Fig. 3B-D).

Intracellular recording provided an explanation for the results because there was only a narrow window of time for the light-evoked and PP-evoked EPSPs to summate maximally, i.e. to have their peaks align and therefore boost the PP-evoked EPSP significantly (Fig. 3E-G). The ideal timing was for MC optogenetic and PP electrical stimuli to be almost at the same time, like the field potential data. These data suggest a very specific temporal window when MCs can facilitate the PP-evoked GC population spike.

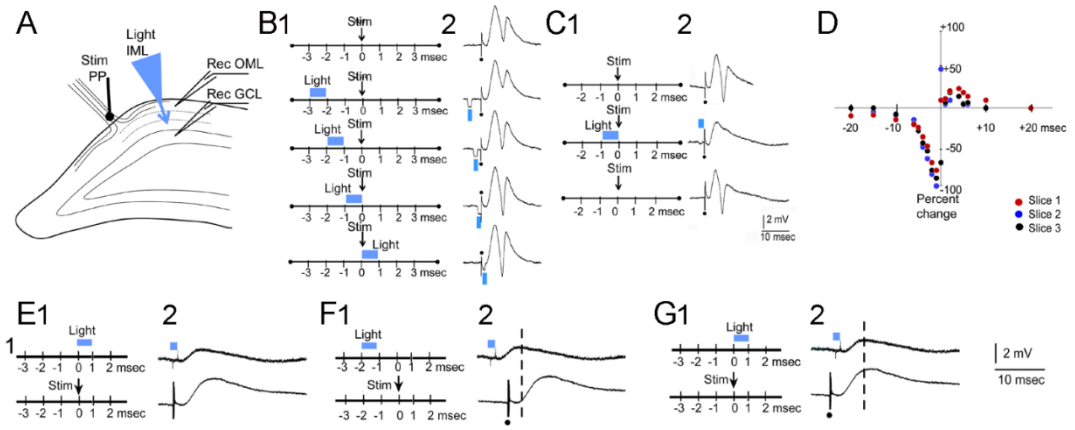

Figure 3. Optogenetic activation of MC axons evokes selective enhancement of the PP input to GCs.

A. A diagram of the experimental arrangement shows light was directed to the IML and extracellular recordings were made in the IML. Electrical stimulation was at the hippocampal fissure beneath the subiculum, on the white fiber bundle of the PP as it divides in the ML. Recordings were made in the GCL to monitor the population spike, and the OML to monitor the corresponding fEPSP. The OML recording sites were placed perpendicular to the GCL recording sites so the GCL and OML recordings monitored similar PP input. Recording sites in the ML were selected where the fEPSP was maximal, so the PP-evoked fEPSP would best reflect that input.

B. 1) The timeline for optogenetic (Light) and electrically-evoked stimuli (Stim).
   2) Optogenetic stimulation facilitated the population spike if the light pulse was triggered 0-1 msec before or after the PP stimulus. The optogenetic stimulus inhibited the population spike if it was triggered over 2 msec before the PP stimulus. Thus, there was a short temporal window for facilitation of the PP input.

C. 1-2) Data from a different slice shows that optogenetic stimulation could block the population spike completely. Note that for B-C, $[K^+]_o$ was elevated to 5 mM because with lower $[K^+]_o$, PP-evoked population spikes are so small that one cannot determine if they can be inhibited.

D. For 3 slices, the interval between the optogenetic stimulus and the PP stimulus is plotted on the X axis and the percent inhibition or facilitation of the population spike is plotted on the Y axis. Facilitation only occurred if the optogenetic stimulus occurred after the PP stimulus. These data are consistent with weak monosynaptic excitation and strong disynaptic inhibition of GCs by the optogenetic stimulus.

E. Optogenetic and PP-evoked EPSPs were compared in the same GC in 3 cells from 3 different mice.
   1) A schematic of the stimulation protocol.
   2) EPSPs evoked by light or PP electrical stimulation are shown.

F. 1) The optogenetic stimulus was triggered shortly before PP stimulation.
   2) The optogenetically-evoked and PP-evoked EPSPs are shown. Their peaks do not coincide (dotted line).

G. 1) Light was triggered shortly after PP stimulation.
   2) There was synchronization of the optogenetic- and PP stimulation evoked-EPSP peaks. The data suggest why facilitation of the population spike occurred when optogenetic stimuli were triggered within 1 msec of the PP stimulus: this timing allows the peaks of both EPSPs to summate.

IV. Conditions that strengthen MC→GC excitation

A. Frequency of MC firing

Although paired pulse facilitation was weak, facilitation could increase if more than two optogenetic stimuli were triggered (Fig. 4). When ISI was 40 msec (25 Hz), facilitation could occur (Fig. 4A-B). When the interval was 200 msec (5 Hz) some stimuli evoked facilitated EPSPs (Appendix Fig. 6). Therefore, increasing frequency from 0.05 to 5 and then to 25 Hz could increase GC EPSPs. Higher frequencies were not effective because ChR2 itself is unable to stimulate at 50-100Hz (Appendix Fig. 6; (Wang et al., 2007).

We hypothesized that during the 5 and 25 Hz stimulus trains the NMDA receptor component of the MC→GC EPSP increased because a 40 msec interval between 2 stimuli would time the second stimulus late in an EPSP, usually when there is an NMDA receptor-dependent phase. To address this hypothesis we unblocked NMDA receptors by reducing $[Mg^{2+}]_o$ from 1.5 to nominal 0 mM. We found that there was a dramatic increase in the MC→GC EPSP at RMP, even to a single stimulus (Fig. 4C-D).

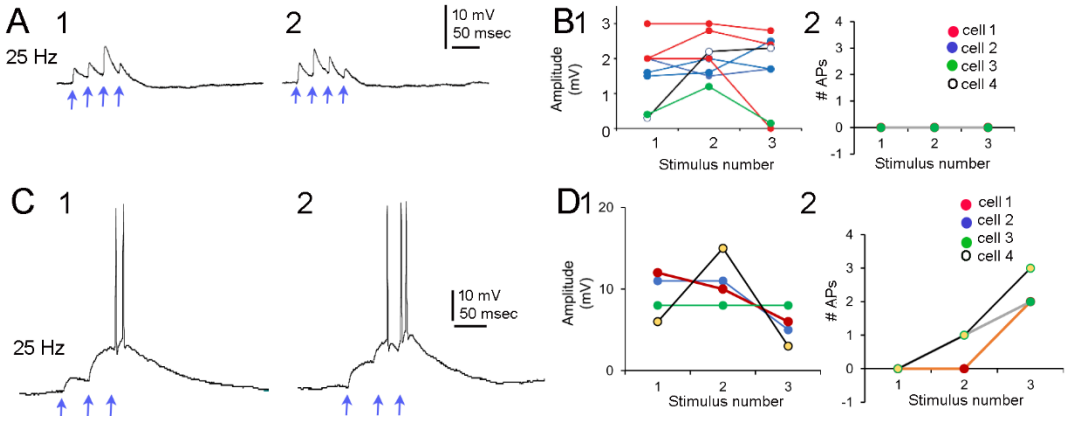

Figure 4. GC EPSPs evoked by optogenetic activation of MC axons are increased by trains of MC input and NMDA receptors.

A. 1-2) Trains of optogenetic stimuli were triggered at 25 Hz. Two examples are shown from the same GC. MC→GC EPSPs sometimes facilitated during the train.

B. 1) EPSP amplitudes during the first 3 stimuli of trains are plotted. Each color designates a different GC.
2) The number of APs evoked during the train are shown. No APs occurred. Therefore, facilitation of EPSPs could occur at 25 Hz, but not enough to reach threshold.

C. 1-2) The response of 2 different GCs to a 25 Hz train with 0 mM $[Mg^{2+}]_o$ to unblock NMDA receptors. Facilitation was greatly enhanced and reached threshold.

D. 1) Comparison of EPSP amplitudes shows large facilitation during trains.
2) Comparison of the number of APs. With 0 mM $[Mg^{2+}]_o$, APs were evoked.

Based on these data, indicating a strong and important NMDA receptor-mediated phase to optogenetically-evoked EPSPs, we further examined the NMDA receptor component. For these experiments, there were typically 2-3 viral injections in one hippocampus. Multiple injections were made to maximize viral expression. Slices were made contralaterally (Table 1). All mice were injected in the left hemisphere as follows: 3 mice received dorsal injections, 2 were ventral, and 6 had one injection that was in between (“mid”). Another 12 mice had 2 injections (either 1 mid and 1 ventral or 1 dorsal and 1 ventral) and the remaining 3 mice had 3 injections (1 dorsal, 1 mid, and 1 ventral).

Crlr-Cre mice were only injected once, in the dorsal DG, for reasons discussed above (Appendix Fig. 5).

Although small at RMP, EPSPs developed a large late phase if the GC was depolarized (Fig. 5A-B). The increase in duration at depolarized potentials was significant (one-way ANOVA; F(5,87)=3.33; p=0.005; Fig. 5C). In contrast to the late EPSP, the initial peak of the EPSP did not increase in amplitude with depolarization, consistent with its dependence on AMPA receptors (one-way ANOVA, F(5,87)=0.24; p=0.944; Fig. 5D). APs were rare during the initial peak of the EPSP, but common during the late EPSP (Fig. 5E). The early EPSP was blocked by DNQX (10 μM; n=3; Fig. 5A) and the late EPSP was reduced by the NMDA receptor antagonist DL-APV (50 μM; n=3; Fig. 5F), confirming it was mediated by NMDA receptors. The effect of APV was observed primarily at depolarized potentials, not hyperpolarized potentials (Fig. 5F), consistent with the observation of NMDA receptor-mediated EPSPs emerging at depolarized potentials. Thus, if GCs were depolarized, MC→GC excitation strengthened.

B. Depolarization increases GC input resistance and facilitates MC input at depolarized potentials

Figure 5G shows that input resistance (R_{in}) increases in GCs with depolarization, potentially making afferent input have a greater effect. An increase in GC R_{in} with depolarization was reported before using rats and sharp electrodes (Scharfman, 1994b) as well as rat cortical pyramidal neurons (Thomson and Deuchars, 1997) so it is not surprising. Here we asked if the same was true in *Drd2*-Cre and *Crlr*-Cre mice. R_{in} was tested in two ways. First, increasing current steps were triggered from RMP (Fig. 5G1). The responses to a step increment increased as steps depolarized the GCs more (Fig. 5G1). For example, a 30 pA step led to a voltage change far exceeding 3x the voltage change produced by a 10 pA step.

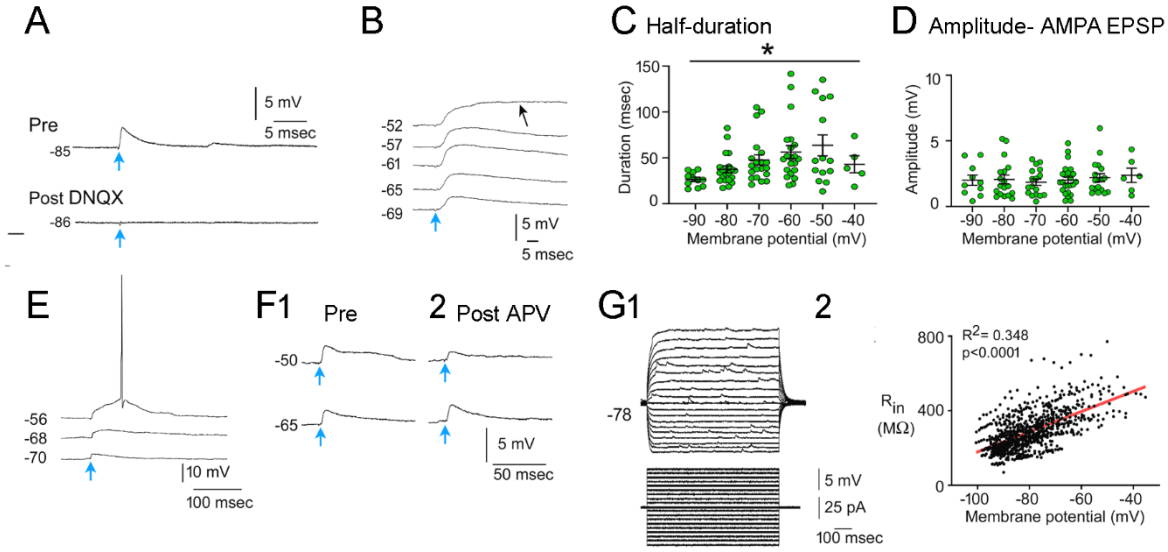

Figure 5. GC EPSPs evoked by optogenetic activation of MC axons increase when GCs are depolarized.

A. A representative example of an EPSP before (Pre) and after blockade by the AMPA receptor antagonist DNQX (10 μM; n=3 GCs, 3 mice) is shown.

B. An example of a response to optogenetic stimulation in a different GC illustrates the gradual emergence of a late EPSP at potentials depolarized to -60 mV (-52 mV, arrow).
C. A one-way ANOVA showed that there was a significant increase in half-duration of EPSPs with depolarization. Responses evoked within a 10 mV range of membrane potentials were pooled (e.g., -85 to -95 mV). The mean for each range of membrane potentials is plotted at the membrane potential corresponding to the middle of the range (e.g., -90 mV for the range between -85 and -95 mV).
D. A one-way ANOVA showed no significant effects of depolarization on the initial peak of the EPSPs. The data in 1 and 2 suggest there is an early EPSP and voltage-dependent late EPSP afterwards.
E. Example of a GC response to an optogenetic stimulus at 3 membrane potentials illustrating the emergence of a late EPSP as the cell was depolarized. An AP was triggered from late, rather than the early. Therefore, the late EPSP appeared to promote MC→GC excitation.
F. Late EPSPs could be blocked by the NMDA receptor antagonist DL-APV.
   1) A response to an optogenetic stimulus is shown at two membrane potentials before DL-APV (50 μM; Pre).
   2) The same stimuli were triggered after exposure to DL-APV (Post APV). The late phase of the EPSP, detected primarily at the more depolarized membrane potential (-50 mV, Top), was reduced by DL-APV. The early EPSP was the primary phase of the EPSP at hyperpolarized potentials (-65 mV, Bottom), and showed little effect of DL-APV. Note that the early EPSP was reduced by DL-APV at -50 mV (Top), suggesting that the late EPSP starts during the early EPSP.
G. 1) An example of a recording from a GC with responses to progressively increased current steps. The incremental changes in current were the same but the change in voltage response increased at depolarized potentials.
   2) R_{in} measured at RMP (n=48 GCs) showed a significant correlation of membrane potential and R_{in}, with R_{in} higher in GCs with more depolarized RMPs. Data in 1 and 2 suggest that GCs increase R_{in} at depolarizing potentials. A higher GC R_{in} at depolarized potentials is significant because it would increase effects of MC input.

R_{in} was also measured at RMP using a current step approximately 5 pA in amplitude. There was a significant correlation between RMP and R_{in}, with greater R_{in} in cells that had more depolarized RMPs (n=48 GCs, Fig. 5G2). In addition, we found that the slopes of the I-V curves for GCs changed at depolarized potentials, reflecting an increased R_{in} (not shown). These data indicate that there could be two factors that make GCs more likely to discharge at depolarized potentials if a MC input is active: NMDA receptors and increased GC R_{in}.

C. Carbachol

GCs and MCs receive cholinergic input, primarily from the basal forebrain cholinergic neurons such as those in the medial septum (Leranth and Frotscher, 1987). The actions of these afferents can be simulated by exposure to a muscarinic cholinergic agonist such as carbachol. Therefore, we asked if exposure to a cholinergic agonist would increase MC→GC EPSPs. Carbachol was added to the ACSF (1-5 μM, 9 cells, 3 mice; Fig. 6). GCs depolarized, but the depolarization was small. Less than -10 pA holding current was required to maintain GCs at their RMP (Fig. 6A).

We found a depolarization-activated inward current developed when cells were exposed to carbachol (Fig. 6B, current clamp; Fig. 6C, voltage clamp). The inward current reached >50 pA and was slow (Fig. 6B-D). In current clamp it developed during

depolarizing steps from RMP to -50 to -60 mV (Fig. 6B1). Small spontaneous synaptic potentials occurred during the inward current (Fig. 6B1).

Next, we triggered an optogenetic pulse early in the current step or at the end, when the inward current developed. An optogenetic response that was weak when it was triggered early in the step was greater if triggered later, and triggered an AP (Fig. 6B2). Thus, the MC→GC input increased in the presence of carbachol to the point that it reached threshold.

Fig. 6C shows the responses in voltage clamp of GCs that were held at -80 mV and depolarized to successively more depolarized potentials by voltage steps. As increasing concentrations of carbachol were applied, an increasing inward current developed. Fig. 6D shows measurements of the current, defined as the difference between the start and end of the step. RMANOVA showed that all concentrations of carbachol were significantly different from baseline ($F(3,6)=85.48$; $p < 0.0001$; Dunnett's post-hoc tests, baseline vs. 1 μM, $p=0.0056$; 2 μM, $p=0.0001$; 5 μM, $p=<0.0001$). Fig. 6E shows that there was a slow return to baseline after the step, consistent with a slow current.

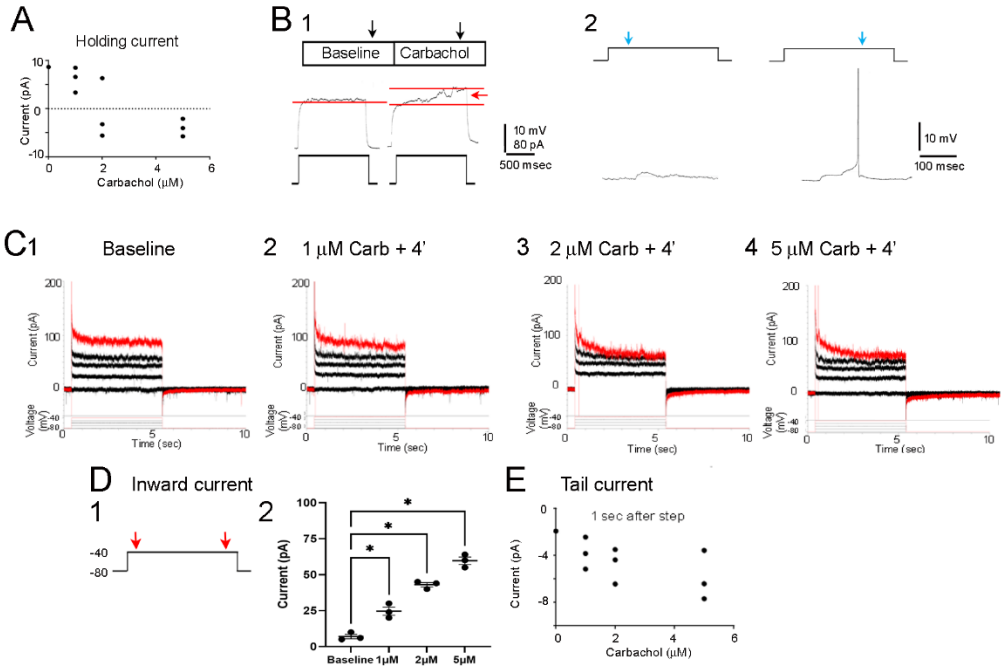

Figure 6. The muscarinic cholinergic agonist carbachol promotes MC→GC excitation.

A. Following the addition of carbachol to the ACSF, GC RMP hyperpolarized in response to the lowest dose (2-4 mV, 1 μM, n=3/3 cells in 3 mice). There was a mixed effect at the next highest dose (2 μM, 3 cells in 3 mice), and a consistent depolarization at 5 μM (2-3 mV, n=3/3 cells in 3 mice). The holding current is graphed, indicating decreased holding current after 1 μM, mixed effects after 2 μM, and increased holding current after 5 μM, respectively.

B. 1) Before carbachol exposure (Baseline), a step was triggered and it depolarized GCs. After carbachol, the step triggered a slow depolarization (red arrow).

2) Left. In the presence of 5 μM carbachol, an optogenetic stimulus during the start of the step (schematized at the top) led to a small EPSP (bottom).
Right. The same stimulus, triggered at the end of the step, evoked an AP. Therefore, MC→ GC excitation was increased after carbachol.

C. Current responses to a series of increasing voltage steps are shown in the baseline and after increasing concentration of carbachol. After carbachol, there was a slow inward current when the voltage steps were greatest (red traces).
1) Baseline; 2) 1 μM; 3) 2 μM; 4) 5 μM.

E. 1) The steady-state current for voltage commands from -80 mV to -40 mV was greatest for higher concentrations of carbachol.
2) The current remaining 1 sec after the end of the voltage step shows the slow kinetics of the inward current.

IV. CA3 activity evoked by MC→GC excitation

Because MC→GC excitation was weak but could strengthen, we tested the hypothesis that it could have significant effects under certain conditions. One reflection of strong effects would be activation of CA3 PCs. This might occur even if MCs caused relatively few GCs to reach threshold because each GC→PC synapse is powerful (von Kitzing et al., 1994; Henze et al., 2000). Also, a single PC can activate many other PCs because the PCs are strongly interconnected by recurrent collaterals (Miles and Wong, 1986). In fact, activating a single CA3 PC is sufficient to trigger a sharp wave-like event in CA3 (Miles and Wong, 1983).

We found that a single optogenetic stimulus to the IML did not trigger detectable activity in the PCL under control conditions (Fig. 7A-B; n=4 slices, 3 mice). However, after a 10 sec train of electrical stimuli (25 Hz) to the mossy fibers (Fig. 7B1), a single optogenetic stimulus triggered a CA3 sharp wave (Fig. 7B2-C). This result can potentially be explained by the ability of the train to potentiate the MC→GC synapse, and is consistent with prior studies in slices showing LTP of the MC→GC synapse (Hashimotodani et al., 2017) or DG commissural pathway (Hetherington et al., 1994; Namgung et al., 1997; Kleschevnikov and Routtenberg, 2003). The data are also consistent with the ability of a 10 sec, 25 Hz train to induce LTP of the GC→PC mossy fiber synapse (Harte-Hargrove et al., 2015).

Interestingly, the delay between the GC EPSP peak and CA3 SPW-R was more than a monosynaptic delay (>4 msec; Fig. 7B2-C). Therefore, polysynaptic circuits contributed. When we found a rare GC that discharged in response to the optogenetic stimulus, the delay from the GC AP peak to the onset of the SPW-R was also >4 msec (Fig. 7C1). One polysynaptic circuit that could explain these data is diagrammed in Fig. 7D. In the diagram, mossy fiber synapses trigger a subset of GCs to become active, the GCs activate CA3 PCs, and PC recurrent collaterals activate other PCs to ultimately produce a synchronized spike (a sharp wave) in a subset of PCs. To show that GCs are critical to this circuit, we added a selective antagonist of mossy fiber transmission to the ACSF (DCG-IV, 1 uM; Yoshino et al., 1996). The SPW-R was blocked but not the optogenetic activation of the GC (Fig. 7C2), consistent with a dependence of the SPW-R on mossy fibers.

If the interpretation was correct, activating more GCs by MCs would lead to activation of more PCs by mossy fibers, and less need to recruit additional PCs for a SPW-R to occur. The result would be CA3 SPW-R after a short delay from GC APs. Therefore we increased MC→GC activation by lowering $[Mg^{2+}]_o$ to 0 mM and depolarizing GCs with an increase in $[K^+]_o$ from 2.5 mM to 3.5 mM (n= 3 GCs, 3 mice; Fig. 7E). $[Mg^{2+}]_o$ was lowered only for a short time so that spontaneous activity did not occur in the slices. Afterwards, a single optogenetic pulse evoked a burst discharge in

the same GC (Fig. 7E1). A SPW-R occurred in area CA3 after the GC burst with a short delay between the first GC AP and the onset of the SPW-R (<4 msec) consistent with a monosynaptic pathway (Fig. 7E inset). Dependence of the SPW-R on the GC mossy fibers was confirmed by block of the SPW-R by DCG-IV (Fig. 7E2). These data suggest that when the GCs are activated strongly by the MCs, the mossy fibers are sufficient to trigger SPW-Rs without the requirement of polysynaptic circuits.

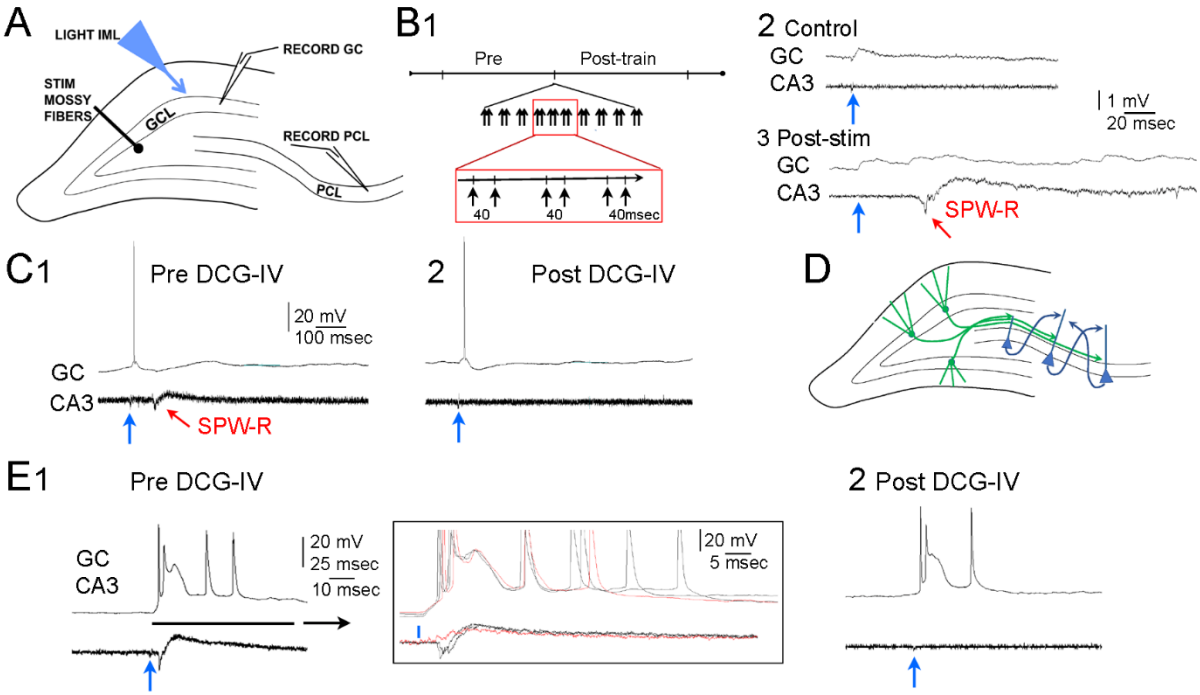

Figure 7. Conditional MC activation of CA3 SPW-Rs.

A. A schematic illustrates sites of recording and stimulation for B-E. A GC was patched and an extracellular recording was made in the PCL. The fiber optic was pointed at the IML, and the mossy fibers were stimulated electrically.

B. 1) A diagram of the stimulus trains used for mossy fiber stimulation.
2) Before trains of mossy fiber stimuli, a control response illustrates a typical small GC EPSP in response to optogenetic stimulation, and no detectable CA3 activity.
3) After a 10 sec train of paired pulses to the mossy fibers, the same optogenetic stimulus evoked a SPW-R (red arrow). Note the GC EPSP duration appeared to be longer, but this was not a consistent finding.

C. 1) A recording in a different GC after a 10 sec train. The optogenetic stimulation evoked an AP. A SPW-R occurred afterwards (red arrow).
2) After exposure to a selective antagonist of mossy fiber transmission, DCG-IV (1 μM), the SPW-R was blocked, suggesting SPW-Rs depended on mossy fibers. The GC response to the optogenetic stimulus was not affected, consistent with the specificity of DCG-IV for mossy fiber synapses.

D. A schematic illustrates how a GC could trigger mossy fiber-dependent SPW-Rs at a long latency. The diagram shows only a few GCs are activated above threshold by the MCs because MC→GC excitation is typically weak. After a small number of PCs were activated by the GCs, other PCs can be recruited by CA3 recurrent collaterals. After sufficient CA3 recruitment, a network event like a SPW-R could occur.

E. 1) Slices were treated to unblock NMDA receptors by reducing $[Mg^{2+}]_o$ to nominal 0 mM. No spontaneous bursts were detected in any cell layer (not shown). The optogenetic stimulus

was triggered, and it evoked a strong response in GCs, similar to an epileptiform burst discharge. The strong activation of GCs was followed by a SPW-R with a very short latency. The inset shows the latency was consistent with a monosynaptic pathway because the GC AP was immediately followed by the onset of the SPW-R.

2) The SPW-R was blocked by DCG-IV, suggesting it was dependent on mossy fibers. Together the data suggest that a train of MC stimuli can lead to sufficient GC excitation to trigger SPW-R in CA3.

These data suggested that MCs could drive CA3 PCs under some conditions. To confirm this effect in vivo we selective activated MCs with chemogenetics (DREADDs; Fig. 8). Adult *Drd2*-Cre$^{+/-}$ (Cre+) or *Cre*$^{-/-}$ (Cre-) control mice were injected with AAV encoding the excitatory DREADD (eDREADD) hM3D(Gq) in four sites (dorsal and ventral DG, bilaterally; Botterill et al., 2021b) in the DG to express eDREADDs in numerous MCs. After 3 weeks for expression to occur, mice were injected with clozapine-N-oxide (CNO; 10 mg/kg in saline, s.c.). After 60 min for CNO to reach a stable brain level, mice were exposed to two novel objects in their home cage for 5 min (Botterill et al., 2021b). Ninety min later the mice were perfused and sections were made to stain for the immediate early gene c-Fos, a marker of active neurons. The results showed that eDREADD activation in Cre+ mice increased the number of hilar c-Fos+ cells greatly, consistent with the ability of eDREADDs to activate MCs. CNO in Cre+ mice also increased CA3c c-Fos-ir (Fig. 9). However, GCL c-Fos-ir was not significantly altered (Fig. 8). Interestingly, dorsal CA3 c-Fos increased, but ventral CA3 did not (Fig. 8). In controls (Cre- mice injected with CNO) there was weak CA3 labeling by c-Fos (Fig. 8). Therefore, the behavior itself did not activate CA3 unless MCs were activated by eDREADDs at the same time. These data supported the hypothesis that MC activation could excite CA3 PCs. Moreover, GC firing, reflected by c-Fos-ir, did not need to increase significantly. Finally, dorsal MCs have these effects but not ventral MCs.

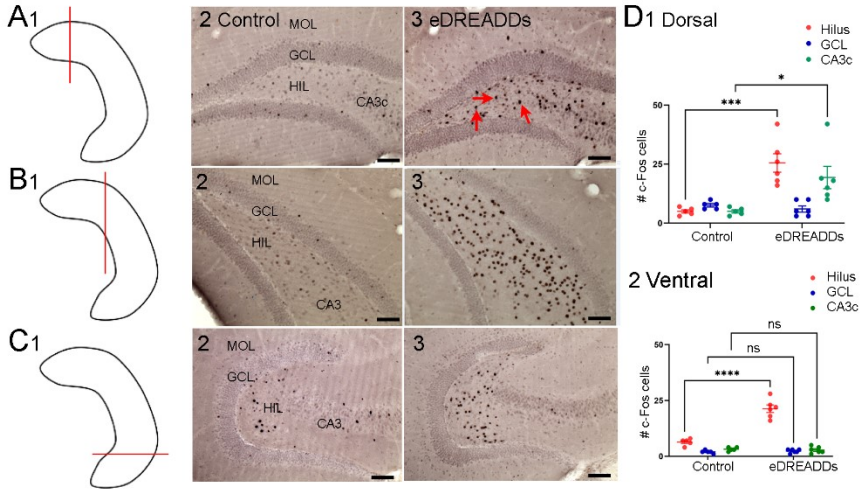

Figure 8. Activation of dorsal CA3 by MC optogenetic stimulation during novel object exploration.

A. 1) A diagram of one hippocampus shows the plane of section (coronal) used to assess dorsal DG.

2-3) CNO was injected in a *Drd2*-Cre$^{-/-}$ mouse (Cre-, control) and a *Drd2*-Cre$^{+/-}$ mouse (Cre+, eDREADDs). After 60 min, novel objects were placed in the home cage (home cage novel object exploration or HCNOE; (Bernstein et al., 2019; Botterill et al., 2021b). Ninety min later, mice were perfused. Sections were stained with an antibody to c-Fos. More hilar and CA3 cells expressed c-Fos (arrows) in Cre+ mice compared to Cre- mice. Calibration here and elsewhere in this Figure, 100 µm.

B. 1) A diagram shows the septotemporal level used for 2-3.
2-3) Similar results were obtained as A2-3.
C. 1) The section plane used to assess ventral DG.
2-3) Ventral CA3 showed little c-Fos after eDREADDs in Cre+ mice.
D. 1) A two-way ANOVA with genotype and subfield as factors showed a significant effect of genotype ($F(1,27)=22.26$; $p<0.001$) and subfield ($F(2,27)=4.42$; $p=0.021$) and an interaction ($F(2,27)=7.86$; $p=0.002$). Tukey-Kramer post-hoc tests showed differences for hilus ($p<0.001$), CA3 ($p=0.017$), but not GCL ($p=0.998$). Thus, eDREADDs activated MCs and CA3 but few GCs.
2) In ventral DG, there was a significant effect of genotype ($F(1,27)=47.18$; $p<0.001$) and subfield ($F(2,27)=108.5$; $p<0.001$) and an interaction ($F(2,27)=47.58$; $p<0.001$). Tukey-Kramer post-hoc tests showed differences for hilus ($p<0.001$), but not CA3 ($p=0.997$), nor GCL ($p=0.998$). Thus, eDREADDS activated ventral MCs but had no significant effects on ventral CA3.

V. Increased calcium fluctuations in GCs after optogenetic stimulation of MCs in vivo.

To examine MC activation of the GC population in vivo, we performed in vivo two-photon (2P) imaging of GC calcium activity with the genetically encoded calcium indicator GCaMP6s while optogenetically stimulating MCs with a red-shifted excitatory opsin (bReaches or ChRimson). The mice were head-fixed and ran on a treadmill with optogenetic stimulation at a specific position (see Methods).

By administering epochs of red LED light, triggered between imaging frames as mice ran on the treadmill, we were able to simultaneously stimulate MCs while imaging calcium responses in GCaMP6s-labeled cells in the GCL (Fig. 9A-C; Appendix Fig. 7). The GCL cells were likely to be GCs because the somata were ~10 μm in diameter, like GCs, and GCs are the majority of GCL neurons. Nevertheless, we acknowledge that these cells are “putative” GCs.

We compared calcium event rates in tuned GCs and all cells. Spatial tuning was defined by the laps with optogenetic stimulation. Those cells with increased event rates at the start or during optogenetic stimulation were defined as tuned.

Comparisons of cells were made with and without optogenetic stimulation. We found that a substantial fraction of tuned GCs exhibited increased event rates when dorsal MCs were optogenetically stimulated (Wilcoxon signed rank test, $p=0.00098$, $n=343$ cells from 11 sessions, from 5 mice; Fig. 9D). Notably, GCs excited by MC optogenetic stimulation composed a large portion of tuned GCs. However, MC-stimulated GCs represented a minority of all GCs ($p=0.32$, $n=2220$ cells from the same 11 sessions and 5 mice; Fig. 9E-F).

Similar results were found when the axons of ventral MCs were optogenetically stimulated and GCs were imaged in dorsal DG (Appendix Fig. 7). Thus, a subset of tuned cells increased their rate of calcium events when MC axons were optogenetically -stimulated (Appendix Fig. 7A) but this was not the case for all cells (Appendix Fig. 7B). However, the results for ventral tuned cells were less robust than dorsal tuned cells because there was only a trend in the ventral tuned cells to have higher calcium event rates during MC optogenetic stimulation compared to no stimulation (Wilcoxon signed rank test, tuned cells: $p=0.062$, $n=129$ cells from 5 sessions in 5 mice; Appendix Fig. 7C-D). Like the pooled group of all dorsal GCs, event rates for all ventral GCs showed

no differences in calcium event rates when laps were compared with and without optogenetic stimulation (p=0.625; Appendix Fig. 7C-D).These data indicate that a subpopulation of dorsal GCs that are spatially tuned are consistently excited by dorsal MCs, but most GCs are not. Axons of ventral MCs show weaker effects.

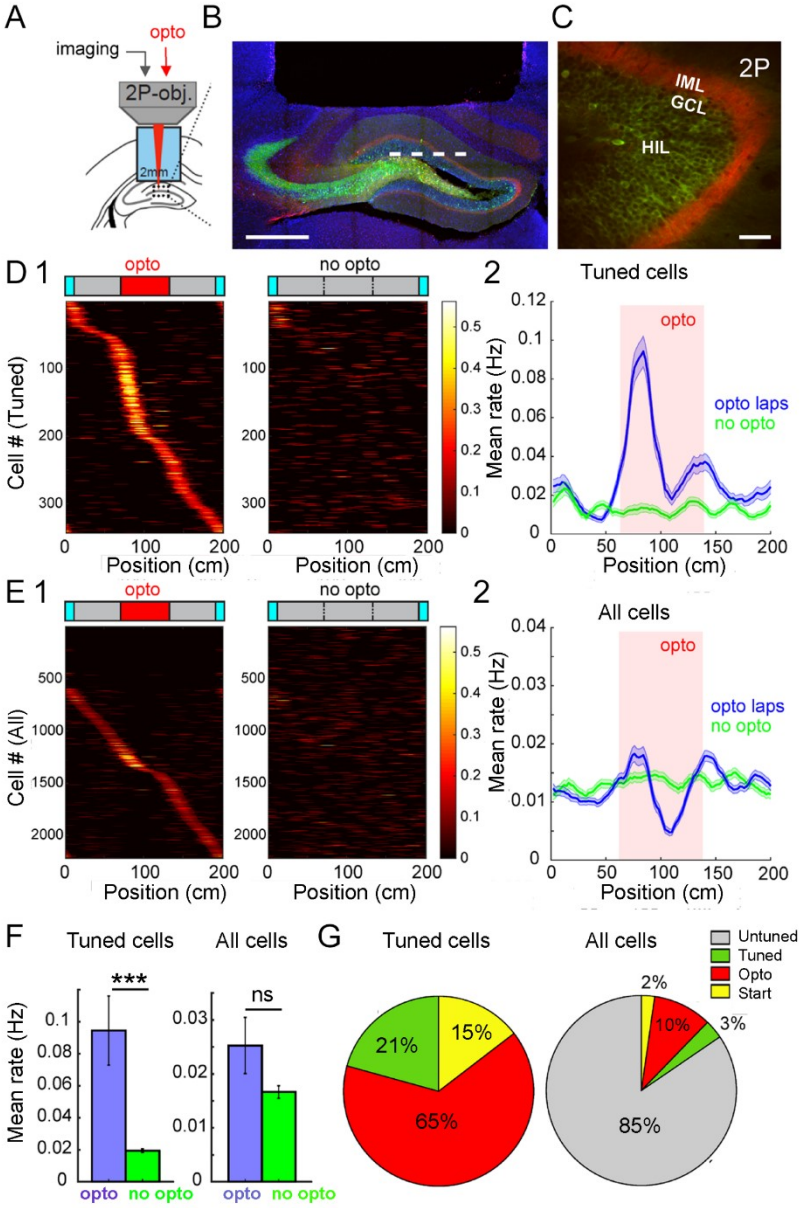

Fig. 9. Simultaneous optogenetic stimulation of MCs and 2P imaging of calcium activity in GCs.

A. Schematic of the chronic imaging window above the DG, through which red LED optogenetic stimulation and 2P imaging was performed.

B. Confocal image of fixed tissue from a *Drd2*-Cre$^{+/-}$ mouse injected with AAV-hSyn-FLEX-ChRimson-tdTomato (red) and AAV-hSyn-GCaMP6s (green) in the dorsal hilus, with a chronic imaging window implanted over the DG (blue: DAPI; calibration, 500 µm).

C. In vivo 2P image of GCaMP6s expression in the GCL (green), and ChRimson-tdTomato expression (red) in axons from dorsal MCs in the IML. Calibration, 50 µm.

D. 1) Left. Average calcium event rates of significantly tuned putative GCs (n=343) on laps where optogenetic stimulation was triggered, sorted by peak firing position (n=11 sessions from 5 mice). Right. Responses from the same cells on laps where no optogenetic stimulation was administered.
2) Average calcium event rates for all tuned cells (n=343 cells).

E. 1) Left. Average calcium event rates of all cells, regardless of tuning (n=2220 cells from same sessions/mice as D). Cells are sorted by position on laps with optogenetic stimulation. Some cells were not active on these laps and those are included in top rows.
Right. Responses from the same cells on laps where no optogenetic stimulation was administered.
2) The mean peak event rate for all sessions during the period of optogenetic stimulation. Blue, laps with optogenetic stimulation; green, laps without.

F. 1) Spatially tuned cells had greater event rates on laps with optogenetic stimulation compared to no stimulation (Wilcoxon signed rank test, optogenetic stimulated laps: 0.1 ± 0.02; laps without stimulation: 0.02 ± 0.003, p=0.0004, n=11 sessions from 5 mice).
2) All cells are compared and showed no significant differences for laps with and without optogenetic stimulation (Wilcoxon signed rank test, optogenetic stimulated laps: 0.024 ± 0.004; laps without stimulation: 0.018 ± 0.001; p=0.32, same sessions as E1, same mice).

G. The percentages of different cell types are compared. Cells were divided into groups based on their calcium activity during laps with optogenetic stimulation. Gray, untuned cells (calcium event rates did not increase significantly at any position); green, "tuned" cells (increased activity either at the start or at the position when optogenetic stimulation occurred); yellow, cells that increased activity but not at the start or during optogenetic stimulation; red, cells that increased calcium event rates only at the start of the lap.
Left. Tuned cells (total 343 cells). There were 78 start cue cells and 147 cells that increased activity during optogenetic stimulation.
Right. All cells (total 2220 cells). There were 1877 untuned cells and147 cells that increased activity during optogenetic stimulation.

VI. Variables affecting MC excitation of GCs

A. Sex

Field EPSPs were studied in 11 male mice (30 slices) and 3 female mice (7 slices). Female data showed a much greater variance (Appendix Fig. 8A). Therefore, data were transformed by taking the reciprocal of each data point for all data. A two-way ANOVA showed no main effect of sex (F(1,70)=0.29; p=0.589) but there were differences in values for slope and amplitude (F(1,70)=8.42; p=0.005). There was no interaction (F(1,70)=0.13; p=0.724). Non-parametric statistics on the raw data also showed no significant effects of sex (Mann-Whitney *U* tests, slope, p=0.887, *U*,101; amplitude, p=0.603; *U*, 91; latency, p=0.109; *U*, 65.5).

For comparisons of sex and other variables described below, EPSPs were compared at -65 to -75 mV. A two-way ANOVA was conducted with sex and EPSP measurement (amplitude, latency to onset, rise time, or half-duration) as main factors. There was no significant effect of sex (F(3,99)=0.24; p=0.866) but there were differences between measurements F(3,99)=24.70; p<0.0001), as one would expect (i.e., latency to onset < half-duration). There was no interaction of factors (F(1,99)=0.11; p=0.746; Appendix Fig. 8B).

B. Septotemporal comparisons

1) Slice location

The hippocampus was divided into a dorsal, mid and ventral region, defining each part as one-third of the hippocampus. For fEPSPs, two-way ANOVA was conducted with slice location and type of measurement (slope or amplitude) as main factors. There was no effect of slice location (F(2,72)=0.03; p=0.969) but there were differences between the values for slope and amplitude (F(1,72)=6.12; p=0.016; Appendix Fig. 9A). There was no interactions (F(2,72)=0.45; p=0.637).

EPSPs were also analyzed by two-way ANOVA. There was no effect of slice location (F(2,93)=0.10; p=0.905) but the measurements were different (F(3,93)=40.10; p<0.0001). There was no interaction F(6,93)=0.10; p=0.996; Appendix Fig. 9A).

2) Dorsal vs. ventral viral injection sites

There was no effect of dorsal vs. ventral injection site on fEPSP slope or amplitude (Appendix Fig. 9B). Thus, a two-way ANOVA showed no effect of injection site location ($F(1,72)=0.0005$; $p=0.981$) but there were differences in the type of measurement (slope vs. amplitude; $F(1,72)=6.50$; $p=0.013$). There was no interaction ($F(1,72)=1.17$; $p=0.282$). Latencies of fEPSPs also were not different (Mann-Whitney *U* test, $p=0.350$; *U*,120.5; Appendix Fig. 9B).

We also asked if the dorsal MCs had different effects at their distal terminal zones in ventral DG compared to effects of ventral MCs on dorsal GCs (Appendix Fig. 9B). This question was of interest because dorsal MCs make a broader projection in the molecular layer in ventral DG than ventral MCs do in dorsal DG (Botterill et al., 2021a; Houser et al., 2021). However, we did not detect differences. Slices of ventral DG from dorsally-injected mice were compared to slices of dorsal DG from ventrally-injected mice. A two-way ANOVA with location and type of measurement (slope or amplitude) showed no effects of location ($F(1,24)=1.05$; $p=0.315$) but slopes were distinct from amplitudes ($F(1,24)=5.51$; $p=0.028$), without interaction of factors ($F(1,24)=0.019$; $p=0.891$). There were no differences in latency (Mann-Whitney *U* test, $p=0.695$, *U*, 17; Appendix Fig. 9B).

3) Ipsilateral vs. contralateral recording sites

Recording sites that were ipsilateral to the injection site were divided into those that were close to it ("near") or far from it ("far"). The definitions for 'near' or 'far' slices were based on studying ChR2 expression and finding that slices at least 800 µm away from the injection site had few (<5) MC somata expressing ChR2. Therefore these slices seemed far from the injection site. On this basis, at least 800 µm from the injection site was "far". In contrast, slices at the injection site or adjacent to it were called "near" (Appendix Fig. 10A).

Ipsilateral and 'near' the viral injection site, ipsilateral 'far', and contralateral recording sites were compared (Appendix Fig. 10A). There were no significant differences by Kruskal-Wallis ANOVAs in fEPSP slope ($p=0.126$; Kruskal-Wallis statistic, 4.14) or amplitude ($p=0.302$; Kruskal-Wallis statistic 2.40) or latency to onset ($p=0.830$; Kruskal-Wallis statistic 0.37; Appendix Fig. 10B).

EPSPs were recorded either ipsilateral near or contralateral. A two-way ANOVA with location and EPSP measurement as main factors showed a borderline effect of location ($F(1,87)=3.72$; $p=0.057$), differences in the measurements ($F(3,87)=23.14$; $p<0.0001$). There was a significant interaction ($F(3,87)=2.96$; $p=0.037$), with half-duration significantly longer for contralateral GCs relative to ipsilateral GCs (Tukey-Kramer post-hoc test, $p=0.013$; Appendix Fig. 10C).

C. Comparisons of different IML recording sites within the DG blades

For the purposes of this study, the GCL was divided into three parts, the superior blade, the crest and the inferior blade. As shown in Appendix Fig. 11A, the superior blade refers to the part of the IML that is closest to area CA1; the inferior blade refers to the blade furthest from area CA1; the crest is between the two blades (Scharfman and Witter, 2007).

Statistical comparisons were restricted to the superior blade and crest because optogenetic stimuli were tested in the lower blade in very few slices. For fEPSPs, Mann-

Whitney *U*-tests were conducted because variance was heterogeneous and could not be resolved by transformation. There was no significant difference between the GCs in the superior blade and crest for slope (p=0.157, *U*=83.5), amplitude (p=0.070; *U*=73.5), or latency (p=0.164; *U*=85.5; Appendix Fig. 11B).

For EPSPs, the variances were not significantly different between groups so a two-way-ANOVA was conducted with location (superior blade or crest) and type of measurement (EPSP amplitude, latency to onset, rise time and half-duration) as main factors. There was no effect of location (F(1,59)=0.9365; p=0.337) although there were significant differences between the type of measurement (F(3,59)=46.1; p<0.0001; Appendix Fig. 11C). There was no interaction of factors (F(3,59)=0.313; p=0.816). The same percentage of EPSPs were recorded in the superior blade (10 GCs showed EPSPs/21 total GCs with EPSPs or 47.6%) and crest (10/21 GCs or 47%).

D. Viral incubation time

Viral expression was examined between 10 and 40 days after viral injection, and there was no evidence that results depended on the delay between viral injection and recordings. For fEPSPs, the correlations between time after injection (27.7± 2.2 days, range 13-40, n=24 slices, 14 mice) and fEPSP latency, slope and amplitude were not significant (slope, Pearson r=0.143, p=0.562; amplitude (Pearson r=0.378, p=0.121) or latency (Spearman's r=0.389, p=0.874; Appendix Fig. 12A).

For whole-cell recordings, there were no significant correlations between incubation time (42.4 ± 10.9 days; range: 15-95, n=26 slices, 15 mice) and amplitude (Pearson r=0.012; p=0.956), rise time (Pearson r=-0.128; p=0.960), latency (Pearson r=-0.015; p=0.940), or half-duration (Pearson r=0.023; p=0.919; Appendix Fig. 12B).

E. Age

Age did not appear to influence fEPSPs because there was no correlation between age (89.2 ± 4.6 days, range: 64-132 days, n=37 slices, 20 mice) and fEPSP slope (Pearson's r=-0.308 p=0.246), amplitude (Pearson's r=-0.0529 p=0.852) or latency (Spearman's r=-0.368, p=0.162; Appendix Fig. 13A).

For EPSPs, there was no correlation between age (mean: 105.2 ± 5.4 days; range: 73-146 days, n=26 slices,18 mice) and amplitude (Pearson r=0.108; p=0.624), rise time (Pearson r =-0.161; p=0.464), latency (Pearson r =0.003; p=0.990), or half-duration (Pearson r =-0.070; p=0.757; Appendix Fig. 13B).

F. Drd2-Cre vs. Crlr-Cre mice

fEPSPs of *Drd2*-Cre and *Crlr*-Cre mice were compared by two-way ANOVA with strain and type of measurement (slope or amplitude) as main factors. There was no effect of strain (F(1,48)=0.73; p=0.397) but there was a difference between slope and amplitude (F(1,4= 5.48; p=0.024). There was no interaction (F(1,48)=1.33; p=0.254; Appendix Fig. 14A-B). There were no differences in latency between *Drd2*-Cre and *Crlr*-Cre mice (Mann-Whitney *U* test, p=0.929, *U*, 158; Appendix Fig. 14C).

For EPSPs, there were many more Drd2-Cre mice (n>20) than Crlr-Cre mice (n=4). Still, a two-way ANOVA showed no effect of strain (F(3,111)=0.26; p=0.849) but there were differences in the type of measurement (F(3,111)=32.72; p<0.001). There was no interaction (F(1,111)=0.36; p=0.550).

DISCUSSION

I. Summary

This study showed that MCs have weak excitatory effects on GCs that are extremely common, so much so that a field potential reflecting the EPSP could be recorded in the IML. Also, EPSPs were common to all parts of the MC projection. Both sexes, dorsal and ventral GCs, GCs from different parts of the GCL, mice with different viral incubation times and ages, and two different Cre lines exhibited fEPSPs extracellularly and EPSP/Cs in single GCs. Results were reproduced with sharp electrode intracellular recording and whole cell recording using current or voltage clamp.

The excitatory effects are described here as weak because EPSPs were small and subthreshold at RMP even with the maximal light stimulus and multiple viral injections. Although weak using standard conditions, MC excitation was sufficient to boost the PP input – but only within a highly restricted temporal window, so that the timing of the MC-evoked GC EPSP coincided with the PP-evoked GC EPSP. This temporally constrained boost of the PP input contrasted with MC-evoked inhibition of GCs, which was produced with a far less restricted temporal window.

Although MC-evoked excitation was weak, it could be strengthened. Manipulations that strengthened excitation included depolarizing GCs or lowering $[Mg^{2+}]_o$ to unblock NMDA receptors and increase GC R_{in}, or increasing stimulus frequency from 5 to 25 Hz. In addition, exposure to carbachol promoted MC→GC excitation.

The ability to strengthen synapses is likely to be significant because after a train of optogenetic stimuli or transient lowering of $[Mg^{2+}]_o$, a single MC optogenetic stimulus could elicit a SPW-R in CA3. The SPW-Rs were GC-dependent, suggesting a MC→GC→PC circuit. SPW-Rs are significant because they are considered to be important to hippocampal dependent memory (Buzsaki, 1986, 1989, 2015). To determine if MC excitation can activate CA3 in vivo, we used chemogenetics to excite MCs and coupled the excitation to a behavior we previously showed was able to activate MCs, but not CA3 (HCNOE; Bernstein et al., 2019). Chemogenetic excitation of MCs during this behavior activated CA3 in vivo, using c-Fos-ir as a proxy for neural activity. These data supported the idea that MCs can activate CA3, but few GCs were activated, suggesting that the number of GCs that are required for CA3 activation might be smaller than one would think, possibly due to the powerful GC→CA3 mossy fiber synapses, which are unusually large and packed with glutamatergic vesicles (Laatsch and Cowan, 1966; von Kitzing et al., 1994; Henze et al., 2000). To pursue the in vitro and in vivo studies further we used MC optogenetics in vivo while calcium imaging GC activity in awake-head-fixed mice on a treadmill. These studies confirmed that MC optogenetics activates few GCs, except for a small subset of the GC population. Interestingly, this GC subpopulation was spatially tuned to positions on the treadmill belt, and primarily dorsal.

Taken together, the results suggest that MC excitation of GCs is weak but widespread within the GC population. Although weak under normal conditions, 1) MC GC excitation can promote the PP input to GCs, although only in a restricted temporal window, 2) MC→ GC excitation can be strengthened under specific conditions (Fig. 10A-B), and 3) a subset of GCs appear to be strongly activated by MCs, and those are

part of the GC population that is responsive to spatial cues (Fig. 10). These new findings help address the gap in knowledge concerning the role of MC→GC excitation in a circuit where MCs also indirectly inhibit GCs.

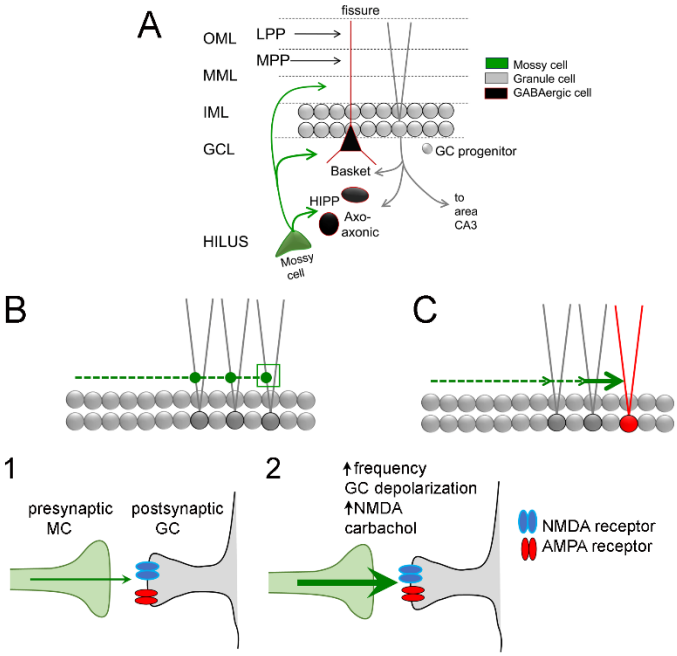

Figure 10. Summary diagram.

A. A simplified circuitry diagram of the DG showing the major cell types: granule cells (GCs, grey), mossy cells (green), and diverse GABAergic neurons (black with red outlines). Not all cell types or connections are shown. GCs project to hilar cell dendrites and CA3 proximal dendrites. Mossy cells project to the hilus and inner molecular layer (IML), where they mainly innervate GC proximal dendrites. The lateral perforant path (LPP) and medial PP (MPP) inputs are shown, but other inputs are not.

B. A diagram of MC en passant synapses having weak excitatory effects on GCs.
   1) The MC→GC synapse in the box is shown in more detail. MCs excite GCs by AMPA receptors under standard conditions, but NMDA receptors are present.
   2) MC→GC excitation strengthens conditionally. Frequency facilitation, GC depolarization, opening NMDA receptors, and the muscarinic agonist carbachol are examples of conditions that promote MC→GC excitation.

C. A different hypothesis from B, that MCs have strong effects on GCs, but only a small subset. Note the two hypothesis are not mutually exclusive.

II. MC→GC excitation is common but weak

This study showed that MC→GC excitation has characteristics that have not been recognized previously. One aspect of MC→GC excitation that has been assumed, but not well documented, is that it is widespread. Within a hippocampal slice, numerous GCs have EPSPs when MC axons in the IML are activated optogenetically. This is reflected by the ability to record a fEPSP in the IML in response to MC optogenetic stimulation. Also, EPSPs are elicited in almost all GCs when they are patched at random in a slice. This occurs whether slices are selected relatively near or far from the injection site, and if injection sites are dorsal or ventral. The results were obtained in both sexes. Our data are consistent with in vitro studies showing numerous synapses on GCs in the IML and in vivo analysis of the distant axon projection of MCs showing numerous MC→GC synapses (Buckmaster et al., 1996; Wenzel et al., 1997).

On the other hand, almost every GC was excited only weakly, so threshold was rarely reached. In vivo activation of MCs by eDREADDs did not result in numerous c-Fos-stained GCs. Also in vivo, a small subset of GCs were strongly excited, but it was a small subpopulation. The results are consistent with the literature showing MC optogenetic stimulation evoked EPSCs in GCs in slices (Chancey et al., 2014; Hashimotodani et al., 2017) which exhibited LTP (Wright and Jackson, 2014; Hashimotodani et al., 2017). The prior studies did not examine how widespread EPSCs

were, or if they were subthreshold, but APs were not shown. Other in vitro studies of the commissural input to the DG showed strong inhibitory neuron activation, as well as EPSCs (Hsu et al., 2015). In vivo, one study has suggested that MCs only excite GCs weakly (Bauer et al., 2021) but others suggest MCs inhibit GCs (Sloviter, 1994; Jinde et al., 2012; Senzai and Buzsaki, 2017; Bui et al., 2018). Notably, many studies that conclude MCs inhibit GCs primarily used recordings of GCs firing or population spikes, so they did not assay subthreshold events. In summary, our results are mainly consistent with the past literature. Where they are not, technical differences might be the reason.

One limitation of our in vitro results is that few recordings were made of GCs at the viral injection site. This is important because the local projections of MCs to GCs may be different from the distant projections to GCs. However, the in vivo calcium imaging studies were conducted near the injection site. Another limitation of the study is that it did not explore MC→GC excitation in relation to wakefulness vs. sleep. This is limiting because MC excitation of GCs may increase under conditions when CA3 has SPW-Rs such as awake immobility and sleep, because the backprojection to MCs is activated by CA3 excitation (Scharfman, 2007). However, the experiments using carbachol potentially provide insight into sleep because heightened cholinergic tone in rapid eye movement (REM) sleep are simulated, somewhat, by experiments with carbachol. The results of those experiments suggest that MCs may increase their excitation of GCs during times of heightened cholinergic tone, like REM.

III. PP excitation of GCs is promoted by MCs but only within a restricted temporal window

Another aspect of MC excitation that is new is the ability to increase the PP input within a very restricted temporal window. We found that the MC input has a bidirectional effect on the PP input, in contrast to many prior views that it is unidirectional and inhibitory. For example, a previous study using optogenetic stimulation of commissurally-projecting neurons from the contralateral hemisphere, the majority of which are MCs. The investigators examined effects of an optogenetic stimulus to a subsequent molecular layer electrical stimulus. Evoked population spikes were inhibited (Lien). Our results were the same but we also tested concurrent stimuli and an optogenetic stimulus after the PP stimulus. Then we found a facilitation of the population spike. Intracellular recording showed that this timing allowed the peaks of the optogenetically-evoked GC EPSP and PP-evoked GC EPSP to summate, explaining the effect.

Our results agree with the view of one study that MCs boost the PP input in slices (Houser). That result was based on ventral MCs, which is important because some of the studies that concluded MCs inhibit the PP input to GCs used dorsal MCs only (Sloviter, Lien, Jinde). On the other hand, we found the bidirectional effects in both dorsal and ventral hippocampus.

Presumably the tight window for facilitation keeps the activation of GCs selective, consistent with a GC population that is a filter or gate (Acsady and Kali, 2007; Hsu, 2007; Krook-Magnuson et al., 2015), contributes to pattern separation (Leutgeb et al., 2007; Myers and Scharfman, 2009; Yassa and Stark, 2011; Newman and Hasselmo, 2014; Knierim and Neunuebel, 2016), and fires sparsely (Jung and McNaughton, 1993;

Myers and Scharfman, 2009; Diamantaki et al., 2016; Pilz et al., 2016; Danielson et al., 2017; GoodSmith et al., 2017; Senzai and Buzsaki, 2017; Hainmueller and Bartos, 2020).

IV. Conditions that strengthen MC→GC excitation

Although under most conditions MC→GC excitation appears to be weak, there were several experimental manipulations that increased GC activation. Some of these are relevant to the intact brain, when the frequency of MC action potentials may increase due to increased afferent input. Regarding frequency, 25 Hz optogenetic stimuli resulted in facilitation of some EPSPs whereas 5 Hz had a modest facilitatory effect. The frequency of 25 Hz is in the beta range (approximately 15-30 Hz; (Chapman et al., 1998) which is notable because of the suggestions that beta activity is involved in memory (Kay, 2014), and the suggestions that MCs contribute to memory processing in the DG-CA3 (Buckmaster and Schwartzkroin, 1994; Lisman et al., 2005; Henze and Buzsáki, 2007; Myers and Scharfman, 2009, 2011; Knierim and Neunuebel, 2016; Nakazawa, 2017; Bui et al., 2018). It is also relevant that 5 Hz is at the low end of theta rhythm in rodents, and MCs have been implicated in theta-associated spatial exploration (Soltesz et al., 1993; GoodSmith et al., 2017; Hashimotodani et al., 2017; Senzai and Buzsaki, 2017; Bui et al., 2018; Jung et al., 2019)

One of the reasons that 25 Hz was able to facilitate EPSPs might have been related to the NMDA component of the MC→GC EPSP. Thus, when two stimuli are timed at 25 Hz, the second stimulus occurs during the late phase of the MC-evoked GC EPSP. At that time, GCs are more depolarized which increases their Rin and could make them more responsive to afferent input. Depolarization would also reduce the voltage-dependent block of NMDA receptors.

Carbachol increased the effects of MC optogenetic stimulation on GCs. GCs were depolarized by carbachol, and a depolarization-activated inward current developed. MC optogenetic stimulation led to a small EPSP in the absence of carbachol and after carbachol, this stimulus led to an AP. These data suggest that acetylcholine acting on muscarinic receptors could be another way that MC→GC excitation is enhanced. This effect may be relevant to behavioral states when cholinergic tone rises, such as REM sleep. Therefore, strengthening of the excitatory effects of MCs on GCs may occur during sleep. This effect might be amplified by other changes during sleep, such as inhibition of hippocampal GABAergic neurons by septal GABAergic afferents (Freund and Gulyas, 1997). Also, CA3 SPW-Rs occur during sleep (Buzsaki, 1986, 2015) and activate MCs (Scharfman, 2007). That idea is consistent with studies of slices with spontaneous SPW-Rs where MCs are activated (Swaminathan et al., 2018).

Cholinergic afferents to the DG are likely to also exert effects on MCs, based on work conducted in vitro. Hofman and Frazier (Hofmann and Frazier, 2010) showed that muscarinic activation of MCs leads to their depolarization and an afterdepolarization which prolonged their AP. Furthermore, prolonged MC APs led to release of cannabinoids which in turn depressed GABAergic transmission. These effects on MCs are important because they would synergize with those described by Ogando et al. (2021) and Martinello et al. (2015). The studies support the idea that muscarinic cholinergic signaling would increase the likelihood that MC→GC excitation would strengthen.

What other conditions might increase MC → GC excitation? Pathological conditions that increase excitability are examples, such as traumatic brain injury and seizures (Santhakumar et al., 2000; Botterill et al., 2019; Nasrallah et al., 2022). During the onset of hyperexcitability accompanying trauma or seizures, GCs depolarize, NMDA receptors become stronger, and GABAergic inhibition weaker or even excitatory (Zhang et al., 2012; Botterill et al., 2019). At this time, MCs appear to cause the GCs to become 'detonators' (Santhakumar et al., 2000; Botterill et al., 2019).

In some normal conditions there may also be increased MC→GC excitation. One example is reduced CB1 endogenous agonism. Another is LTP of the MC→GC synapse (Hashimotodani et al., 2017). Another example involves the noradrenergic brainstem projection. When activated, the noradrenergic input depolarizes GCs (Haas and Rose, 1987; Lacaille and Schwartzkroin, 1988; Stanton et al., 1989). The result is that GCs are placed in a membrane potential range when a subsequent MC input would produce a greater late EPSP. In addition, enhanced MC→GC excitation may occur when tonic inhibition of GCs wanes at times during the estrous cycle (Maguire et al., 2005). Agonists of the glucagon-like peptide 1 receptor, involved in feeding, and oxytocin, involved in diverse social behaviors, excite MCs [(Steiner et al., 2022; Hung et al., 2023), but see (Harden and Frazier, 2016)]. Finally, activation of extrasynaptic kainate receptors drives hilar mossy cell activity (Ramos et al., 2022)

V. MC activation of CA3 in vitro and in vivo

In vitro, MC optogenetic stimulation did not activate CA3 neurons, most likely because it activated few GCs over threshold. However, after a high frequency train of MC optogenetic stimuli to increase GC excitation, CA3 SPW-Rs occurred. The SPW-Rs were blocked by an antagonist of GC-CA3 transmission, suggesting that some GCs reached threshold and these GCs activated CA3. The data are consistent with in vitro and in vivo studies suggesting that MC→GC synapses exhibit LTP (Hetherington et al., 1994; Kleschevnikov and Routtenberg, 2003; Hashimotodani et al., 2017). In addition, MC plasticity has been inferred from its expression of molecules like GAP-43 (Namgung et al., 1997; Maroto et al., 2023).

The delay between MC optogenetic simulation and the onset of the SPW-Rs was well over the typical synaptic delay, suggesting polysynaptic circuitry. This is consistent with the idea that recurrent circuitry between CA3 PCs is required to synchronize sufficient PCs so that a SPW-R occurs. Notably, only a single CA3 PC is required to synchronize sufficient PCs to produce a field potential spike (Miles and Wong, 1983)

These data suggest that MC excitation of subsets of GCs can robustly activate CA3 PCs. To pursue this idea in vivo, we used eDREADDs to activate MCs. Although normally eDREADDs did not activate PCs in a robust manner, when eDREADDS coincided with behavior they did. Notably, behavior without eDREADDs was not effective. The task that was chosen is known to cause c-Fos expression to increase in MCs, so the behavior may have induced synaptic plasticity observed in the in vitro studies. Notably, few GCs expressed c-Fos protein either with or without the eDREADDs, consistent with the idea that few GCs needed to be active to strongly activate PC. However, in the in vivo experiment we do not know that GCs were required. We assume it because the only pathway that would excite CA3 after MC excitation is via GCs.

VI. Two-photon calcium imaging of GCs after optogenetic stimulation of MCs in head-fixed mice

To address the findings with additional in vivo data, we turned to calcium imaging of GCs while mice were head-fixed on a treadmill. MCs were optogenetically stimulated. A subset of GCs had extremely strong calcium signals during the laps with MC optogenetic stimulation. These data support the idea that a subset of GCs are strongly activated. Why these particular GCs are strongly activated is unclear, but their tuning is a clue. They may be the GCs with the greatest input from the EC, because the EC conveys information about the environment to the DG, either information about objects, place, or sensory information. However, it has not been shown, to our knowledge, that a subset of GCs have more EC input than another subset. Another possibility is that the GCs that were strongly activated were young adult-born neurons. When extremely young (<4 weeks-old), MCs form a major input to them (Chancey et al., 2014). When they are older but still considered young (~6 weeks-old), they exhibit differences in their PP input from mature GCs (Dieni et al., 2016; Luna et al., 2019).

VII. Septotemporal homogeneity

It was surprising to find little evidence of septotemporal differences in optogenetic responses, both fEPSPs and EPSPs. It was especially notable to find no evidence of differences in mice that were injected to label dorsal MCs vs. ventral injection sites. That is important because dorsal MCs project to the distant DG in both the IML and MML whereas ventral MCs project only to the IML (Botterill et al., 2021a; Houser et al., 2021). The caveat is that when a difference is not detected it could be that other methods or analyses might reveal them.

Regarding the results from c-Fos studies that were conducted after MCs were stimulated with eDREADDs and HCNOE, c-Fos protein expression in dorsal CA3 was increased relative to controls but not ventral CA3. These data suggest dorsal-ventral differences in the MC excitation of CA3. One explanation is based on the finding that ventral MCs express more c-Fos protein than dorsal MCs in response to HCNOE and other tasks that involve the memory of novelty (Duffy et al., 2013; Bernstein et al., 2019). This is important because greater activity in ventral MCs could lead to more activation of dorsal CA3. The reason is that ventral MCs primarily project to GCs in the dorsal DG and dorsal GCs primarily project to dorsal CA3.

Calcium imaging also showed a potentially stronger effect of MCs on dorsal GCs. However, the comparison was not identical: ventral MCs had only their axons optogenetically stimulated whereas dorsal MCs potentially had both MC somata and MC axons activated. Also, bReaches was used for dorsal MC optogenetics but Chrimson for ventral MCs. Finally, although the ventral data showed a trend and not statistical differences, the trend for the same effect observed for dorsal MCs was evident in the data. Therefore a dorsal-ventral difference was not compelling.

Why excitation of GCs by MCs is weak - mechanisms

A natural question is why MC-driven EPSPs in GCs are weak. One possibility is that MCs are neuromodulatory to GCs (Jung et al., 2019). This is consistent with the idea that MCs, GCs, and CA3 PCs form a circuit with MCs helping ensure pattern separation

(GoodSmith et al., 2019). It is not consistent with the idea that MCs impart their own functional role (Nakazawa, 2017; GoodSmith et al., 2019) having stronger and more flexible place fields than GCs (Neunuebel and Knierim, 2012; GoodSmith et al., 2017; Senzai and Buzsaki, 2017).

Another question is why the MC have high spontaneous rates of APs (Scharfman and Schwartzkroin, 1988; Scharfman, 1993; Larimer and Strowbridge, 2008; Danielson et al., 2017) if the effect of the axon is weak. A possible explanation is that there may be inhibitory regulation of MC terminals to keep it from exciting GCs most of the time. Indeed there are cannabinoid receptor type 1 (CB1 receptors) on MCs that suppress MC glutamate release on GCs (Chiu and Castillo, 2008; Maroto et al., 2023). D2 dopamine receptors are on MC terminals and inhibit glutamate release (Gulfo et al., 2023). This idea is consistent with the high failure rate of the MC → GC synapse (Scharfman, 1995a).

Conclusions

The results support the hypothesis that MC excitation of GCs is widespread, as the anatomical data suggest, but weak because APs are rarely generated under normal conditions. The data are also consistent with the studies which examines GC firing, and see little evidence of MC excitation of GCs over threshold. However, subthreshold excitation is potentially important because it can boost the PP input, although the temporal constraints are tight. The restricted time window is consistent with the need for GCs to fire in a highly selective manner. Importantly, there are many conditions that increase MC excitatory effects on GCs so they reach threshold. These data also suggest that MC excitation of GCs is highly selective, requiring specific conditions. Remarkably, MC excitation could trigger SPW-Rs in CA3 in vitro or CA3 c-Fos protein expression in vivo, results which help explain why MCs appear to be important to behavior. The findings from calcium imaging of GCs in vivo were consistent with the slice experiments, showing most GCs are excited weakly by MCs. They also suggested a novel idea, that MCs excite a subset of GCs in a robust manner, but not the majority.

Thus, MC→GC excitation may usually be weak, but it is widespread and can strengthen (Fig. 10A-B). Both normally and after strengthening, MCs exert an influence on GCs and CA3. Moreover, we provide evidence that a select subset of GCs are excited strongly by MCs (Fig. 10C).

Tables

Table 1. Stereotaxic coordinates used for injection of AAV encoding ChR2-eYFP or eYFP.

	Coordinate (mm)	Range (±)
A-P	2.0	0.1
M-L	1.3	0.1
Depth	2.1	0.1
A-P	3.0	0.1
M-L	2.4	0.2
Depth	2.6	0.2
A-P	3.4	0.3
M-L	2.6	0.2
Depth1	2.2	0.0
Depth2	3.0	0.3

Table 1 Legend.

The coordinates for injection of AAVs are shown. Distances are relative to Bregma. The top set of coordinates were for injections in dorsal DG, the middle row shows sites for a relatively caudal and ventral location, and the bottom set of coordinates was used for the most ventral DG. When a single dorsal injection was made, only the top row was used. When a single ventral injection was made, only the middle or bottom coordinates were used. Note that coordinates used for in vivo studies of GC calcium fluctuations used one dorsal or one ventral injection and coordinates are provided in the section about those experiments.

Table 2. Characteristics of optogenetically-evoked fEPSPs.

	Pulse duration	Latency from onset of pulse	Latency from end of pulse	Slope	Amplitude	Rise time	Half-duration
Mean	2.43	4.62	2.31	0.11	1.78	2.42	10.35
SEM	0.37	0.76	0.38	0.02	0.39	0.29	0.60
N	19	20	20	17	19	14	10
Min	0.40	0.00	0.00	0.01	0.20	1.50	7.90
Max	5	10	5	0.45	7.2	6.6	15.9

Table 2 Legend.
Characteristics of fEPSPs evoked by optogenetic stimulation are shown. Pulse duration is the duration of optogenetic stimulation. The latency to the onset of the fEPSP from either the start or end of the light pulse is shown to the right. Slope was defined as the maximum slope of the fEPSP, amplitude was measured from pre-stimulus baseline to peak, and rise time was measured from the EPSP onset to the peak. Half-duration was measured from the fEPSP onset to the point on the EPSP decay where amplitude had declined to half.

Table 3. Intrinsic properties of GCs.

	RMP	Rin	τ	AP amp from RMP	AP amp from threshold	Threshold	AP Rising slope	AP Decay slope
	mV	MΩ	msec	mV	mV	mV	V/s	V/s
Cells with Response								
Mean	-81.69	301.88	26.14	114.56	71.58	-37.53	232.84	-72.32
SEM	1.16	16.74	1.70	1.94	1.94	1.00	12.33	2.24
n	47	39	36	43	43	43	43	43
Min	-91.11	130.50	12.68	76.47	45.56	-48.70	98.90	-94.26
Max	-55.18	540.40	52.60	134.68	93.75	-23.59	395.06	-38.77
Cells without Response								
Mean	-80.95	267.30	32.24	119.03	79.31	-38.44	260.59	-80.22
SEM	1.85	12.16	5.16	2.67	3.19	1.55	12.86	4.34
n	7	7	7	7	7	7	7	7
Min	-86.27	229.90	17.87	107.49	69.55	-43.21	206.32	-100.43
Max	-73.90	325.00	60.80	128.41	93.26	-32.00	294.26	-67.16
t-test	0.813	0.394	0.179	0.372	0.129	0.724	0.378	0.182

Table 3 Legend.
The properties of GCs with and without detectable optogenetic responses are shown. For definitions and methods of measuring properties, see Methods. There were no significant differences between the two groups of GCs.

.

APPENDIX

Appendix Figure 1
AMPA receptors, but not $GABA_A$ receptors, contribute to MC→GC optogenetic excitation.

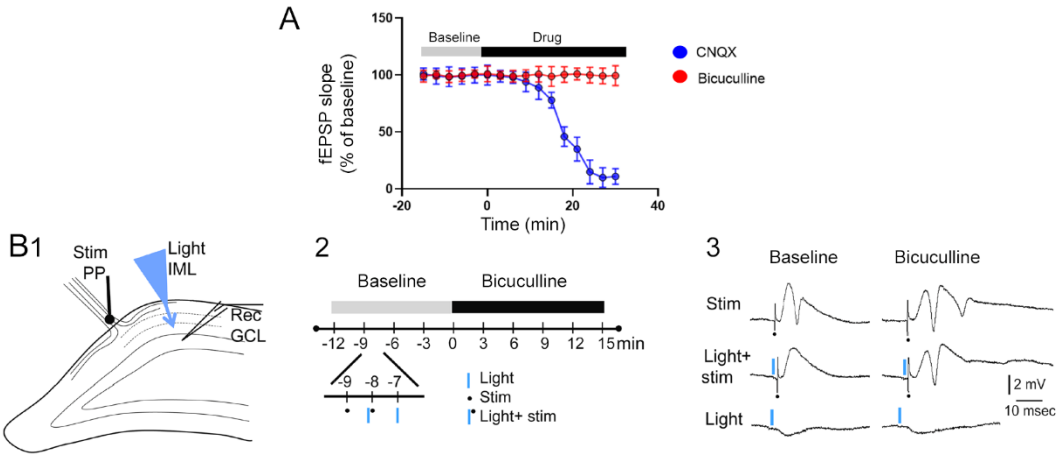

A. Optogenetc stimuli were triggered to evoke EPSPs. FEPSPs decreased in amplitude upon exposure to 10 μM CNQX (3 slices, 3 mice) but not 10 μM BMI (3 slices, 3 mice).

B.

1) A schematic of the recording arrangement.
2) A schematic of the experimental timeline. Stimuli were triggered every minute in this order: electrical stimulation of the PP, optogenetic stimulation, both PP and optogenetic stimulation. For the latter, the optogenetic stimulus was triggered with the same delay before the PP stimulus. This sequence was repeated throughout the experiment. There was a control period to confirm responses were stable, and then the slice was exposed to 10 μM BMI.
3) Responses are shown for before (Baseline) and after BMI was added to the ACSF (BMI). In the control period, a PP stimulus (Baseline, Stim) evoked a large population spike and a prepulse of light inhibited it (Baseline, Light + Stim). When light was triggered by itself (Baseline, Light), a small fEPSP occurred. After BMI, the light pulse no longer inhibited the population spike elicited by PP stimulation (BMI, Light + Stim). The fEPSP evoked by the light pulse appeared to be unaffected by BMI (BMI, Light), which is consistent with the idea that optogenetic stimulation evoked a fEPSP mediated by glutamate, not GABA. Note that the second population spike evoked in the presence of BMI (BMI, Stim), was inhibited by the light pulse (BMI, Light + Stim). This result is consistent with BMI-resistant $GABA_B$ receptors causing a slow inhibition after the optogenetic stimulus. Results were replicated in 5 slices from 5 mice.

Appendix Figure 2
Optogenetic activation of MCs leads to weak GC excitation even when the PP evokes strong excitation in the same slice.

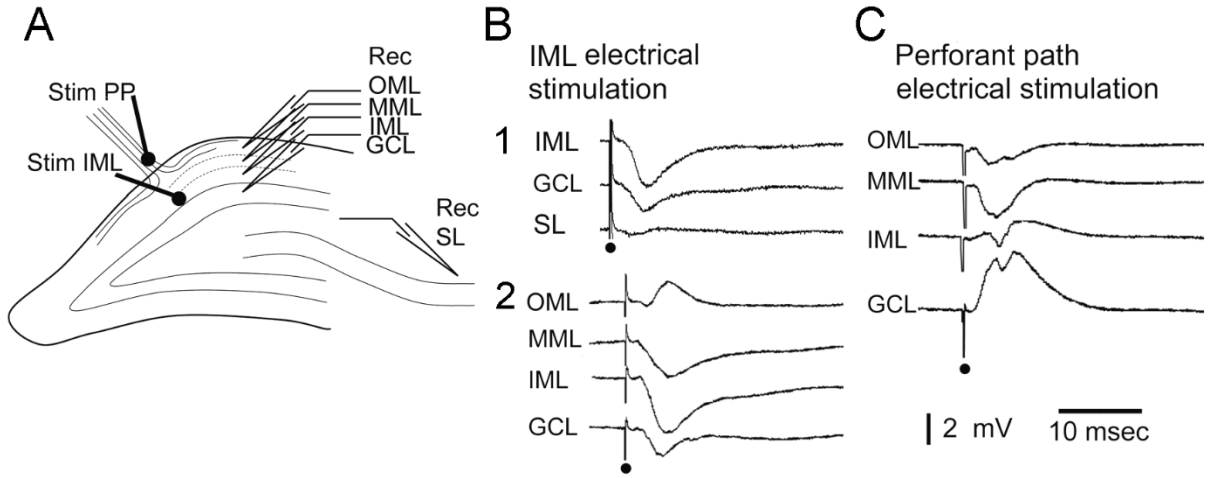

A. A shows the recording site in the GCL and the stimulating electrode in the PP. The site of stimulation was on the hippocampal fissure rather than the ML to avoid direct stimulation of DG neurons (Scharfman, 1995b). Light was directed to the IML near the GCL recording site.

B. 1) Example of a fEPSP elicited by electrical stimulation of the IML. Sequential recordings in different layers showed the largest responses in the IML, consistent with preferential stimulation of the IML axons. Note there is no population spike, consistent with weak activation of the IML inputs. Electrical stimulation is not selective for MC axons, so to make electrical stimulation as specific as possible for the IML we used a stimulus electrode that was small in diameter (25 μm diameter) and weak currents (10-50 μsec, 50 μA). In this way, current would not be likely to spread to the MML and activate PP axons. In addition, we only used slices where an electrical stimulus to the IML evoked a fEPSP that was larger in the IML than the MML.

2) Another example of fEPSPs elicited by IML electrical stimulation, demonstrating IML axons were preferentially stimulated, because the fEPSP that was maximal in the IML was small in the MML and flipped polarity in the OML.

C. In contrast to IML stimulation, electrical stimulation of the PP elicited a fEPSP that could trigger a population spike in the GCL. Same slice as B. The PP stimulus strength was adjusted so the fEPSP was no greater in amplitude than the fEPSP generated in the IML by IML stimulation. These data suggest that the MC input to GCs is weakly excitatory compared to the PP input.

Appendix Figure 3
Experimental approach and viral expression in *Drd2-Cre* mice.

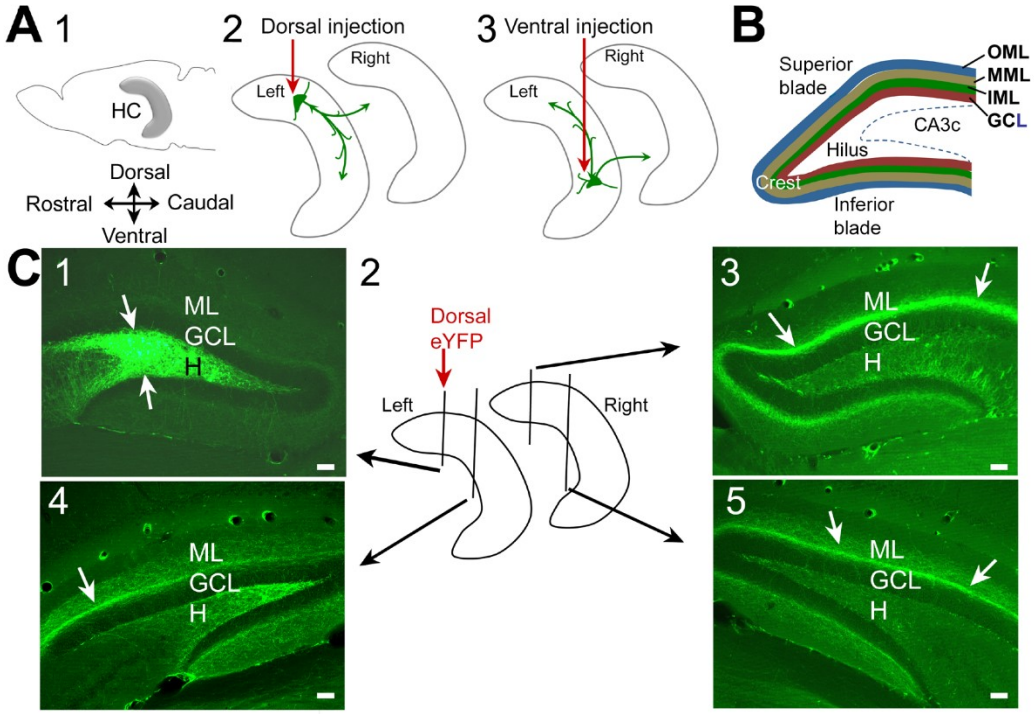

A. 1) A schematic of the rodent brain (side view) illustrates the location of the hippocampus (HC) in gray. Dorsal is up; Rostral is to the left.
2-3) A diagram illustrates the injection of AAV either in dorsal (2) or ventral (3) hippocampus. The axon of a dorsal MC (green arrows) is indicated, reflecting the major projection, which extends ipsi- and contralaterally, terminating distant to the cell body in the IML (for review, see Scharfman and Myers 2012). Green lines without arrowheads represent axon collaterals in the hilus, which are mostly near the cell body of MCs (Scharfman and Myers 2012).

B. A schematic of the dorsal mouse DG and CA3c in the coronal plane shows the layers: outer molecular layer (OML); middle molecular layer (MML); inner molecular layer (IML); granule cell layer (GCL); hilus; pyramidal cell layer (PCL). ML in part C and elsewhere refers to all three sublayers (OML, MML, IML). Superior and inferior refer to the two DG blades.

C. Representative example of widespread septotemporal and bilateral expression of virus in MC axons after a single dorsal injection.
1) Two weeks after dorsal injection of AAV2-eYFP, there was strong fluorescence in the left dorsal hilus near the injection site (arrows). H=hilus.
2) Schematic of the injection and locations of sections shown in C1, C3, C4, and C5.
3) Expression in the contralateral hemisphere at a dorsal location. Arrows mark staining of axons in the IML, reflecting the termination of contralateral MC axons.
4) A section ipsilateral and caudal to the injection site shows that dorsal MCs project to the caudal IML.
5) A section contralateral to the injection site, caudal to the injection site. Expression is mainly in the IML (arrows). Calibrations, 50 μm.

Appendix Figure 4
Specificity of *Drd2*-Cre mice.

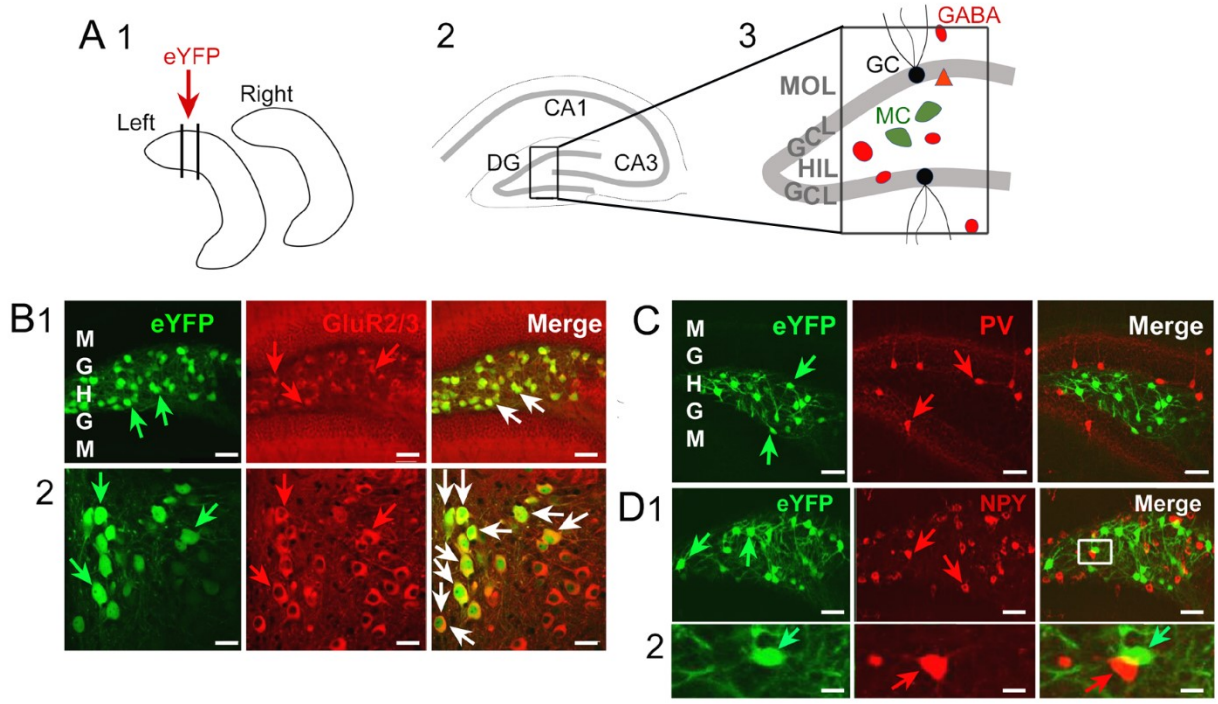

A. 1) A schematic illustrates the injection of AAV2-eYFP in the left dorsal DG. Sections were taken from the area near the injection site because the area with the most concentrated virus would be most likely to have nonspecific labeling.
2) The orientation of the tissue sections in B-D.
3) The area outlined by the box in 2 is expanded and cell types are illustrated schematically. MCs are green. GCs are black. GABAergic neurons are red. All subtypes of GABAergic neurons are not included. The boxed area is shown in B-D.

B.1) Tissue sections were processed using an antibody to the 2/3 subunit of the ionotropic glutamate receptor (GluR2/3) to stain glutamatergic cells. In the hilus, the vast majority of GluR2/3 cells are MCs (Leranth et al., 1996).
Left: EYFP-expressing cells are denoted by the green arrows.
Center: GluR2/3-labeled cells in the hilus (red arrows). In the mice injected in dorsal hippocampus (n=3), 538/545 (98.6%) of hilar eYFP-expressing cells also expressed GluR2/3. For the mice injected ventrally (n=3), 661/695 (94.8%) cells were double-labelled. Sections were selected from the injection site and areas next to it (5-7 sections/mouse). The hilus was defined as zone 4 of Amaral (Amaral, 1978).
Right: The merged image of eYFP and GluR2/3 immunofluorescence shows that eYFP-expressing hilar cells also expressed GluR2/3 (white arrows). Calibration, 50 μm. M, molecular layer; G, granule cell layer; H, hilus.
2) The same sections as B1 are shown at higher gain. Calibration, 20 μm.
C. No eYFP-expressing cells were labeled using an antibody to PV, which stains a major subclass of DG GABAergic neurons called basket cells (also called

perisomatic targeting cells; (Sloviter, 1994; Freund and Buzsaki, 1996; Houser, 2007; Hosp et al., 2014). Calibration, 50 μm.

Left: eYFP-fluorescent hilar cells (green arrows).

Center: PV-immunoreactive cells (red arrows).

Right: The merged image shows no double-labeling.

D. 1) Neuropeptide Y (NPY) is expressed in a major subset of hilar GABAergic cells called HIPP cells (GABAergic neurons with a ***Hi***lar cell body and projection to the terminal zone of the ***P***erforant ***P***ath; (Bering et al., 1997; Freund and Gulyas, 1997; Scharfman et al., 2002; Scharfman and Gray, 2006; Sperk et al., 2007). Double-labeling occurred in 4/337 (1.2%) of hilar cells that also expressed eYFP (for dorsal injections) and 9/328 (2.7%) for ventral injections. These data suggest that up to 3% of cells with NPY expression were not MCs in *Drd2*-Cre$^{+/-}$ mice. Calibration, 20 μm.

Left and Center: Many hilar neurons expressed eYFP (green arrows) or NPY (red arrows).

Right: Double-labeled cells (yellow) were rare.

2) The area outlined by the box in D1 is shown at higher gain.

Left: A cell expressing eYFP is noted by the green arrow.

Center: The red arrow points to a different cell with NPY immunofluorescence.

Right: The merged image shows that the cells at the arrows overlap and therefore yellow is observed, but they are two different cells. Thus, yellow reflected 2 overlapping cells but not double-labeling. Such falsely double-labeled cells were not included when counts of double-labeled cells were made. Calibration, 10 μm.

Appendix Figure 5
Specificity of *Crlr*-Cre mice.

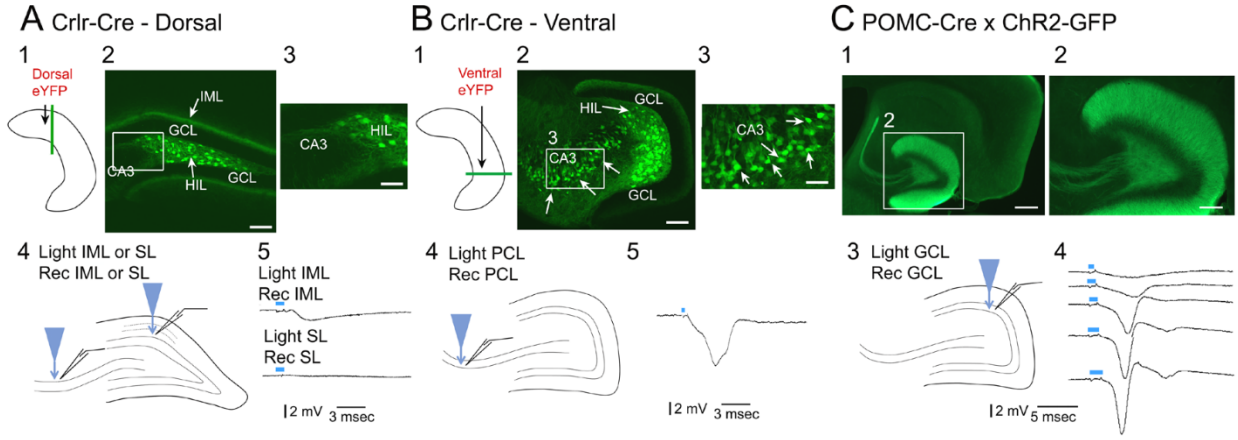

A. 1) A schematic shows a dorsal injection of AAV2-eYFP to evaluate specificity for MCs.
   2) A dorsal coronal section shows hilar and IML fluorescence (arrows), indicating labeling of MCs. The area surrounded by the box is between the hilus and CA3 and is expanded in 3.
   3) Dorsal area CA3 showed no fluorescent cells. Calibrations:100 µm (2), 50 µm (3).
   4) A schematic illustrates recording sites in slices that were prepared approximately two weeks after AAV2-ChR2-eYFP injection. The optical fiber was either directed towards the IML and extracellular recordings were made there, or light was directed at stratum lucidum (SL) in CA3 and extracellular recordings were made there.
   5) Top: An optogenetic stimulus to the IML elicited a fEPSP in the IML. Bottom: An optogenetic stimulus to SL did not elicit a response in SL. No responses were elicited from the PCL either (not shown). Similar data were elicited from 4 other slices (n=5; 1 slice/mouse).

B. 1) A schematic illustrates ventral injection of AAV2-eYFP. Approximately 3 weeks after ventral injection, horizontal sections were made of the ventral HC.
   2) A ventral horizontal section shows hilar and IML fluorescence (arrows). The area surrounded by the box is expanded in 3.
   3) Arrows point to fluorescent CA3 neurons. Calibrations, 100 µm (2); 50 µm (3).
   4) A schematic illustrates the light fiber direction towards the CA3 cell layer and recording at that location.
   5) A robust light response was evoked with a short latency (also in 2 other slices; n=3 slices, 2 mice). These data suggest a lack of specificity for MCs in ventral hippocampus of *Crlr*-Cre$^{+/-}$ mice.

C. 1-2) Experiments were conducted to confirm CA3 PCs were activated in B5 because the response morphology (waveform) was different from a population spike elicited by afferent stimulation (Scharfman et al., 2003). Therefore, we checked another mouse line with ChR2 in another cell layer, the GCL. In this mouse line, Cre is expressed in cells with the proopiomelanocortin (POMC) promoter (POMC-Cre$^{+/-}$ mice). This mouse line was crossed to a ChR2 reporter line (see Methods). Progeny had robust ChR2-GFP expression in GCs with a high degree of specificity as

previously reported (Overstreet et al., 2004). The box that is outlined is shown at higher gain in 2. Calibrations, 100 μm (1); 50 μm (2).

3) A schematic of the experimental arrangement for a POMC-Cre x ChR2-GFP mouse. The optogenetic stimulus was directed towards the GCL and recordings were made in the GCL.

4) Activation of GCs with increasing light durations shows increasing responses that appear more and more like a population spike. One of the weaker responses (third from the top) is similar qualitatively to the CA3 response in *Crlr*-Cre$^{+/-}$ mice, suggesting that recordings in *Crlr*-Cre$^{+/-}$ mice reflect weak activation of CA3. In summary, *Crlr*-Cre$^{+/-}$ mice expressed ChR2 in CA3 of ventrally-injected mice, and expression was sufficient to activate CA3. Therefore, viral injection in *Crlr*-Cre$^{+/-}$ mice were only made in dorsal DG.

Appendix Figure 6
Additional analysis of frequency-dependence of MC-evoked GC EPSPs.

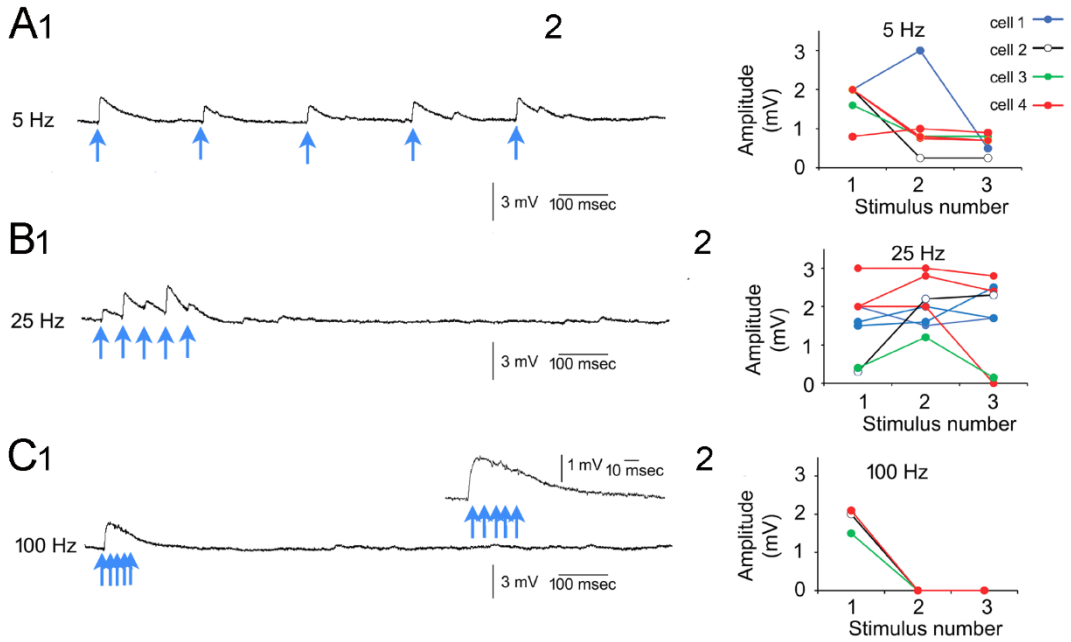

A.
1) A train of optogenetic stimuli were triggered at 5 Hz. MC→GC EPSPs could facilitate during the train.
2) Plot of the first three EPSPs of 5 Hz trains. Each color reflects a different GC. Some EPSPs were facilitated during the train.

B.
1) The response of 2 different GCs to a 25 Hz train. MC→GC EPSPs could facilitate during the train.
2) Plot of the first three EPSPs with different GCs in different colors. Some EPSPs were facilitated during the train.

C.
1) An example of a response to a 100 Hz train with an inset (top right) showing the higher gain of the response to the train.
2) The first three EPSPs are plotted for each GC. The stimuli stopped evoking EPSPs during the train, consistent with the demonstration that ChR2 does not follow frequencies between 50-100 Hz (Wang et al., 2007).

Appendix Figure 7
Weaker effects of ventral MC optogenetic stimulation on dorsal GCs compared to dorsal MCs.

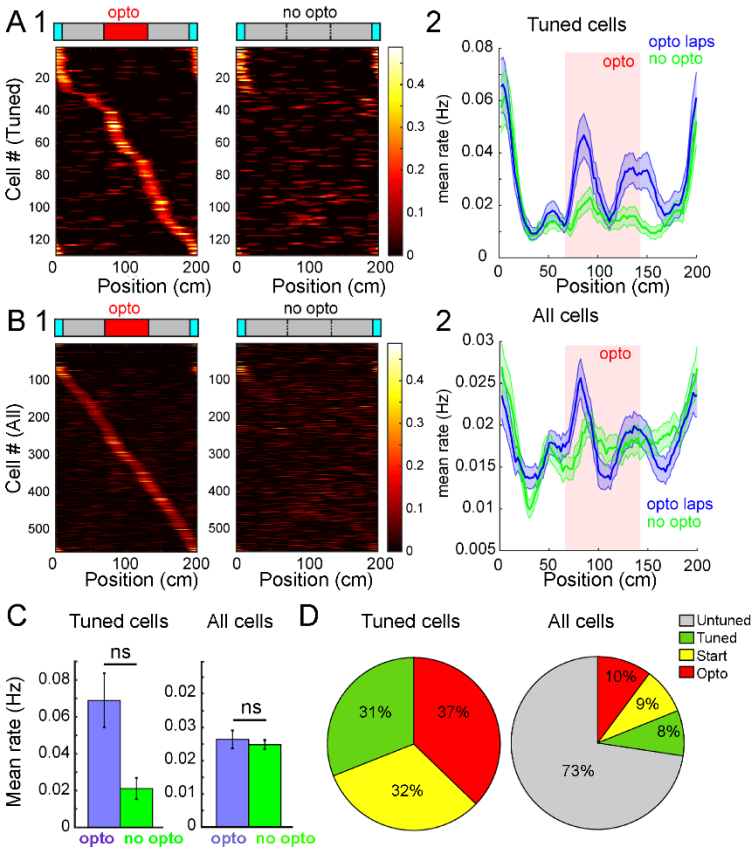

A. Analogous to Fig. 9, but ventral mossy cell axons were stimulated instead of dorsal MCs while 2P imaging of calcium activity in dorsal GCs.
   1) Left. Average calcium event rates of 129 significantly tuned putative GCs on laps with optogenetic stimulation (sorted by peak firing position; n=5 sessions, 5 mice).
      Right. Responses from the same cells during laps with no optogenetic stimulation (n=5 sessions from 5 mice).
   2) Average calcium event rates for the cells (n=129 cells).

B. Average calcium event rates of all cells, regardless of tuning consistency (n=560 cells from same sessions/mice as A.). Cells are sorted by calcium event rate during laps with (1) and without (2) optogenetic stimulation. Note that some cells were not active on these laps so they are included in the top rows.

C. Peak average calcium event rate during the position on the lap where optogenetic stimulation occurred.
   Left. Tuned cells had a higher mean calcium event rate during laps with optogenetic stimulation (0.07±0.01) but there was only a trend for significance compared to laps without (0.02±0.006, p=0.062, Wilcoxon signed rank test, n=11 sessions from 5 mice).
   Right. The differences were not significant for all cells (laps with optogenetic stimulation: 0.026±0.003, laps without: 0.025±0.001, p=0.630, Wilcoxon signed rank test, same sessions, same mice).

D. Fraction of cell response types (see Figure 10 for definitions).
   Left. Spatially tuned cells (total 129 cells, 41 start cue cells, 38 cells which increased calcium activity during optogenetic stimulation).
   Right. All cells (total 560 cells, 431 untuned, 38 which increased calcium activity during optogenetic stimulation).

Appendix Figure 8
No sex differences in optogenetic responses of GCs to MC axon stimulation.

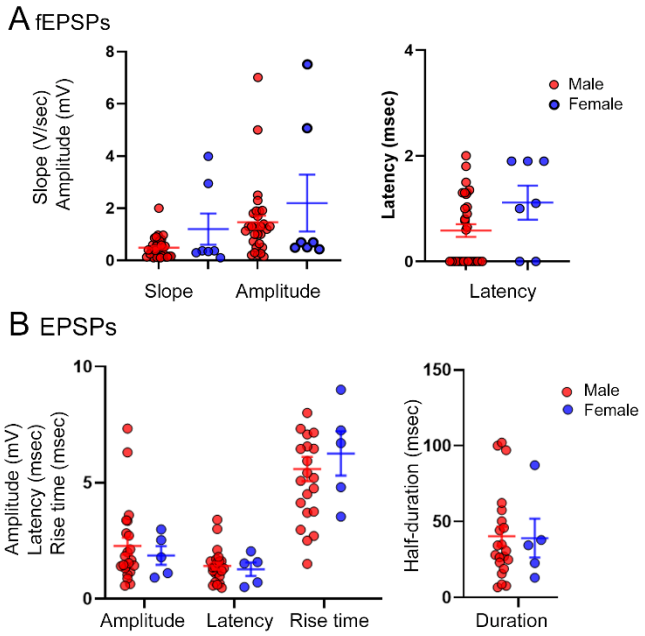

A. There were no differences between males and females in the slope or amplitude of fEPSPs, and no differences in latency. A two-way ANOVA showed no effect of sex ($F(1,70)=0.29$; $p=0.589$) but there were differences in values for slope and amplitude ($F(1,70)=8.42$; $p=0.005$). There was no interaction ($F(1,70)=0.13$; $p=0.724$). A Mann-Whitney *U* test showed no effects of sex on latency ($p=0.109$; *U*, 65.5).

B. EPSPs were compared in females and males at -65 to -75 mV membrane potential. A two-way ANOVA showed that there was no effect of sex in EPSP amplitude, latency to onset, rise time or half-duration ($F(3,99)=0.243$; $p=0.866$) but there was a main effect of the type of measurement ($F(3,99)=24.70$; $p<0.0001$), as one would expect (i.e., latency to onset < half-duration). There was no interaction of factors ($F(1,99)=0.106$; $p=0.746$).

Appendix Figure 9
Lack of dorsal-ventral differences in optogenetic responses of GCs to MC stimulation.

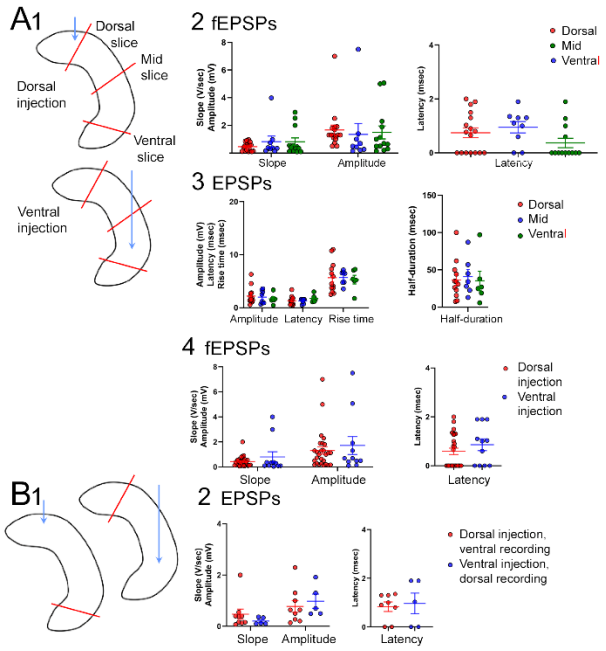

A.

1) Diagrams show the use of dorsal or ventral injections (blue arrows) and locations of slices (red lines). For A2-3, the slices were for dorsal and ventral injections were pooled. For A4, slices from dorsal, mid and ventral locations were pooled for mice injected in dorsal DG and compared to all slices from ventrally-injected mice.
2) For fEPSPs, there were no significant differences in slopes or amplitudes (two-way ANOVA, effect of slice location, F(2,72)=0.0317; p=0.969; effect of type of measurement, F(1,72)=6.120; p=0.016). There was no interaction (F(2,72)=0.453; p=0.637). There were no significant differences in latency to onset between slices from the dorsal, mid, and ventral DG (Kruskal-Wallis, p=0.970; Kruskal-Wallis statistic, 4.68).
3) For EPSPs, there were no significant differences in amplitude, latency to onset, risetime, or half-duration. Thus, two-way ANOVA showed no effect of slice location (F(2,93)=0.100; p=0.905). There was a main effect of the type of measurement (F(3,93)=40.10; p<0.0001). There was no interaction of factors (F(6,93)=0.097; p=0.996).
4) There were no differences in fEPSP slopes, amplitudes or latencies. Thus, a two-way ANOVA showed no effect of injection site location (F(1,72)=0.0005; p=0.981) but there were differences in the type of measurement (slope vs. amplitude; F(1,72)=6.50; p=0.013). There was no interaction (F(1,72)=1.17; p=0.282). Latencies of fEPSPs were not different (Mann-Whitney *U* test, p=0.350; *U*, 120.5).

B.

1) A diagram shows that mice with dorsal injections were compared to mice injected in ventral DG. Only those slices from the ipsilateral distal projection were compared, i.e., ventral slices for dorsal injections and dorsal slices for ventral injections.
2) There were no differences in fEPSP slopes, amplitudes or latencies. A two-way ANOVA with location and type of measurement (slope or amplitude) showed no effects of location (F(1,24)=1.05; p=0.315) but slopes were distinct from amplitudes (F(1,24)=5.51; p=0.028), without an interaction of factors (F(1,24)=0.019; p=0.891). There were no differences in latency (Mann-Whitney *U* test, p=0.695, *U*, 17).

Appendix Figure 10
Effects of ipsilateral and contralateral recording site on GC optogenetic responses to MC axon stimulation.

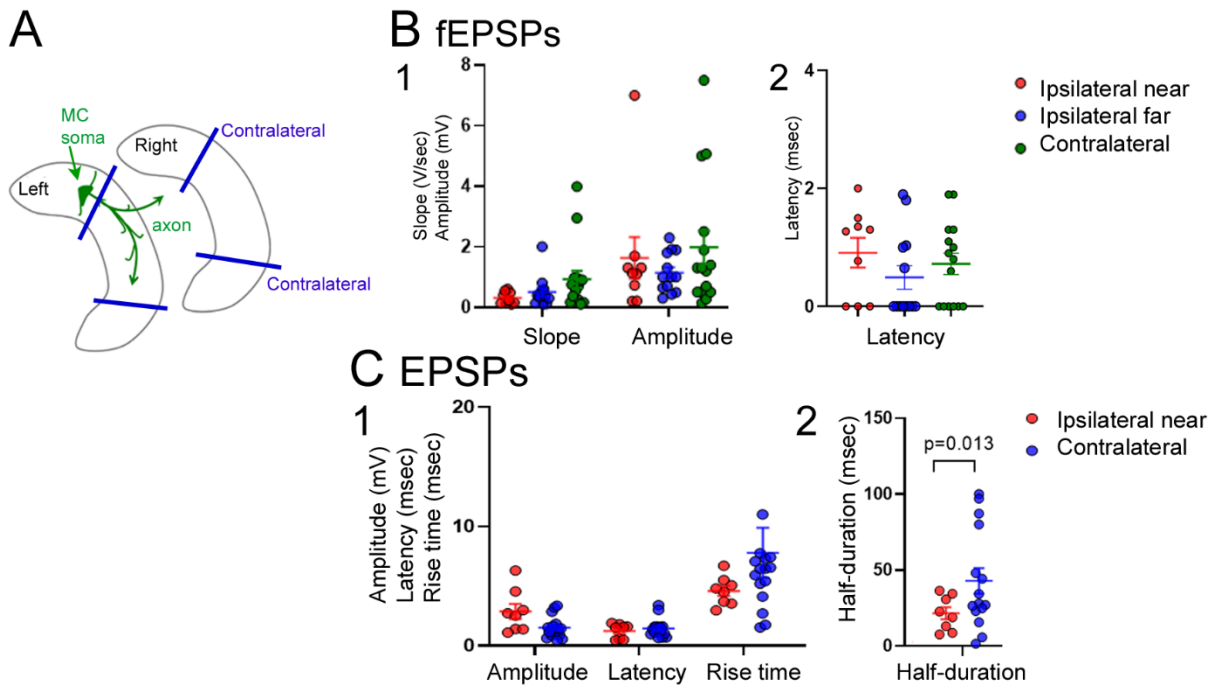

A. Recording sites that were ipsilateral to the injection site were divided into those that were close to it ("near") or far from it ("far"). The definitions for 'near' or 'far' slices were based on studying ChR2 expression and finding that slices at least 800 µm away from the injection site had few (<5) MC somata expressing ChR2. Therefore these slices seemed far from the injection site. On this basis, at least 800 µm from the injection site was "far". In contrast, slices at the injection site or adjacent to it were called "near". Ipsilateral and 'near' the viral injection site, ipsilateral 'far', and contralateral recording sites were compared.

B.
1) For the three recording site locations, there were no significant differences in fEPSP slope (Kruskal-Wallis, p=0.126, Kruskal-Wallis statistic, 4.14) or amplitude (Kruskal-Wallis, p=0.302, Kruskal-Wallis statistic, 2.40)
2) There were no differences in latency to onset (Kruskal-Wallis, p=0.830, Kruskal-Wallis statistic, 0.37).

C. EPSPs were recorded either ipsilateral "near" or contralateral.
1) A two-way ANOVA with location and type of EPSP measurement as main factors showed a trend for an effect of location ($F(1,87)=3.72$; $p=0.057$), and significant differences in the type of measurement ($F(3,87)=23.14$; $p<0.001$). There was a significant interaction ($F(3,87)=2.96$; $p=0.037$).
2) Consistent with an interaction of factors, half-duration was significantly longer for contralateral GCs relative to ipsilateral GCs (Tukey-Kramer post-hoc test, p=0.013).

Appendix Figure 11
No differences in optogenetic responses recorded from GCs in different parts of the GCL.

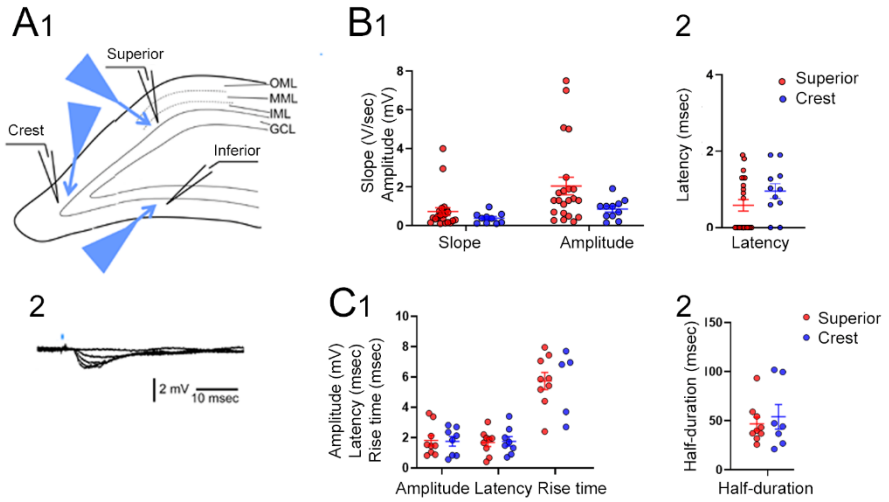

A.
1) A diagram of the three different parts of the DG, superior blade, crest, or inferior blade, used to compare optogenetic responses.
2) Example of fEPSPs elicited by increasing durations of optogenetic stimulation.

B. fEPSPs
1) There were no significant differences in fEPSP slope (Mann-Whitney *U* test, p=0.157, *U*=83.5) or amplitude (Mann-Whitney *U* test, p=0.070; *U*=73.5) between superior blade and crest.
2) There were no differences in latency (Mann-Whitney *U* test, p=0.164; *U*=85.0)The sample size (2 slices) for the lower blade was too small for statistical comparisons but values were in the same range as the other locations.

C. There were no significant effects of location on GC EPSPs in the superior blade vs. crest (two-way ANOVA, main effect of location, F(1,59)=0.94; p=0.337) although there was a main effect of the type of measurement (F(3,59)=46.10; p<0.0001). There was no interaction of factors (F(3,59)=0.31; p=0.816).
1) Amplitude, latency and rise time.
2) Half-duration.

Appendix Figure 12

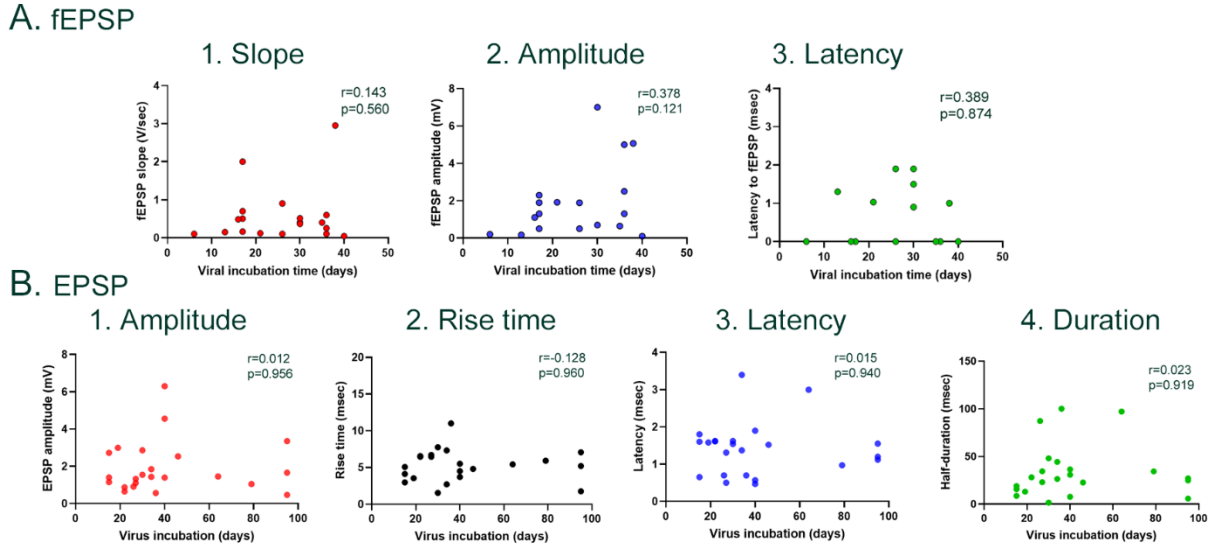

The duration of viral incubation did not correlate with characteristics of fEPSPs or EPSPs.

Viral expression was examined between 10 and 40 days after viral injection.

A. For fEPSPs, the correlations between time after injection (27.7± 2.2 days, range 13-40, n=14 mice, 34 slices) and fEPSP slope (1), amplitude (2) and latency (3) were not significant (slope, Pearson r=0.143, p=0.560; amplitude, Pearson r=0.378, p=0.121; latency, Spearman's r=-0.389, p=0.874).

B. For whole-cell recordings, there were no significant correlations between incubation time (42.4 ± 10.9 days; range: 15-95, n=15 mice, 26 slices) and 1) amplitude (Pearson r=0.012; p=0.956), 2) rise time (Pearson r=-0.128; p=0.960), 3) latency (Pearson r=0.015; p=0.940), or 4) half-duration (Pearson r=-0.023; p=0.919).

Appendix Figure 13

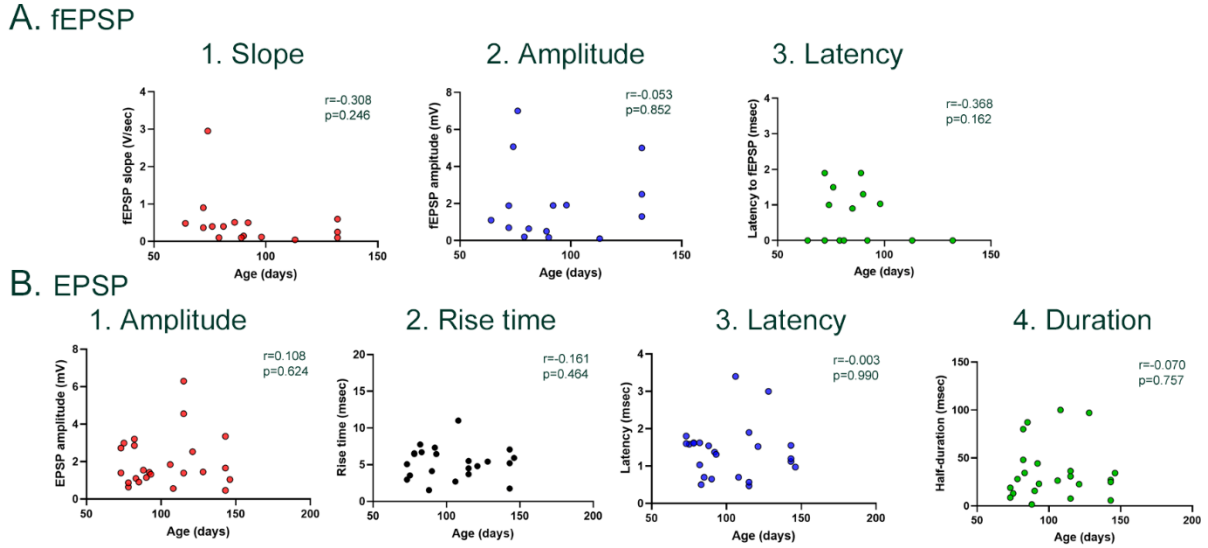

Characteristics of optogenetic fEPSPs and EPSPs were not correlated with age.

A. Age (89.2 ± 4.6 days, range: 64-132 days was examined in 37 slices of 20 mice. There was no correlation of age with fEPSP (1) slope (Pearson's r=-0.308 p=0.246), (2) amplitude (Pearson's r=-0.053, p=0.852) and (3) latency (Spearman's r=-0.368, p=0.162).

B. For EPSPs, there was no correlation between age (mean: 105.2 ± 5.4 days; range: 73-146 days, n=18 mice, 26 slices) and (1) amplitude (Pearson r=0.108; p=0.824), (2) rise time (Pearson r =-0.161; p=0.464), (3) latency (Pearson r =-0.003; p=0.990), or (4) half-duration (Pearson's r=-0.070; p=0.757).

Appendix Figure 14
Similar optogenetic fEPSPs in *Drd2*-Cre and *Crlr*-Cre mice.

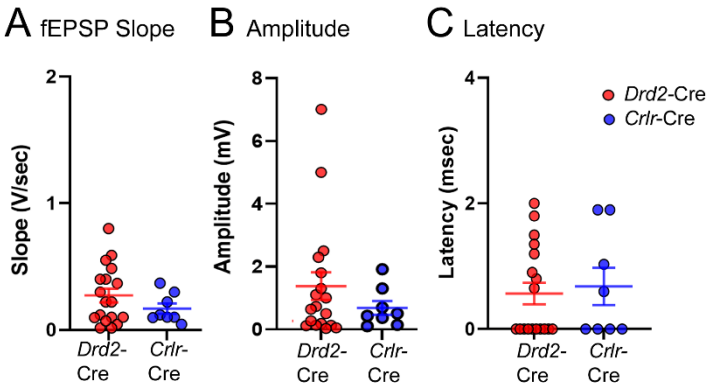

A-B. fEPSPs of *Drd2*-Cre and *Crlr*-Cre mice were compared by two-way ANOVA with strain and type of measurement (slope or amplitude) as main factors. There was no effect of strain ($F(1,48)=0.73$; $p=0.397$) but there was a difference between slope (A) and amplitude (B; $F(1,4= 5.48$; $p=0.024$). There was no interaction ($F(1,48)=1.33$; $p=0.254$).

C. There were no differences in latency between *Drd2*-Cre and *Crlr*-Cre mice (Mann-Whitney *U* test, $p=0.929$, *U*, 158).

REFERENCES

Acsady L, Kali S (2007) Models, structure, function: The transformation of cortical signals in the dentate gyrus. Prog Brain Res 163:577-599.

Amaral D (1978) A golgi study of cell types in the hilar region of the hippocampus in the rat. J Comp Neurol 15:851-914.

Amaral DG, Scharfman HE, Lavenex P (2007) The dentate gyrus: Fundamental neuroanatomical organization (dentate gyrus for dummies). Prog Brain Res 163:3-22.

Azevedo EP, Pomeranz L, Cheng J, Schneeberger M, Vaughan R, Stern SA, Tan B, Doerig K, Greengard P, Friedman JM (2019) A role of drd2 hippocampal neurons in context-dependent food intake. Neuron 102:873-886 e875.

Bauer JP, Rader SL, Joffe ME, Kwon W, Quay J, Seanez L, Zhou C, Conn PJ, Lewis AS (2021) Modeling intrahippocampal effects of anterior hippocampal hyperactivity relevant to schizophrenia using chemogenetic excitation of long axis-projecting mossy cells in the mouse dentate gyrus. Biol Psychiatry Glob Open Sci 1:101-111.

Bering R, Draguhn A, Diemer NH, Johansen FF (1997) Ischemia changes the coexpression of somatostatin and neuropeptide y in hippocampal interneurons. Exp Brain Res 115:423-429.

Bernstein HL, Lu YL, Botterill JJ, Scharfman HE (2019) Novelty and novel objects increase c-Fos immunoreactivity in mossy cells in the mouse dentate gyrus. Neural Plast 2019:1815371.

Blumcke I, Suter B, Behle K, Kuhn R, Schramm J, Elger CE, Wiestler OD (2000) Loss of hilar mossy cells in ammon's horn sclerosis. Epilepsia 41 Suppl 6:S174-180.

Botterill JJ, Gerencer KJ, Vinod KY, Alcantara-Gonzalez D, Scharfman HE (2021a) Dorsal and ventral mossy cells differ in their axonal projections throughout the dentate gyrus of the mouse hippocampus. Hippocampus 31:522-539.

Botterill JJ, Vinod KY, Gerencer KJ, Teixeira CM, LaFrancois JJ, Scharfman HE (2021b) Bidirectional regulation of cognitive and anxiety-like behaviors by dentate gyrus mossy cells in male and female mice. J Neurosci 41:2475-2495.

Botterill JJ, Lu YL, LaFrancois JJ, Bernstein HL, Alcantara-Gonzalez D, Jain S, Leary P, Scharfman HE (2019) An excitatory and epileptogenic effect of dentate gyrus mossycells in a mouse model of epilepsy. Cell Rep 29:2875-2889 e2876.

Buckmaster PS, Schwartzkroin PA (1994) Hippocampal mossy cell function: A speculative view. Hippocampus 4:393-402.

Buckmaster PS, Wenzel HJ, Kunkel DD, Schwartzkroin PA (1996) Axon arbors and synaptic connections of hippocampal mossy cells in the rat in vivo. J Comp Neurol 366:271-292.

Bui AD, Nguyen TM, Limouse C, Kim HK, Szabo GG, Felong S, Maroso M, Soltesz I (2018) Dentate gyrus mossy cells control spontaneous convulsive seizures and spatial memory. Science 359:787-790.

Buzsaki G (1986) Hippocampal sharp waves: Their origin and significance. Brain Res 398:242-252.

Buzsaki G (1989) Two-stage model of memory trace formation: A role for "noisy" brain states. Neuroscience 31:551-570.

Buzsaki G (2015) Hippocampal sharp wave-ripple: A cognitive biomarker for episodic memory and planning. Hippocampus 25:1073-1188.

Chancey JH, Poulsen DJ, Wadiche JI, Overstreet-Wadiche L (2014) Hilar mossy cells provide the first glutamatergic synapses to adult-born dentate granule cells. J Neurosci 34:2349-2354.

Chapman CA, Xu Y, Haykin S, Racine RJ (1998) Beta-frequency (15-35 hz) electroencephalogram activities elicited by toluene and electrical stimulation in the behaving rat. Neuroscience 86:1307-1319.

Chartampila E, Elayouby KS, Leary P, LaFrancois JJ, Alcantara-Gonzalez D, Jain S, Gerencer K, Botterill JJ, Ginsberg SD, Scharfman HE (2023) Choline supplementation in early life improves and low levels of choline can impair outcomes in a mouse model of Alzheimer's disease. bioRxiv.

Chiu CQ, Castillo PE (2008) Input-specific plasticity at excitatory synapses mediated by endocannabinoids in the dentate gyrus. Neuropharmacology 54:68-78.

Danielson NB, Turi GF, Ladow M, Chavlis S, Petrantonakis PC, Poirazi P, Losonczy A (2017) In vivo imaging of dentate gyrus mossy cells in behaving mice. Neuron 93:552-559 e554.

Diamantaki M, Frey M, Berens P, Preston-Ferrer P, Burgalossi A (2016) Sparse activity of identified dentate granule cells during spatial exploration. Elife 5.

Dieni CV, Panichi R, Aimone JB, Kuo CT, Wadiche JI, Overstreet-Wadiche L (2016) Low excitatory innervation balances high intrinsic excitability of immature dentate neurons. Nat Commun 7:11313.

Duffy AM, Schaner MJ, Chin J, Scharfman HE (2013) Expression of c-fos in hilar mossy cells of the dentate gyrus in vivo. Hippocampus 23:649-655.

Esposito MS, Piatti VC, Laplagne DA, Morgenstern NA, Ferrari CC, Pitossi FJ, Schinder AF (2005) Neuronal differentiation in the adult hippocampus recapitulates embryonic development. J Neurosci 25:10074-10086.

Fredes F, Shigemoto R (2021) The role of hippocampal mossy cells in novelty detection. Neurobiol Learn Mem 183:107486.

Freund TF, Buzsaki G (1996) Interneurons of the hippocampus. Hippocampus 6:347-470.

Freund TF, Gulyas AI (1997) Inhibitory control of gabaergic interneurons in the hippocampus. Can J Physiol Pharmacol 75:479-487.

Gangarossa G, Longueville S, De Bundel D, Perroy J, Herve D, Girault JA, Valjent E (2012) Characterization of dopamine d1 and d2 receptor-expressing neurons in the mouse hippocampus. Hippocampus 22:2199-2207.

Ge S, Yang CH, Hsu KS, Ming GL, Song H (2007) A critical period for enhanced synaptic plasticity in newly generated neurons of the adult brain. Neuron 54:559-566.

Giovannucci A, Friedrich J, Gunn P, Kalfon J, Brown BL, Koay SA, Taxidis J, Najafi F, Gauthier JL, Zhou P, Khakh BS, Tank DW, Chklovskii DB, Pnevmatikakis EA (2019) Caiman an open source tool for scalable calcium imaging data analysis. Elife 8.

GoodSmith D, Lee H, Neunuebel JP, Song H, Knierim JJ (2019) Dentate gyrus mossy cells share a role in pattern separation with dentate granule cells and proximal CA3 pyramidal cells. J Neurosci 39:9570-9584.

GoodSmith D, Kim SH, Puliyadi V, Ming GL, Song H, Knierim JJ, Christian KM (2022) Flexible encoding of objects and space in single cells of the dentate gyrus. Curr Biol 32:1088-1101 e1085.

GoodSmith D, Chen X, Wang C, Kim SH, Song H, Burgalossi A, Christian KM, Knierim JJ (2017) Spatial representations of granule cells and mossy cells of the dentate gyrus. Neuron 93:677-690 e675.

Grovola MR, Paleologos N, Wofford KL, Harris JP, Browne KD, Johnson V, Duda JE, Wolf JA, Cullen DK (2020) Mossy cell hypertrophy and synaptic changes in the hilus following mild diffuse traumatic brain injury in pigs. J Neuroinflammation 17:44.

Gulfo MC, Lebowitz JJ, Ramos C, Hwang DW, Nasrallah K, Castillo PE (2023) Dopamine d2 receptors in mossy cells reduce excitatory transmission and are essential for hippocampal function. bioRxiv.

Haas HL, Rose GM (1987) Noradrenaline blocks potassium conductance in rat dentate granule cells in vitro. Neurosci Lett 78:171-174.

Hainmueller T, Bartos M (2020) Dentate gyrus circuits for encoding, retrieval and discrimination of episodic memories. Nat Rev Neurosci 21:153-168.

Hajos N, Freund TF (2002) Pharmacological separation of cannabinoid sensitive receptors on hippocampal excitatory and inhibitory fibers. Neuropharmacology 43:503-510.

Harden SW, Frazier CJ (2016) Oxytocin depolarizes fast-spiking hilar interneurons and induces GABA release onto mossy cells of the rat dentate gyrus. Hippocampus 26:1124-1139.

Harte-Hargrove LC, Varga-Wesson A, Duffy AM, Milner TA, Scharfman HE (2015) Opioid receptor-dependent sex differences in synaptic plasticity in the hippocampal mossy fiber pathway of the adult rat. J Neurosci 35:1723-1738.

Hashimotodani Y, Nasrallah K, Jensen KR, Chavez AE, Carrera D, Castillo PE (2017) Ltp at hilar mossy cell-dentate granule cell synapses modulates dentate gyrus output by increasing excitation/inhibition balance. Neuron 95:928-943 e923.

Henze DA, Buzsáki G (2007) Hilar mossy cells: Functional identification and activity in vivo. Prog Brain Res 163:199-216.

Henze DA, Urban NN, Barrionuevo G (2000) The multifarious hippocampal mossy fiber pathway: A review. Neuroscience 98:407-427.

Hetherington PA, Austin KB, Shapiro ML (1994) Ipsilateral associational pathway in the dentate gyrus: An excitatory feedback system that supports n-methyl-d-aspartate-dependent long-term potentiation. Hippocampus 4:422-438.

Hofmann ME, Frazier CJ (2010) Muscarinic receptor activation modulates the excitability of hilar mossy cells through the induction of an afterdepolarization. Brain Res 1318:42-51.

Hosp JA, Struber M, Yanagawa Y, Obata K, Vida I, Jonas P, Bartos M (2014) Morpho-physiological criteria divide dentate gyrus interneurons into classes. Hippocampus 24:189-203.

Houser CR (2007) Interneurons of the dentate gyrus: An overview of cell types, terminal fields and neurochemical identity. Prog Brain Res 163:217-232.

Houser CR, Peng Z, Wei X, Huang CS, Mody I (2021) Mossy cells in the dorsal and ventral dentate gyrus differ in their patterns of axonal projections. J Neurosci 41:991-1004.

Hsu D (2007) The dentate gyrus as a filter or gate: A look back and a look ahead. Prog Brain Res 163:601-613.

Hsu TT, Lee CT, Tai MH, Lien CC (2015) Differential recruitment of dentate gyrus interneuron types by commissural versus perforant pathways. Cereb Cortex.

Hung YC, Wu YJ, Chien ME, Lin YT, Tsai CF, Hsu KS (2023) Loss of oxytocin receptors in hilar mossy cells impairs social discrimination. Neurobiol Dis 187:106311.

Jinde S, Zsiros V, Nakazawa K (2013) Hilar mossy cell circuitry controlling dentate granule cell excitability. Front Neural Circuits 7:14.

Jinde S, Zsiros V, Jiang Z, Nakao K, Pickel J, Kohno K, Belforte JE, Nakazawa K (2012) Hilar mossy cell degeneration causes transient dentate granule cell hyperexcitability and impaired pattern separation. Neuron 76:1189-1200.

Jung D, Kim S, Sariev A, Sharif F, Kim D, Royer S (2019) Dentate granule and mossy cells exhibit distinct spatiotemporal responses to local change in a one-dimensional landscape of visual-tactile cues. Sci Rep 9:9545.

Jung MW, McNaughton BL (1993) Spatial selectivity of unit activity in the hippocampal granular layer. Hippocampus 3:165-182.

Kay LM (2014) Circuit oscillations in odor perception and memory. Prog Brain Res 208:223-251.

Kim SH, GoodSmith D, Temme SJ, Moriya F, Ming GL, Christian KM, Song H, Knierim JJ (2023) Global remapping in granule cells and mossy cells of the mouse dentate gyrus. Cell Rep 42:112334.

Kim WB, Cho JH (2020) Encoding of contextual fear memory in hippocampal-amygdala circuit. Nat Commun 11:1382.

Kleschevnikov AM, Routtenberg A (2003) Long-term potentiation recruits a trisynaptic excitatory associative network within the mouse dentate gyrus. Eur J Neurosci 17:2690-2702.

Knierim JJ, Neunuebel JP (2016) Tracking the flow of hippocampal computation: Pattern separation, pattern completion, and attractor dynamics. Neurobiol Learn Mem 129:38-49.

Krook-Magnuson E, Armstrong C, Bui A, Lew S, Oijala M, Soltesz I (2015) In vivo evaluation of the dentate gate theory in epilepsy. J Physiol 593:2379-2388.

Laatsch RH, Cowan WM (1966) Electron microscopic studies of the dentate gyrus of the rat. I. Normal structure with special reference to synaptic organization. J Comp Neurol 128:359-395.

Lacaille JC, Schwartzkroin PA (1988) Intracellular responses of rat hippocampal granule cells in vitro to discrete applications of norepinephrine. Neurosci Lett 89:176-181.

Larimer P, Strowbridge BW (2008) Nonrandom local circuits in the dentate gyrus. J Neurosci 28:12212-12223.

Leranth C, Frotscher M (1987) Cholinergic innervation of hippocampal gad- and somatostatin-immunoreactive commissural neurons. J Comp Neurol 261:33-47.

Leranth C, Szeidemann Z, Hsu M, Buzsáki G (1996) AMPA receptors in the rat and primate hippocampus: A possible absence of glur2/3 subunits in most interneurons. Neuroscience 70:631-652.

Leutgeb JK, Leutgeb S, Moser MB, Moser EI (2007) Pattern separation in the dentate gyrus and CA3 of the hippocampus. Science 315:961-966.

Lisman JE, Talamini LM, Raffone A (2005) Recall of memory sequences by interaction of the dentate and CA3: A revised model of the phase precession. Neural Netw 18:1191-1201.

Luna VM, Anacker C, Burghardt NS, Khandaker H, Andreu V, Millette A, Leary P, Ravenelle R, Jimenez JC, Mastrodonato A, Denny CA, Fenton AA, Scharfman HE, Hen R (2019) Adult-born hippocampal neurons bidirectionally modulate entorhinal inputs into the dentate gyrus. Science 364:578-583.

Maguire JL, Stell BM, Rafizadeh M, Mody I (2005) Ovarian cycle-linked changes in GABA(a) receptors mediating tonic inhibition alter seizure susceptibility and anxiety. Nat Neurosci 8:797-804.

Maroto IB, Costas-Insua C, Berthoux C, Moreno E, Ruiz-Calvo A, Montero-Fernandez C, Macias-Camero A, Martin R, Garcia-Font N, Sanchez-Prieto J, Marsicano G, Bellocchio L, Canela EI, Casado V, Galve-Roperh I, Nunez A, Fernandez de Sevilla D, Rodriguez-Crespo I, Castillo PE, Guzman M (2023) Control of a hippocampal recurrent excitatory circuit by cannabinoid receptor-interacting protein GAP43. Nat Commun 14:2303.

Miles R, Wong RK (1983) Single neurones can initiate synchronized population discharge in the hippocampus. Nature 306:371-373.

Miles R, Wong RK (1986) Excitatory synaptic interactions between CA3 neurones in the guinea-pig hippocampus. J Physiol 373:397-418.

Miller LN, Weiss C, Disterhoft JF (2022) Learning-related changes in cellular activity within mouse dentate gyrus during trace eyeblink conditioning. Hippocampus 32:776-794.

Moretto JN, Duffy AM, Scharfman HE (2017) Acute restraint stress decreases c-fos immunoreactivity in hilar mossy cells of the adult dentate gyrus. Brain Struct Funct 222:2405-2419.

Myers CE, Scharfman HE (2009) A role for hilar cells in pattern separation in the dentate gyrus: A computational approach. Hippocampus 19:321-337.

Myers CE, Scharfman HE (2011) Pattern separation in the dentate gyrus: A role for the CA3 backprojection. Hippocampus 21:1190-1215.

Nakazawa K (2017) Dentate mossy cell and pattern separation. Neuron 93:465-467.

Namgung U, Matsuyama S, Routtenberg A (1997) Long-term potentiation activates the gap-43 promoter: Selective participation of hippocampal mossy cells. Proc Natl Acad Sci U S A 94:11675-11680.

Nasrallah K, Frechou MA, Yoon YJ, Persaud S, Goncalves JT, Castillo PE (2022) Seizure-induced strengthening of a recurrent excitatory circuit in the dentate gyrus is proconvulsant. Proc Natl Acad Sci U S A 119:e2201151119.

Neunuebel JP, Knierim JJ (2012) Spatial firing correlates of physiologically distinct cell types of the rat dentate gyrus. J Neurosci 32:3848-3858.

Newman EL, Hasselmo ME (2014) CA3 sees the big picture while dentate gyrus splits hairs. Neuron 81:226-228.

Oh SJ, Cheng J, Jang JH, Arace J, Jeong M, Shin CH, Park J, Jin J, Greengard P, Oh YS (2020) Hippocampal mossy cell involvement in behavioral and neurogenic responses to chronic antidepressant treatment. Mol Psychiatry 25:1215-1228.

Oh YS, Gao P, Lee KW, Ceglia I, Seo JS, Zhang X, Ahn JH, Chait BT, Patel DJ, Kim Y, Greengard P (2013) Smarca3, a chromatin-remodeling factor, is required for p11-dependent antidepressant action. Cell 152:831-843.

Overstreet LS, Hentges ST, Bumaschny VF, de Souza FS, Smart JL, Santangelo AM, Low MJ, Westbrook GL, Rubinstein M (2004) A transgenic marker for newly born granule cells in dentate gyrus. J Neurosci 24:3251-3259.

Pilz GA, Carta S, Stauble A, Ayaz A, Jessberger S, Helmchen F (2016) Functional imaging of dentate granule cells in the adult mouse hippocampus. J Neurosci 36:7407-7414.

Pnevmatikakis EA, Soudry D, Gao Y, Machado TA, Merel J, Pfau D, Reardon T, Mu Y, Lacefield C, Yang W, Ahrens M, Bruno R, Jessell TM, Peterka DS, Yuste R, Paninski L (2016) Simultaneous denoising, deconvolution, and demixing of calcium imaging data. Neuron 89:285-299.

Puighermanal E, Biever A, Espallergues J, Gangarossa G, De Bundel D, Valjent E (2015) Drd2-cre:Ribotag mouse line unravels the possible diversity of dopamine d2 receptor-expressing cells of the dorsal mouse hippocampus. Hippocampus 25:858-875.

Ramos C, Lutzu S, Yamasaki M, Yanagawa Y, Sakimura K, Tomita S, Watanabe M, Castillo PE (2022) Activation of extrasynaptic kainate receptors drives hilar mossy cell activity. J Neurosci 42:2872-2884.

Ratzliff A, Santhakumar V, Howard A, Soltesz I (2002) Mossy cells in epilepsy: Rigor mortis or vigor mortis? Trends Neurosci 25:140-144.

Ribak CE, Seress L, Amaral DG (1985) The development, ultrastructure and synaptic connections of the mossy cells of the dentate gyrus. J Neurocytol 14:835-857.

Salin PA, Scanziani M, Malenka RC, Nicoll RA (1996) Distinct short-term plasticity at two excitatory synapses in the hippocampus. Proc Natl Acad Sci U S A 93:13304-13309.

Santhakumar V, Bender R, Frotscher M, Ross ST, Hollrigel GS, Toth Z, Soltesz I (2000) Granule cell hyperexcitability in the early post-traumatic rat dentate gyrus: The 'irritable mossy cell' hypothesis. J Physiol 524 Pt 1:117-134.

Scharfman HE (1991) Dentate hilar cells with dendrites in the molecular layer have lower thresholds for synaptic activation by perforant path than granule cells. J Neurosci 11:1660-1673.

Scharfman HE (1993) Characteristics of spontaneous and evoked EPSPs recorded from dentate spiny hilar cells in rat hippocampal slices. J Neurophysiol 70:742-757.

Scharfman HE (1994a) EPSPs of dentate gyrus granule cells during epileptiform bursts of dentate hilar "mossy" cells and area CA3 pyramidal cells in disinhibited rat hippocampal slices. J Neurosci 14:6041-6057.

Scharfman HE (1994b) Evidence from simultaneous intracellular recordings in rat hippocampal slices that area CA3 pyramidal cells innervate dentate hilar mossy cells. J Neurophysiol 72:2167-2180.

Scharfman HE (1995a) Electrophysiological evidence that dentate hilar mossy cells are excitatory and innervate both granule cells and interneurons. J Neurophysiol 74:179-194.

Scharfman HE (1995b) Electrophysiological diversity of pyramidal-shaped neurons at the granule cell layer/hilus border of the rat dentate gyrus recorded in vitro. Hippocampus 5:287-305.

Scharfman HE (2007) The CA3 "backprojection" to the dentate gyrus. Prog Brain Res 163:627-637.

Scharfman HE (2016) The enigmatic mossy cell of the dentate gyrus. Nat Rev Neurosci 17:562-575.

Scharfman HE, Schwartzkroin PA (1988) Electrophysiology of morphologically identified mossy cells of the dentate hilus recorded in guinea pig hippocampal slices. J Neurosci 8:3812-3821.

Scharfman HE, Gray WP (2006) Plasticity of neuropeptide y in the dentate gyrus after seizures, and its relevance to seizure-induced neurogenesis. EXS:193-211.

Scharfman HE, Witter MP (2007) Preface. In: The dentate gyrus: A comprehensive guide to structure, function, and clinical implications (Scharfman HE, ed), pp ix-xvii. New York: Elsevier.

Scharfman HE, Myers CE (2012) Hilar mossy cells of the dentate gyrus: A historical perspective. Front Neural Circuits 6:106.

Scharfman HE, Goodman JH, Sollas AL (2000) Granule-like neurons at the hilar/CA3 border after status epilepticus and their synchrony with area CA3 pyramidal cells: Functional implications of seizure-induced neurogenesis. J Neurosci 20:6144-6158.

Scharfman HE, Sollas AL, Smith KL, Jackson MB, Goodman JH (2002) Structural and functional asymmetry in the normal and epileptic rat dentate gyrus. J Comp Neurol 454:424-439.

Schmidt-Hieber C, Jonas P, Bischofberger J (2004) Enhanced synaptic plasticity in newly generated granule cells of the adult hippocampus. Nature 429:184-187.

Senzai Y, Buzsaki G (2017) Physiological properties and behavioral correlates of hippocampal granule cells and mossy cells. Neuron 93:691-704 e695.

Sloviter RS (1994) The functional organization of the hippocampal dentate gyrus and its relevance to the pathogenesis of temporal lobe epilepsy. Ann Neurol 35:640-654.

Soltesz I, Bourassa J, Deschenes M (1993) The behavior of mossy cells of the rat dentate gyrus during theta oscillations in vivo. Neuroscience 57:555-564.

Soriano E, Frotscher M (1994) Mossy cells of the rat fascia dentata are glutamate-immunoreactive. Hippocampus 4:65-69.

Sperk G, Hamilton T, Colmers WF (2007) Neuropeptide y in the dentate gyrus. Prog Brain Res 163:285-297.

Stanton PK, Mody I, Heinemann U (1989) A role for n-methyl-d-aspartate receptors in norepinephrine-induced long-lasting potentiation in the dentate gyrus. Exp Brain Res 77:517-530.

Steiner A, Owen BM, Bauer JP, Seanez L, Kwon S, Biddinger JE, Huffman R, Ayala JE, Nobis WP, Lewis AS (2022) Glucagon-like peptide-1 receptor differentially controls mossy cell activity across the dentate gyrus longitudinal axis. Hippocampus 32:797-807.

Swaminathan A, Wichert I, Schmitz D, Maier N (2018) Involvement of mossy cells in sharp wave-ripple activity in vitro. Cell Rep 23:2541-2549.

Thomson AM, Deuchars J (1997) Synaptic interactions in neocortical local circuits: Dual intracellular recordings in vitro. Cereb Cortex 7:510-522.

von Kitzing E, Jonas P, Sakmann B (1994) Quantal analysis of excitatory postsynaptic currents at the hippocampal mossy fiber-CA3 pyramidal cell synapse. Adv Second Messenger Phosphoprotein Res 29:235-260.

Wang H, Yuan Y, Zhang Z, Yan H, Feng Y, Li W (2014) Dysbindin-1c is required for the survival of hilar mossy cells and the maturation of adult newborn neurons in dentate gyrus. J Biol Chem 289:29060-29072.

Wang H, Peca J, Matsuzaki M, Matsuzaki K, Noguchi J, Qiu L, Wang D, Zhang F, Boyden E, Deisseroth K, Kasai H, Hall WC, Feng G, Augustine GJ (2007) High-speed mapping of synaptic connectivity using photostimulation in channelrhodopsin-2 transgenic mice. Proc Natl Acad Sci U S A 104:8143-8148.

Wang KY, Wu JW, Cheng JK, Chen CC, Wong WY, Averkin RG, Tamas G, Nakazawa K, Lien CC (2021) Elevation of hilar mossy cell activity suppresses hippocampal excitability and avoidance behavior. Cell Rep 36:109702.

Wenzel HJ, Buckmaster PS, Anderson NL, Wenzel ME, Schwartzkroin PA (1997) Ultrastructural localization of neurotransmitter immunoreactivity in mossy cell axons and their synaptic targets in the rat dentate gyrus. Hippocampus 7:559-570.

Wright BJ, Jackson MB (2014) Long-term potentiation in hilar circuitry modulates gating by the dentate gyrus. J Neurosci 34:9743-9753.

Yassa MA, Stark CE (2011) Pattern separation in the hippocampus. Trends Neurosci 34:515-525.

Yoshino M, Sawada S, Yamamoto C, Kamiya H (1996) A metabotropic glutamate receptor agonist dcg-iv suppresses synaptic transmission at mossy fiber pathway of the guinea pig hippocampus. Neurosci Lett 207:70-72.

Yuan Y, Wang H, Wei Z, Li W (2015) Impaired autophagy in hilar mossy cells of the dentate gyrus and its implication in schizophrenia. J Genet Genomics 42:1-8.

Zhang ZJ, Koifman J, Shin DS, Ye H, Florez CM, Zhang L, Valiante TA, Carlen PL (2012) Transition to seizure: Ictal discharge is preceded by exhausted presynaptic GABA release in the hippocampal CA3 region. J Neurosci 32:2499-2512.

Zhou QG, Nemes AD, Lee D, Ro EJ, Zhang J, Nowacki AS, Dymecki SM, Najm IM, Suh H (2019) Chemogenetic silencing of hippocampal neurons suppresses epileptic neural circuits. J Clin Invest 129:310-323.